1990

Gas Phase Photoelectron Studies Of Organoplatinum Complexes Using Helium I, Helium Ii And Synchrotron Radiation

Dong-sheng Yang

1. Information From Ionization Energy. The ionization energy, often called the electron binding energy, is the difference in total energy between the neutral molecule and the molecular ion in a particular state:[2]

$$I.E. = h\nu - E_k(e^-) = E(M^+) - E(M) \qquad (1\text{-}2)$$

The formal relationship between the ionization energy and the theoretical (one-electron) orbital energy is established by Koopmans' theorem,[18] which states that the ionization energy is the negative of the orbital energy (ε_i)

$$I.E. = -\varepsilon_i \qquad (1\text{-}3)$$

from a Hartree-Fock molecular orbital calculation, provided that the electron distribution of the final (molecular ion) state does not relax from that of the initial molecular state with one electron missing from orbital i. The correlation between theories and experiments can be improved in many cases by considering electron relaxation, electron correlation and relativistic effects in the theoretical calculations.

The ionization energy as well as the ionization energy shift between related molecules is the most important feature of the photoelectron spectrum. In general, the first ionization energy (the lowest ionization energy) of a molecule may be correlated with its electron richness. A high ionization energy indicates relatively stable and inaccessible electrons, while a low ionization energy indicates relatively unstable and available electron density. This feature is directly related to oxidation-reduction reactivity. The ionization energy is also related to the bonding nature. Strong covalent bonding interactions result in ionization bands with generally higher ionization energies, while non-bonding and antibonding orbitals result in ionizations with generally lower ionization energies. The shift in an ionization energy between electronically or chemically related molecules reveals the localized or delocalized character of the electronic states. For example, in the d^8 molecules $(\eta^5\text{-}C_5H_5)Co(CO)_2$ and $(\eta^5\text{-}C_5H_5)Rh(CO)_2$, three of the four metal-based orbital ionizations have large

GAS PHASE PHOTOELECTRON STUDIES OF ORGANOPLATINUM COMPLEXES USING HE I, HE II AND SYNCHROTRON RADIATION

by

Dong-Sheng Yang

Department of Chemistry

Submitted in partial fulfilment

of the requirements for the degree of

Doctor of Philosophy

Faculty of Graduate Studies

The University of Western Ontario

London, Ontario

November 1989

ISBN 0-315-55281-6

ABSTRACT

Gas-phase He I and He II photoelectron spectra of four series of organoplatinum complexes are reported, together with synchrotron radiation photoelectron spectra of $CpPtMe_3$ (Cp = η^5-C_5H_5) and $PtMe_2(COD)$ (COD = 1,5-cyclooctadiene). The platinum complexes investigated with both He I and He II sources include square-planar cis-dimethylplatinum(II), square-planar cis-bis(trifluoromethyl)platinum(II), half-sandwich (η^5-cyclopentadienyl)trimethylplatinum(IV), and octahedral-like (ß-diketonato)trimethylplatinum(IV) complexes. The electronic structures of the complexes studied are discussed using the He I and He II spectral information, such as the ionization energy shifts from ligand substitutions and the resolved vibrational splittings from ligand-based orbitals, and using Xα-SW calculations on some model compounds. The photo-ionization behaviour of the upper valence orbitals of $CpPtMe_3$ and $Me_2Pt(COD)$ is discussed in terms of the branching ratios as a function of the photon energies from 21 to 100 eV.

In the complexes cis-$[PtMe_2L_2]$ {L = PMe_3, PMe_2Ph, $PMePh_2$, PEt_3, $P(NMe_2)_3$, $PMe(OEt)_2$, $P(OMe)_3$, $P(OEt)_3$, $AsMe_3$, CNMe, and CNPh; or L_2 = $Me_2NCH_2CH_2NMe_2$ (TMED), 1,5-cyclooctadiene (COD), and norbornadiene (NBD)} and cis-$[Pt(CF_3)_2L_2]$ {L = PEt_3 and $AsMe_3$, or L_2 = TMED and COD}, the two molecular orbitals with the lowest ionization energies are assigned to Pt-ligand σ-orbitals, and these are followed by four MO's which have mostly nonbonding Pt character. The Me contribution to the Pt-Me σ bonds has essentially C 2p character, while the CF_3 contribution to the Pt-CF_3 bond is C-F antibonding with a significant C 2s character. The σ-donor ability of a ligand L is reflected in its first ionization energy and decreases in the order L = $P(NMe_2)_3$ > TMED > $PMePh_2$ ~ PMe_2Ph > PEt_3 > $AsMe_3$ ~ PMe_3 > $PMe(OEt)_2$ > $P(OEt)_3$ > $P(OMe)_3$ > COD > NBD. The π-

acceptor ability of the ligand is reflected by the energy separation of the Pt $5d_\pi$ orbitals and falls in the order $PMePh_2$ ~ PMe_2Ph ~ $P(OMe)_3$ ~ $P(OEt)_3$ ~ $PMe(OEt)_2$ ~ $P(NMe_2)_3$ > $AsMe_3$ ~ PMe_3 ~ PEt_3 ~ COD ~ NBD > TMED. Both CNMe and CNPh, which cannot be arranged into the above series, have comparable σ-donor ability and the latter has stronger π-acceptor properties.

In the complexes $CpPtMe_3$ and Cp^*PtMe_3 ($Cp^* = \eta^5$-C_5Me_5), the eight upper filled MO's are composed of three Pt 5d-based MO's unevenly sandwiched between the Pt-ligand orbitals. There are strong interactions between the Pt $5d_\sigma$ orbitals and both the Cp e_1'' π and the Me σ sets, together with significant back-donation from the Pt $5d_\pi$ to the empty Cp e_2'' orbitals.

The ionization energies of the first six valence MO's fall in the order π_3 < n < Pt-n_+ < Pt 5d, Pt-Me in the complexes $[PtMe_3(acac)]$ (acac = acetylacetonate), $[PtMe_3(tfa)H_2O]$ (tfa = trifluoroacetylacetonate), and $[PtMe_3(hfa)H_2O]$ (hfa = hexafluoroacetylacetonate), while the ionization energy of the first seven valence MO's in the compound $[PtMe_3(tfa)Me_2S]$ falls in the order Pt-Me_2S<π_3<n_-<Pt-n_+<Pt 5d. There is strong interaction between the platinum 5d orbitals and both the ß-diketonate n_+ and the methyl σ orbitals.

Experimental branching ratios from 21 to 100 eV photon energies are reported, along with theoretical values, for the compounds $CpPtMe_3$ and $Me_2Pt(COD)$. The agreement between experimental branching ratios and the Xα-SW values strongly supports the Xα-SW assignment for both $CpPtMe_3$ and $Me_2Pt(COD)$. The differences in orbital character are generally reflected in the experimental branching ratios in the absence of resonance effects. A possible resonance resulting from a Pt-ligand σ electron transition to an f-like antibonding orbital is observed in $CpPtMe_3$.

ACKNOWLEDGEMENTS

I would like to express my gratitude to my supervisors, Dr. G. M. Bancroft and Dr. R. J. Puddephatt, for the opportunity they provided for me to study and work at the University of Western Ontario, for their guidance, encouragement and patience throughout the course of this work. The years I have spent at Western will be cherished in my memory for the rest of my life.

It is a pleasure to acknowledge the assistance of the many friendly and helpful individuals I have associated with during my studies at Western. Special thanks are extended to Doug Hairsine for his technical assistance with the vacuum pumps in the ESCA photoelectron spectrometer; to John Bozek and John Tse, Ian Jobe and Mehdi Rashidi, Lisa Marie Dignard and Jo-Ann Edith Bice, and Kim Tan and Jeff Cutler, for their respective help in the initial stages of the Xα-SW calculations, syntheses, He source photoelectron, and synchrotron radiation photoelectron experiments. I also wish to acknowledge the other members of the groups, Leighton Coatsworth, Brian Yates, Ian Muir, Margaret Hyland, Masoud Kasrai, Steve Bushby, Jamie Price, Jay Mycroft, ZhiFeng Liu, Douglas Sutherland, Mike Jennings, Nasim Hadj-Bagheri, Ravindranath Ramachandran, Arleen Bradford, Weini Zhou, Khin-Than Aye, Craig Anderson, Sujit Roy and Lucio Gelmini for their friendship and lively discussions.

I am grateful to the University of Western Ontario and the Ontario Ministry of Colleges and Universities for their financial support.

Finally, I am deeply indebted to my wife, Chun Fang, for her love, understanding and support and to our families for their encouragement.

TABLE OF CONTENT

LIST OF TABLES

LIST OF FIGURES

Abbreviations

acac	acetylacetonate
COD	1,5-cyclooctadiene
Cp	η^5-cyclopentadienyl
Cp*	η^5-pentamethylcyclopentadienyl
Et	ethyl
hfa	hexafluoroacetylacetonate
Me	methyl
NBD	norbornadiene
Ph	phenyl
tfa	trifluoroacetylacetonate
TMED	N,N,N',N'-tetramethylenediamine

CHAPTER 1

INTRODUCTION

1.1 INTRODUCTION

The chemistry that occurs at transition metal centres is fundamental to many homogeneous synthesis and catalysis reactions, surface reactions, and bioinorganic processes. Characterization of the structural arrangement of atoms in a molecule is an important step to understand organometallic chemistry. However, the understanding of the properties and behaviour of an organometallic molecule, and our ability to extend this understanding to new systems, requires knowledge of more than just the particular three dimensional arrangement of atoms. A further, more detailed step in characterization of a molecule is to obtain information on the electronic structure in terms of electron distribution, bonding and stability. Electronic structural factors play an important role in defining the physical properties of the molecule and its reaction with its environment. Therefore, full characterization of a molecule must include its electronic structural features in addition to the molecular structure. Photoelectron spectroscopy provides the most direct experimental study of electronic structure, and organometallic molecules provide systems with metal-ligand interactions in a variety of electronic environments suitable for detailed investigation. This thesis presents a detailed gas phase He I/He II and synchrotron radiation photoelectron study of series of organoplatinum molecules which are important to organoplatinum chemistry.

1.2 OVERVIEW OF GAS PHASE UV PHOTOELECTRON SPECTROSCOPY IN ORGANOMETALLIC CHEMISTRY

Basic Concept. The photoelectron spectroscopy experiment[1-12] is conceptually simple. A photon ($h\nu$) provides the energy to eject an electron from an electron bound state of a gas molecule. The kinetic energy, $E_k(e^-)$, of the ejected electron is measured, and the ionization energy (I.E.) for this event, according to Einstein's energy conservation relation to the photoelectric effect[13] is defined as

$$\text{I.E.} = h\nu - E_k(e^-) \qquad (1\text{-}1)$$

For low energy photons ($h\nu$ commonly less than 50 eV) such as He I (21.218 eV), He II (40.814 eV), or Ne I (16.848 eV), the electrons are ejected primarily from the valence shell with a high resolution (~0.02 eV), and the technique is called ultraviolet photoelectron spectroscopy (UPS). For high energy photons ($h\nu$ commonly greater than 1000 eV) such as MgKα (1253.6 eV), AlKα (1486.6 eV), etc., the electrons are ejected primarily from atomic core levels with relatively low resolution (≥0.5 eV), and the technique is called X-ray photoelectron spectroscopy (XPS) or electron spectroscopy for chemical analysis (ESCA). The gap between these two sources can be bridged by a synchrotron radiation source which can span the range from the UV to the X-ray region.[14-16] The synchrotron radiation source, which provides an intense continuum of linearly polarized radiation, can be monochromatized to obtain an intense photon beam of relatively narrow linewidth and allows angular distributions and cross sections or branching ratios to be studied as a function of photon energy. In addition, lasers working in the UV region have been introduced and permit studies of photoelectron spectroscopy of excited states of molecules.[17]

Information from Photoelectron Spectra. A photoelectron spectrum is a scan of intensity versus electron kinetic energy for ejected electrons analyzed at a given angle from the incident photon beam. The characteristic features of an ionization band in the spectrum are its energy, shape, resolved fine structure, and relative intensity. Each feature is generally sensitive to the electronic structure of the molecule.

1. Information From Ionization Energy. The ionization energy, often called the electron binding energy, is the difference in total energy between the neutral molecule and the molecular ion in a particular state:[2]

$$\text{I.E.} = h\nu - E_k(e^-) = E(M^+) - E(M) \qquad (1\text{-}2)$$

The formal relationship between the ionization energy and the theoretical (one-electron) orbital energy is established by Koopmans' theorem,[18] which states that the ionization energy is the negative of the orbital energy (ε_i)

$$\text{I.E.} = -\varepsilon_i \qquad (1\text{-}3)$$

from a Hartree-Fock molecular orbital calculation, provided that the electron distribution of the final (molecular ion) state does not relax from that of the initial molecular state with one electron missing from orbital i. The correlation between theories and experiments can be improved in many cases by considering electron relaxation, electron correlation and relativistic effects in the theoretical calculations.

The ionization energy as well as the ionization energy shift between related molecules is the most important feature of the photoelectron spectrum. In general, the first ionization energy (the lowest ionization energy) of a molecule may be correlated with its electron richness. A high ionization energy indicates relatively stable and inaccessible electrons, while a low ionization energy indicates relatively unstable and available electron density. This feature is directly related to oxidation-reduction reactivity. The ionization energy is also related to the bonding nature. Strong covalent bonding interactions result in ionization bands with generally higher ionization energies, while non-bonding and antibonding orbitals result in ionizations with generally lower ionization energies. The shift in an ionization energy between electronically or chemically related molecules reveals the localized or delocalized character of the electronic states. For example, in the d^8 molecules $(\eta^5\text{-}C_5H_5)Co(CO)_2$ and $(\eta^5\text{-}C_5H_5)Rh(CO)_2$, three of the four metal-based orbital ionizations have large shift magnitudes and one of them has little energy shift,[19] indicating that in this type of molecules, six metal electrons are essentially localized on the metals, while two metal electrons are extensively delocalized on the cyclopentadienyl ligand. More information from the ionization energy shift has been discussed by Bursten[20,21] and Jolly.[22-26]

2. Information From Ionization Band Shape and Resolved Fine Structure. The shapes of ionization bands are governed by the potential energy curves of the molecule in both neutral and ionic states. Figure 1.1 shows potential energy curves for a hypothetical molecule AB in its ground state and the corresponding molecular ion AB^+ in two ionic states. The sublevels in each potential well represent vibrational ones. The ionization bands resulting from the two transitions are shown schematically on the right ordinate. If ionization leads to a final ionic state with potential curve a, in which the ion has the same nuclear configuration as in the molecular ground state, the resulting spectrum will exhibit a very intense $0 \leftarrow 0$ peak followed by a relative short progression with similar vibrational spacing to that in the neutral molecule. If ionization leads to a final ionic state with potential energy curve b, in which internuclear distance is increased from its ground state value, the corresponding spectrum will display the most intensive peak near the middle of a long vibrational progression with smaller vibrational spacing. For small molecules, this vibrational progression can often be resolved, and then useful information concerning the type of electron ejected is provided with the magnitude of the vibrational spacing, i.e. nonbonding and bonding electrons are expected in cases a and b, respectively. For organotransition metal complexes, observation of resolved vibrational fine structure is less likely because of low metal-ligand vibrational frequencies (usually < 0.1 eV) or because several different vibrational progressions are excited by a single ionization. In theses cases the overlapping vibrational

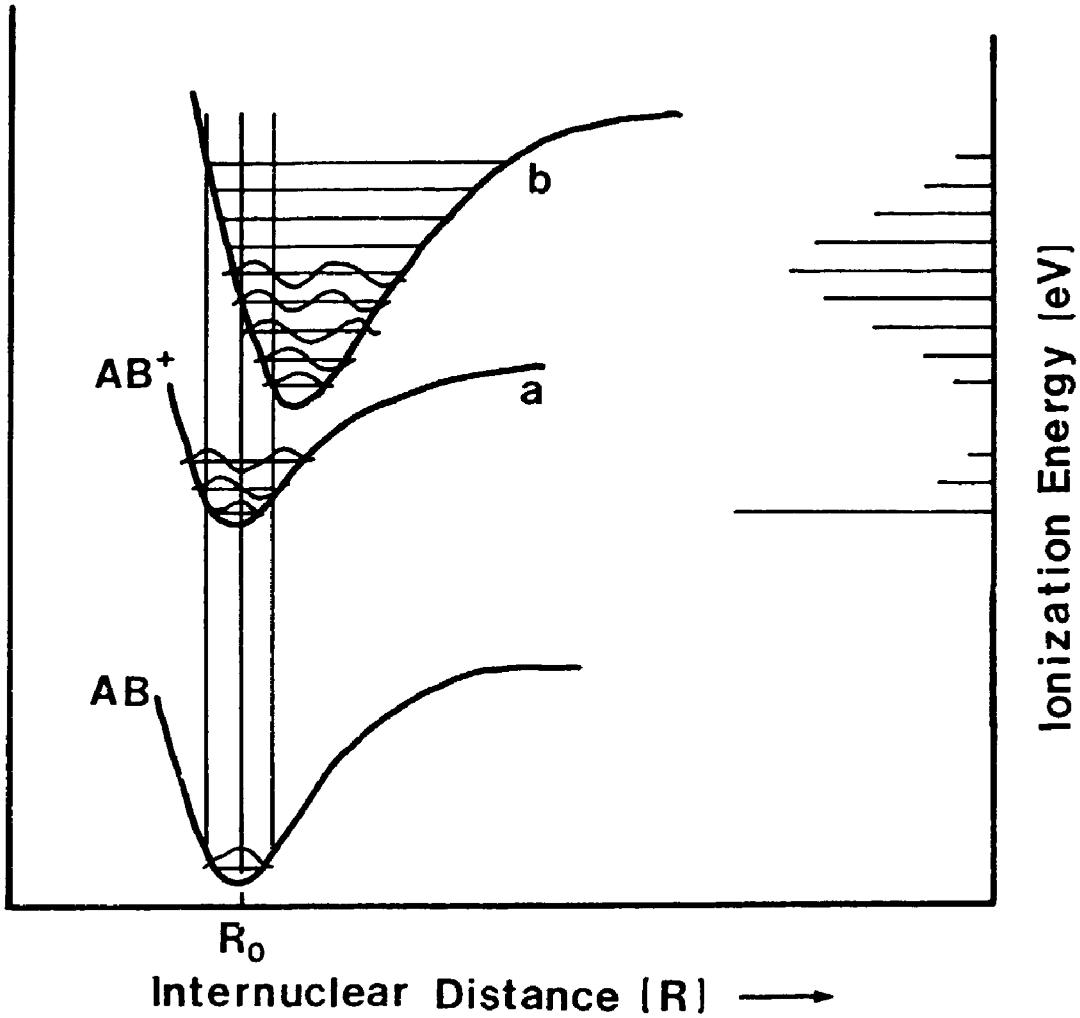

Figure 1.1. Potential energy curves for the hypothetical molecule AB in its ground state and the corresponding molecular ion AB^+ in two different ionic states. Photoelectron bands resulting from the transitions are shown schematically on the right ordinate.

components will blend into a single featureless band, but the breath of the band may be an indication of the nature of electron ejected. Generally, a broad ionization band is associated with the ionization from a strongly bonding orbital, while a narrow band is associated with the ionization from a non-bonding or weak bonding orbital.

Sometimes, it is possible to observe the resolved fine structures of the ionization bands in the spectra of organotransiton metal complexes, subject to related ionization bands being well separated. For example, if an electron is ejected from a metal-based valence d and degenerate molecular orbital, spin-orbital coupling with a relatively large coupling parameter may be observed; on the other hand, if a ligand-based vibrational excitation is accompanied by a metal-ligand orbital ionization and the vibrational spacing is greater than the width of the vibrational peak, then vibrational splitting may be resolved. The resolved fine structures of the ionization band caused by spin-orbital coupling and vibrational coupling can provide information about the degree of the electron localization on the metal and the ligands. One of the b . examples describing the information from resolved fine structure has been discussed in detail in the photoelectron spectra of tungsten hexacarbonyl $W(CO)_6$.[27,28] In this complex, the observed spin-orbital splitting between the twofold degenerate $^2E''$ and fourfold degenerate $^2U'$ bands is 0.26 eV and corresponds to a coupling constant of 0.17 eV. This is smaller than the atomic coupling constant for tungsten of 0.21 eV. The reduction in the coupling constant indicates a decrease of electron density at the metal center and a delocalization of electron density into carbonyl π^* orbitals. On the other hand, the observed vibrational separation from the $^2U'$ band is 0.26 eV (2090 cm^{-1}) and correlates with a short progression in the ν_{CO} stretch vibrational mode at 1998 cm^{-1}. The slightly higher ν_{CO} in the positive ion indicates that the C-O bond is stronger than in the ground state and that the removed electron has some CO π^* antibonding character. It was also reported that the vibrational fine structure corresponding to the W-C stretching mode could be resolved by using some spectral analysis techniques, such as Fourier Transform and spectral simulation.[29]

3. Information From Ionization Band Intensity. The most widely used information from the ionization band intensities is based on the different relative ionization band intensities obtained with the He I and He II excitation sources.[30-32] Main group (especially those of n > 2, such as S, Cl, and Br) p orbitals generally show a smaller He II:He I spectral intensity ratio than most transition metal d orbitals. This can be caused either by a reduction of the He II spectral intensities for main group p orbitals or by an enhancement of the He II spectral intensities for metal d orbitals, or by both factors.

The general physical basis for this empirical observation has been previously discussed.[33,34] In brief, the intensity of an ionization band is determined by the photoionization cross section $\sigma_{nl}(E_k)$ for ejection of an electron with kinetic energy, E_k, from the nl subshell,

$$\sigma_{nl}(E_k) = 4\pi^2\alpha a_0^2/3g(h\nu)[\int\Psi_i \, r \, \Psi_f \, d\tau]^2 \qquad (1\text{-}4)$$

where α is the fine structure constant (= 1/137), a_0 is the Bohr radius (0.529 Å), g is the number of degenerate subshells, and $h\nu$ is the input photon energy (in Rydbergs). The term in brackets which governs the intensity is the electric dipole transition moment integral for transition from the ground state (Ψ_i) to the final state (Ψ_f). Assuming no orbital relaxation, the integral involves only the wavefunction of the electron before and after ionization. Obviously, the photoionization cross section is determined by the input photon energy and the dipole moment integral. The dipole matrix element involved in the cross section expression depends on both the probability distribution and the nodal properties of the initial state and the wavelength and phase of the photoelectron in the final state. The wavelength of the photoelectron is indirectly associated with the input photon energy, as known from the relationship between its wavelength and kinetic energy, $\lambda(Å) = 12.3/(E_k(eV))^{1/2}$. This means the cross section does not simply decrease monotonically with increasing photon energy above the ionization threshold but in fact exhibits a delayed maximum which depends on the l value of the orbital from which the electron is ejected. For transition metals, the main channel for the ionization of d electron is via a free electron f wave. At low photon energies the bound d electron wave function does not have a good overlap with the continuum f electron wave because the centrifugal barrier ($l(l+1)/r^2$) in the radial Schrödinger equation limits core penetration, so the photoionization cross section is low. As the photon energy rises, the overlap increases and the cross section maximizes before falling because of the oscillatory nature of the outgoing electron wave function. For main group elements, the main channel for ionization of a p electron is via a free electron d wave. In these cases, the centrifugal barrier is smaller, and the maximum shifts to lower photon energies. Therefore, the photoionization cross sections of the ligand-based orbitals usually decrease with increasing photon energy in UV photoelectron experiments.

The He I:He II intensity differences provide an experimental indication of the metal or ligand character in the orbitals responsible for the ionizations. Larger He II:He I intensity ratios indicate ionizations from orbitals with mostly metal d character and smaller He II: He I intensity ratios indicate ionizations from orbitals with mostly ligand character. If no significant intensity differences are observed, then the ionizations are expected to be from orbitals with both metal and ligand character. However, caution must be exercised when using this general relationship to elucidate the electron localizations, because of possible resonance effects,[35,36] or changes in shapes of the atomic cross sections as a function of photon energy in different chemical and physical environments.[37-39] Furthermore, the degree of the intensity changes from He I to He II radiations are quite different among the main group p orbitals and among the transition metal d orbitals.[40] The reduction of the He II spectral intensities is undramatic for N, O, and F 2p orbitals (He II:He I ratios of 0.45, 0.67, and 0.90 respectively), but becomes dramatic for the p orbitals of heavier atoms, such S, Cl and Br (He II:He I ratios of 0.14, 0.05 and 0.06 respectively). On the other hand, the enhancement of the He II spectral intensity is generally greater for the 3d metal orbitals than for the 4d/5d orbitals. For example, the He II:He I cross section ratios are 2.10 for Ni 3d, 1.25 for Pd 4d, and 1.06 for Pt 5d orbitals. The above reasons can largely explain why increasing amounts of research have been addressed to synchrotron radiation studies of the ionization cross sections in organometallic photoelectron spectroscopy.[35,41-45]

It should be pointed out that in order to obtain the greatest possible amount of information from photoelectron spectra, the experiment must be adequately designed, since meaningful information hardly ever comes out from a single spectrum of a single molecule.

The first UPS studies of organometallic complexes appeared in 1969. These studies included d^{10} $Ni(CO)_4$ and d^8 $Fe(CO)_5$[46] and d^6 $Mn(CO)_5X$ (X=halogen, etc.).[47] Since then (especially since the middle of 1970's), research in this field has rapidly developed, including studies of a variety of organometallic monomers and clusters, as evidenced by a large number of reviews and research accounts which have appeared in the literature.[21,30,32,48-54] The various systems in turn contributed to developing techniques for spectral assignment and interpretation, based on direct ionization information and on theoretical predictions. The techniques using ionization information include criteria such as energy shifts, He I and He II intensity differences and resolved fine structure to assign metal, metal-ligand and ligand ionization.[40,32,52] Correlations of valence ionizations with core level ionizations can separate bonding effects from charge distribution effects,[22,55] and synchrotron radiation can reveal the detailed ionization cross section behaviour of the metal and ligand orbitals.[35,41-45] The techniques using theoretical calculations are used wherever the direct experimental information is not clear enough to assign and interpret the molecular orbital ionizations, and calculations are sometimes used to quantitatively describe the orbital characters and natures. Among various theoretical methods, Fenske-Hall[56-62], SCF-Xα-SW[63-75] and ab initio[76-84] methods have been mostly employed in UV photoelectron studies of organometallic molecules.

1.3 SCOPE OF THESIS

Of particular interest to this thesis is the study of the electronic structures of organoplatinum(II) and organoplatinum(IV) complexes, in terms of the molecular orbital ionization energies, the electron distribution, as well as the orbital ionization behaviour as a function of the photon energy, using photoelectron spectroscopy. The platinum(II) and (IV) complexes investigated include the square-planar cis-dimethylplatinum(II) complexes (Chapter 2), square-planar cis-bis(trifluoromethyl)platinum(II) complexes (Chapter 3), half-sandwich (η^5-cyclopentadienyl)trimethylplatinum(IV) complexes (Chapter 4), and octahedral-like (ß-diketonato)trimethylplatinum(IV) complexes (Chapter 5). These complexes represent some typical examples of the monomeric platinum(II) and (IV) compounds which are considered the most common and important in organoplatinum chemistry.[85-88] Photoionization sources used in this study are He I, He II and synchrotron radiation. The He I and He II photoelectron spectra are discussed based on the direct experimental information and SCF-Xα-SW calculations. In Chapter 6, the photoionization behaviour of the upper valence orbitals of $CpPtMe_3$ and $Me_2Pt(COD)$ is discussed in terms of the branching ratios as a function of the photon energy.

1.4 REFERENCES

1. D. W. Turner, C. Baker, A. D. Baker and C. R. Brundle, Molecular Photoelectron Spectroscopy, Wiley, London, 1970.
2. J. H. D. Eland, Photoelectron Spectroscopy, 2nd, Butterworths, London, 1984.
3. P. K. Ghosh, Introduction to Photoelectron Spectroscopy, Wiley, New York, 1983.
4. C. R. Brundle and A. D. Baker, Electron Spectroscopy: Theory, Techniques, and Applications, Academic, London, 1977, Vol.1-3.
5. K. Siegbahn, C. Nordling, G. Johansson, J. Hedman, P. F. Heden, K. Hamrin, U. Gelius, T. Bergmark, L. O. Werme, R. Manne and Y. Baer, ESCA Applied to Free Molecules, North-Holland, Amsterdam, 1969.
6. D. N. Hendrickson, Physical Methods in Chemistry, edited by R. S. Drago, Saunders, Philadelphia, 1977
7. J. W. Rabalais, Principles of Ultraviolet Photoelectron Spectroscopy, Wiley, New York, 1977.
8. R. E. Ballard, Photoelectron Spectroscopy and Molecular Orbital Theory, Adam Hilger, Bristol, 1978.
9. T. A. Carlson, Photoelectron and Auger Spectroscopy, Plenum, New York, 1975.
10. J. Berkowitz, Photoabsorption, Photoionization, and Photoelectron Spectroscopy, Academic, New York, 1979.
11. D. Briggs, Handbook of X-ray and Ultraviolet Photoelectron Spectroscopy, Heyden, London, 1977.
12. K. Kimura, S. Katsumata, Y. Achiba, T. Yamazaki and S. Iwata, Handbook of HeI Photoelectron Spectra of Functional Organic MOlecules, Japan Scientific Societies, Tokyo, 1981.
13. A. Einstein, Ann. Phys., 17, 132 (1905).

14. H. Winick and S. Doniach, Synchrotron Radiation Research, Plenum, New York, 1980.

15. J. L. Dehamer, A. C. Parr and S. H. Southworth, Handbook on Synchrotron Radiation, Vol. 2, edited by G. V. Marr, North-Holland, Amsterdam, 1986.

16. G. Margaritondo, Introduction to Synchrotron Radiation, Oxford University, New York, 1988.

17. K. Kimura, in Photodissociation and Photoionization, edited by K. P.Lawley, John Weily & Sons Ltd., London, 1985, P.161.

18. T. Koopmans, Physica (Amsterdam), 1, 104 (1931).

19. D. C. Calabro and D. L. Lichtenberger, Inorg. Chem., 19, 1732 (1980).

20. B. E. Bursten, J. Am. Chem. Soc., 104, 1299 (1982).

21. B. E. Bursten, Prog. Inorg. Chem., 36, 393 (1988).

22. W. L. Jolly, Acc. Chem. Res., 16, 370 (1983).

23. D. B. Beach and W. L. Jolly, Inorg. Chem., 25, 875 (1986).

24. W. L. Jolly, Chem. Phys. Lett., 100, 546 (1983).

25. W. L. Jolly and C. J. Eyermann, J. Phys. Chem., 86, 4834 (1982).

26. W. L. Jolly, J. Phys. Chem., 87, 26 (1983).

27. M. B. Hall, J. Am. Chem. soc., 97, 2057 (1975).

28. B. R. Higginson, D. R. Lloyd, P. Burroughs, D. M. Gibson and A. F. Orchard, J. Chem. Soc., Faraday Trans. II, 69, 1659 (1973).

29. J. L. Hubbard and D. L. Lichtenberger, J. Am. Chem. Soc., 104, 2132 (1982).

30. J. C. Green, Struct. Bonding (Berlin), 43, 37 (1981).

31. J. C. Guest, I. H. Hillier, B. R. Higginson and D. R. Lloyd, Mol. Phys., 29, 113 (1975).

32. A. H. Cowley, Prog. Inorg. Chem., 26, 45 (1979).

33. E. I. Solomon, Comments Inorg. Chem., 3, 227 (1984).

34. S. T. Manson, Adv. Electron. Electron Phys. 44, 1 (1977).

35. G. Cooper, J. C. Green, M. P. Payne, B. R. Dobsen and I. H. Hillier, J. Am. Chem. Soc., 109, 3836 (1987).

36. B. W. Yates, K. H. Tan, G. M. Bancroft, L. L. Coatsworth, J. S. Tse and G. J. Schrobilgen, 84, 3603 (1986) and references therein.

37. G. Rossi, I. Lindau, L. Braicovich and I. Abbati, Phys. Rev. B, 28, 3031 (1983).

38. K. Guertler, K. H. Tan, G. M. Bancroft and P. R. Norton, Phys. Rev. B, 35, 6024 (1987).

39. B. R. Tambe and S. T. Manson, Phys. Rev., 30, 256 (1987).

40. I. Lindau and J. J. Yeu, At. Nucl. Data. Tables, 32, 1 (1987).

41. I. Novak, J. M. Benson, A. Svensson and A. W. Potts, Chem. Phys. Lett., 135, 471 (1987).

42. J. Novak, J. M. Benson and A. W. Potts, J. Phys. B: At. Mol. Phys., 20, 3395 (1987).

43. G. Cooper, J. C. Green and M. P. payne, Mol. Phys., 63, 1031 (1988).

44. J. W. Taylor and G. A. von Wald, J. Electron. Spectrosc. Relat. Phenom. 47, 315 (1988).

45. J. G. Brennan, J. C. Green and C. M. Redfern, J. Am. Chem. Soc, 111, 2373 (1989).

46. D. R. Lloyd nd E. W. Schlag, Inorg. Chem., 8, 2544 (1969).

47. S. Evans, J. C. Green, M. L. H. Green, A. F. Orchard and D. W. Turner, Discuss. Faraday Soc., 47, 112 (1969).

48. A. F. Orchard, Electronic States of Inorganic Compounds: New Experimental Technique, edited by P. Day, P.267, Dordrecht, D. Reidel, 1975.

49. R. F. Fenske, Prog. Inorg. Chem., 21, 179 (1976).

50. C. Furlani and C. Cauletti, Struct. Bonding (Berlin), 35, 119 (1978).

51. C. Cauletti and C. Furlani, Comments Inorg. Chem., 5, 29 (1985).

52. D. L. Lichtenberger and G. E. Kellogg, Acc. Chem. Res., 20, 379 (1987).

53. D. L. Lichtenberger, G. E. Kellogg and L. S. K. Pang, Experimental Organometallic Chemistry: A Practicum in Synthesis and Characterization, ACS Symposium Series, P. 265, Vol. 357, Edited by M. J. Comstock, American Chemical Society, 1987.

54. A. Oskam, Spectroscopy of Inorganic-based Materials, Edited by R. J. H. Clark and R. E. Hester, P. 429, John Weily & Sons Ltd, 1987.

55. D. L. Lichtenberger, G. E. Kellogg and G. H. Landis, J. Chem. Phys., 83, 2759 (1985).

56. R. F. Fenske, Pure. Appl. Chem., 27, 61 (1971).

57. M. B. Hall and R. F. Fenske, Inorg. Chem., 11, 768 (1972).

58. M. T. Ashby, J. H. Enemark and D. L. Lichtenberger, Inorg. Chem., 27, 191 (1988).

59. D. L. Lichtenberger and G. E. Kellogg, J. Am. Chem. Soc., 108, 2560 (1986).

60. D. L. Lichtenberger and J. L. Hubbard, Inorg. Chem., 24, 3835 (1985).

61. D. L. Lichtenberger, D. C. Calabro and G. E. Kellogg, Organometallics, 3, 1623 (1984).

62. D. C. Calabro and D. L. Lichtenberger, J. Am. Chem. Soc., 103, 6846 (1981).

63. J. C. Slater, Int. J. Quantum Chem., 7s, 533 (1973).

64. K. H. Johnson, Advan. Quantum Chem., 7, 147 (1973).

65. S. D. Didziulis, S. L. Cohen, A. A. Gewirth and E. I. Solomon, J. Am. Chem. Soc., 110, 250 (1988).

66. F. A. Cotton, G. G. Stanley, A. H. Cowley and M. Lattman, Organometallics, 7, 835 (1988).

67. G. M. Bancroft, T. C. S. Chan and R. J. Puddephatt, Inorg. Chem., 22, 2133 (1983).

68. J. E. Bice, G. M. Bancroft and L. L. Coatsworth, Inorg. Chem., 25, 2181 (1986).

69. B. E. Bursten, F. A. Cotton and G. G. Stanley, Israel J. Chem., 19, 132 (1980).

70. B. E. Bursten, M. Casarin, S. Di Bella, A. Faug and I. Fragalà, Inorg. Chem., 24, 1241 (1985).

71. G. Guimon, G. Pfister-Guillouzo, B. Chaudret and R. Poilblanc, J. Chem. soc. Dalton Trans., 43 (1985).

72. S. Elbel, M. Grodzicki, L. Pille, G. Rünger, J. Mol. Struct., 175, 441 (1988).

73. M. H. Chisholm, A. H. Cowley and M. Lattman, J. Am. Chem. Soc., 102, 46 (1980).

74. F. A. Cotton, J. L. Hubbard, D. L. Lichenberger and I. Shim, J. Am. Chem. Soc., 104, 679 (1982).

75. G. C. Hancock, N. M. Kostic and R. F. Fenske, Organometallics, 2, 1089 (1983).

76. C. C. J. Roothaan, Rev. Mod. Phys., 23, 69 (1951).

77. G. G. Hall, Proc. Roy. Soc., Ser. A, 205, 541 (1951); ibid., 213, 102, 113 (1952).

78. S. Di Bella, M. Casarin, I. Fragalà, G. Granozzi and T. J. Marks, Inorg. Chem., 27, 3993 (1988).

79. S. Di Bella, I. Fragalà and G. Granozzi, Inorg. Chem., 25, 3997 (1986).

80. J. N. Louwen, R. Hengelmolen, D. M. Grove, D. J. stufkens and A. Oskam, J. Chem. Soc. Dalton Trans., 141 (1986).

81. G. Zangrande, G. Granozzi, M. Casarin, J. P. Daudey and D. Minniti, Inorg. Chem., 25, 2872 (1986).

82. J. N. Louwen, R. Hengelmolen, D. M. Grove, A. Oskam and R. L. Dekock, Organometallics, 3, 908 (1984).

83. D. L. Clark, J. C. Green, C. M. Redfern, G. E. Quelch, I. H. Hillier and M. F. Guest, Chem. Phys. Lett., 154, 326 (1989).

84. D. Moncrieff, I. H. Hillier, V. R. Saunders and W. von Niessen, J. Chem. Soc. Chem. Commun., 779 (1985).

85. F. R. Hartley, in Comprehensive Organometallic Chemistry, Edited by G. Wilkinson, Pergamon, Oxford, 1982, Vol. 6, Chapter 39, P. 471.

86. D. M. Roundhill, in Comprehensive Coordination Chemistry, Edited by G. Wilkinson, Pergamon, Oxford, 1987, Vol. 5, Chapter 52, P. 351.

87. R. J. Puddephatt, Coord. Chem. Rev., 33, 149 (1980).

88. V. K. Jain, G. S. Rao and L. Jain, Adv. Organomet. Chem., 27, 113 (1987).

CHAPTER 2

ELECTRONIC STRUCTURE OF CIS-DIMETHYLPLATINUM(II) COMPLEXES

2.1 INTRODUCTION

Square-planar complexes of Pt(II) play a central role in Pt chemistry, and exhibit a versatile chemistry and possibly catalytic behaviour as a consequence of these complexes being coordinatively unsaturated with only 16 electrons in their valence shell. The complexes cis-$[PtR_2L_2]$, where R = alkyl or aryl and L = a ligand such as a tertiary phosphine, arsine, amine, alkene or isocyanide, are among the simplest representatives of the square-planar complexes of Pt, and they have played an important role in studies of organometallic reaction mechanisms related to catalysts by d^8 complexes, such as those of Pt-C bond cleavage and cis to trans isomerization,[1-3] ligand substitution,[4-6] oxidative addition,[7] reductive elimination,[8-10] and platinum-catalysed hydrogenation[11-13] and cross-coupling.[14] The more volatile compounds are also useful precursors for chemical vapour deposition of platinum.[15]

Although a knowledge of valence orbital energy and bonding nature is important in understanding reactivity and mechanism, surprisingly, there has not be any detailed experimental determination of the relative energy of the valence orbitals, in particular the Pt-C σ and Pt 5d orbitals in these molecules. Some time ago, a short communication of the photoelectron study of the compounds cis-$[PtMe_2(PMe_3)_2]$ and $[PtMe_2(PMe_2Ph)_2]$ was reported.[16] Since only He I spectra and no complemental theoretical calculations were available, the assignments made were in many cases only tentative. Recently, UV photoelectron spectra of trans-$[PtX_2L_2]$, where X = Cl, Br, or I, and L = NR_3, PR_3, or AsR_3, were also published.[17-20] Because of differences in geometries of cis-[PtR_2L_2] and trans-[PtX_2L_2], and in bonding characteristics of halogen group (anionic σ and π donor) versus alkyl group (an anionic σ donor), significant changes between the electronic structure of these molecules are expected.

This chapter will presents a detailed He I and He II photoelectron spectroscopic study of complexes cis-[$PtMe_2L_2$][21] where L = PMe_3, PMe_2Ph, $PMePh_2$, PEt_3, $P(NMe_2)_3$, $PMe(OEt)_2$, $P(OEt_3)$, $AsMe_3$, CNMe and CNPh; or L_2 = $Me_2NCH_2CH_2NMe_2$ (TMED), 1,5-cyclooctadiene (COD) and norbornadiene (NBD), combined with SCF-Xα-SW calculations on the model compounds cis-[$PtMe_2(EH_3)_2$] (E = N, P, As), cis-[$PtMe_2(C_2H_4)_2$] and cis-[$PtMe_2(CNH)_2$].

2.2 UV PHOTOELECTRON SPECTRA

Four typical spectra are shown in Figure 2.1. It is convenient to discuss the region of the spectra in the energy ranges > 10.5 eV and < 10.5 eV separately, and a similar strategy will be followed in the entire thesis.

In the region > 10.5 eV the spectra contain broad envelopes, which are fitted to the minimum number of bands but which contain contributions from ionizations of many ligand-based MO's as well as the lowest energy (largest I. E.) metal-ligand σ MO's. The He II:He I intensity ratio is much lower for these higher energy ionizations than for the bands at energy < 10.5 eV, as expected for ligand based ionizations. This region at > 10.5 eV will not be discussed further, for the following two reasons. First, there are too many ionizations located in these structureless envelopes, which makes any definitely spectral assignment extremely difficult. Secondly, the ionizations in this high energy region are not important to organometallic chemistry.

In the energy region < 10.5 eV (Figures 2.2-2.6), there are often six resolved bands although, for some ligands, extra ligand bands are present (eg. the spectra of phenyl containing compounds in Figure 2.4) and, in some cases, two of the bands

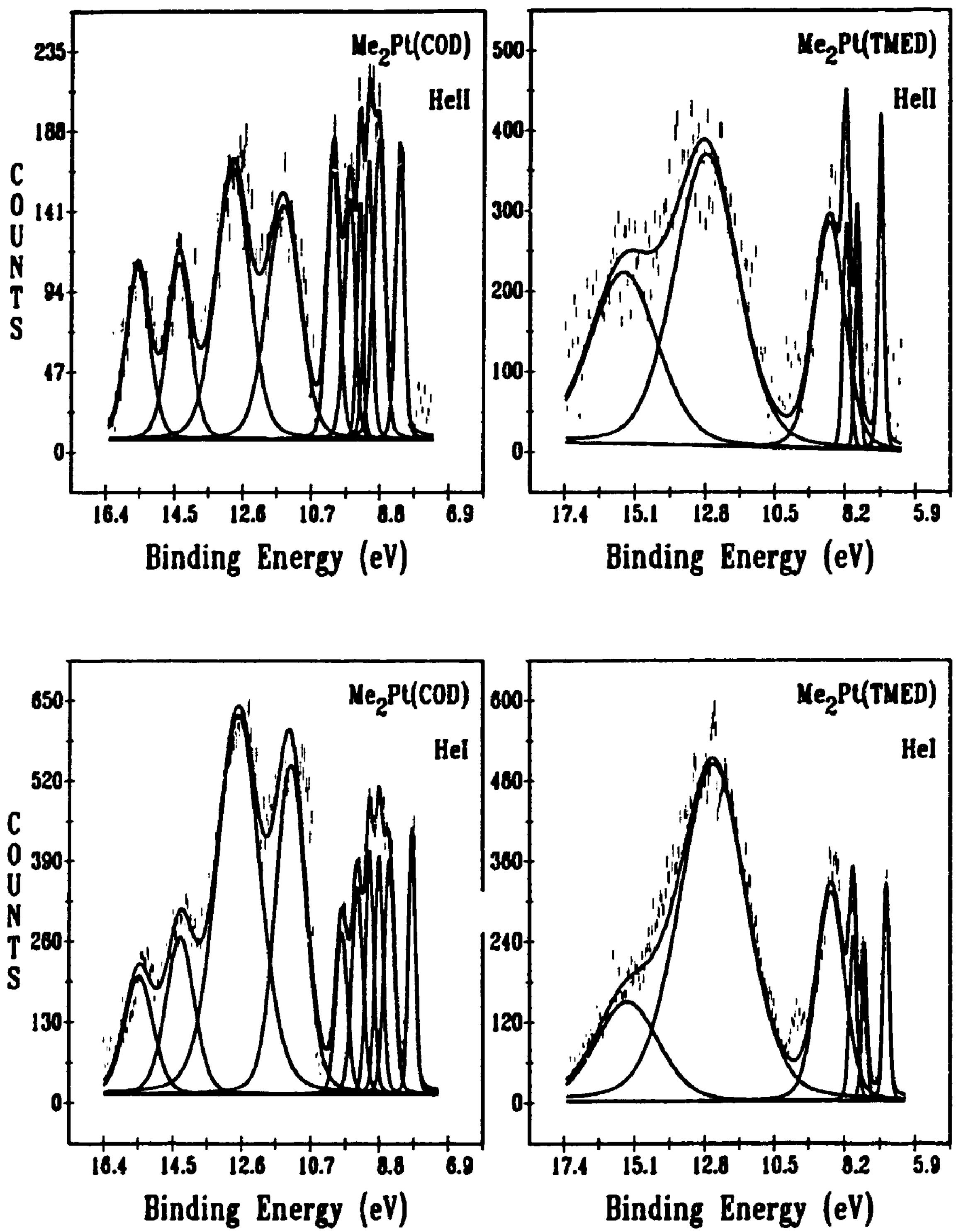

Figure 2.1. He I and He II spectra of $[PtMe_2L_2]$ (L_2 = COD and TMED).

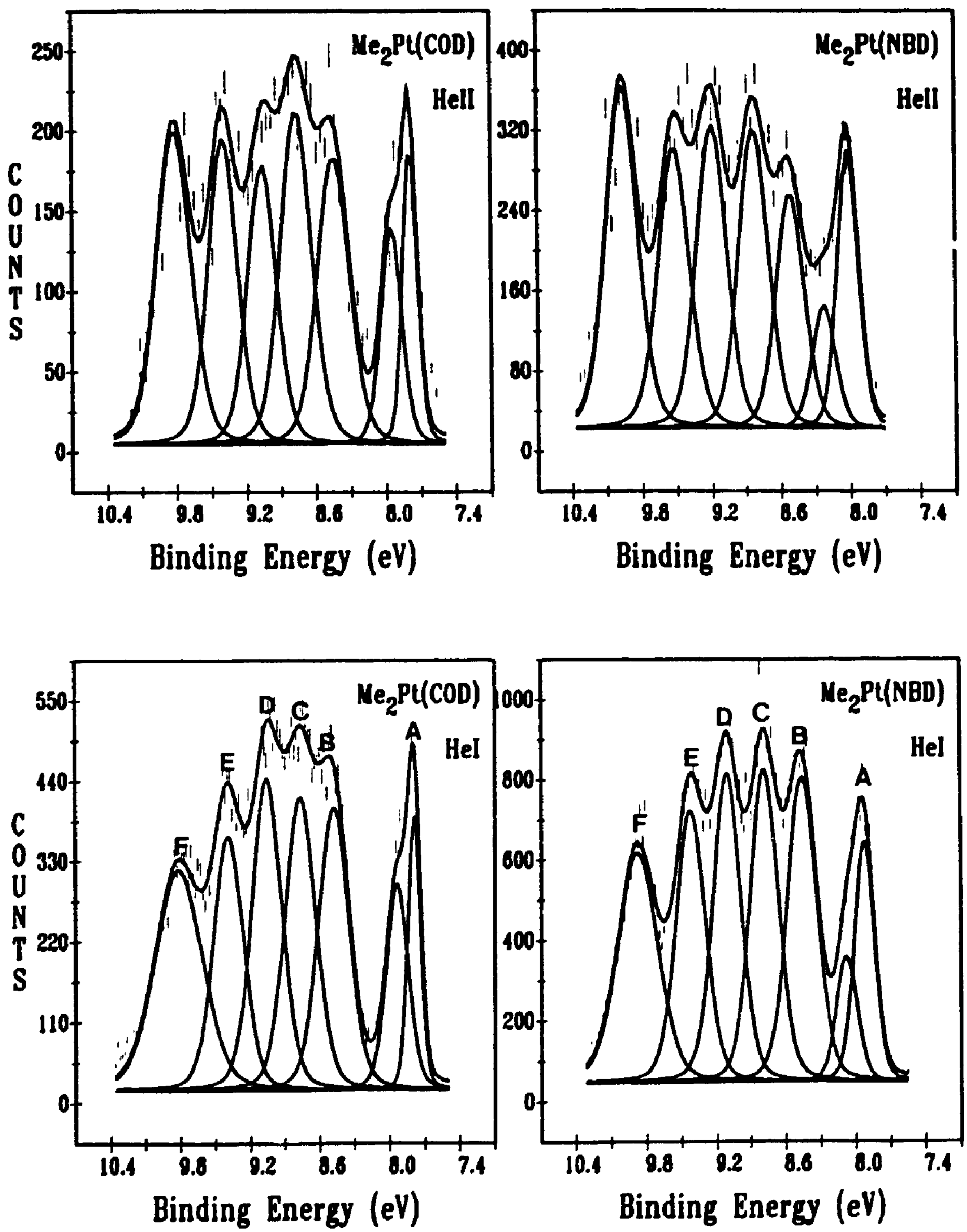

Figure 2.2. The He I and He II spectra in the low ionization energy region of $[PtMe_2L_2]$ (L_2 = COD and NBD).

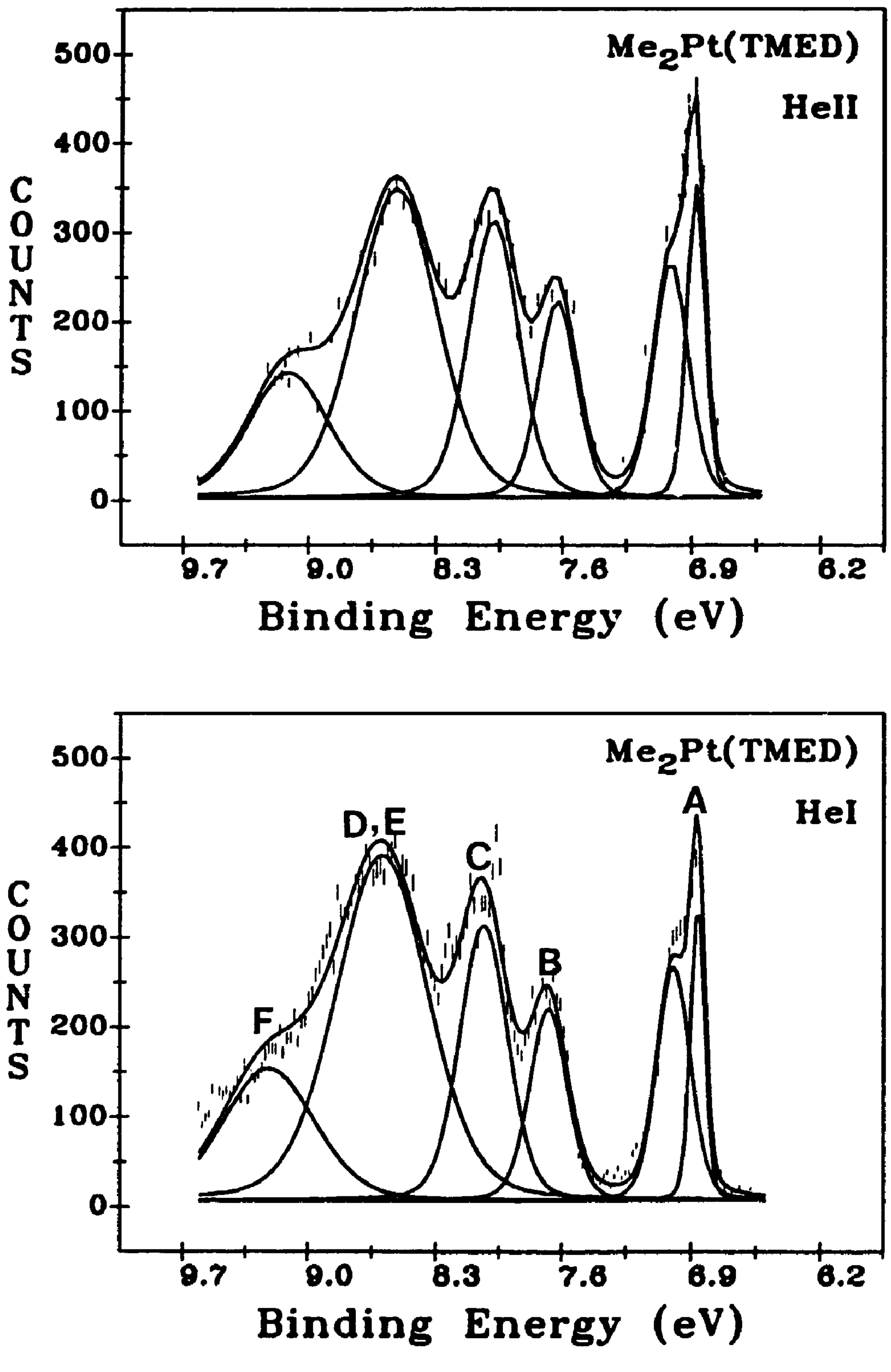

Figure 2.3. The He I and He II spectra of [PtMe$_2$(TMED).

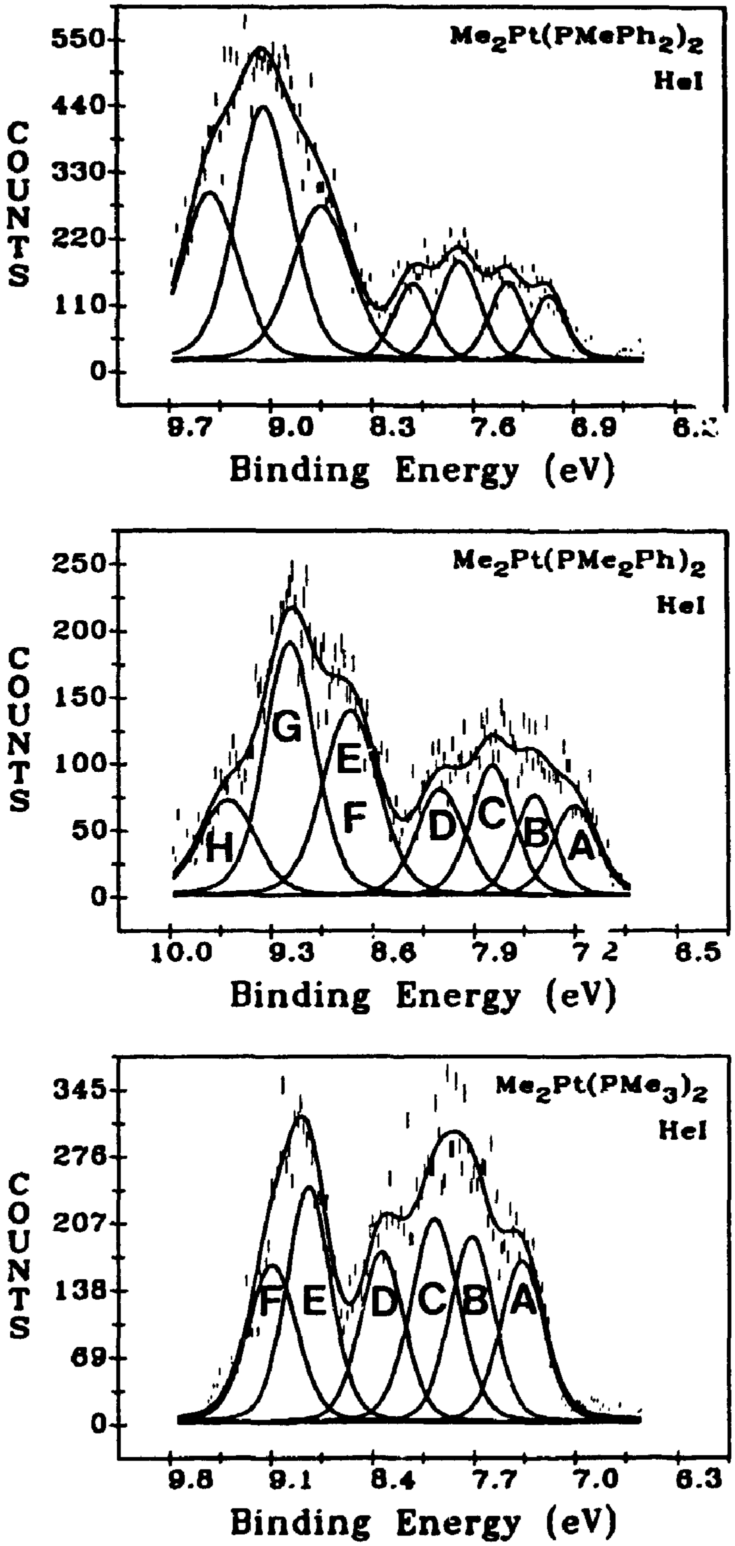

Figure 2.4. The He I spectra of cis-[$PtMe_2L_2$)] where L = PMe_3, PMe_2Ph, and $PMePh_2$.

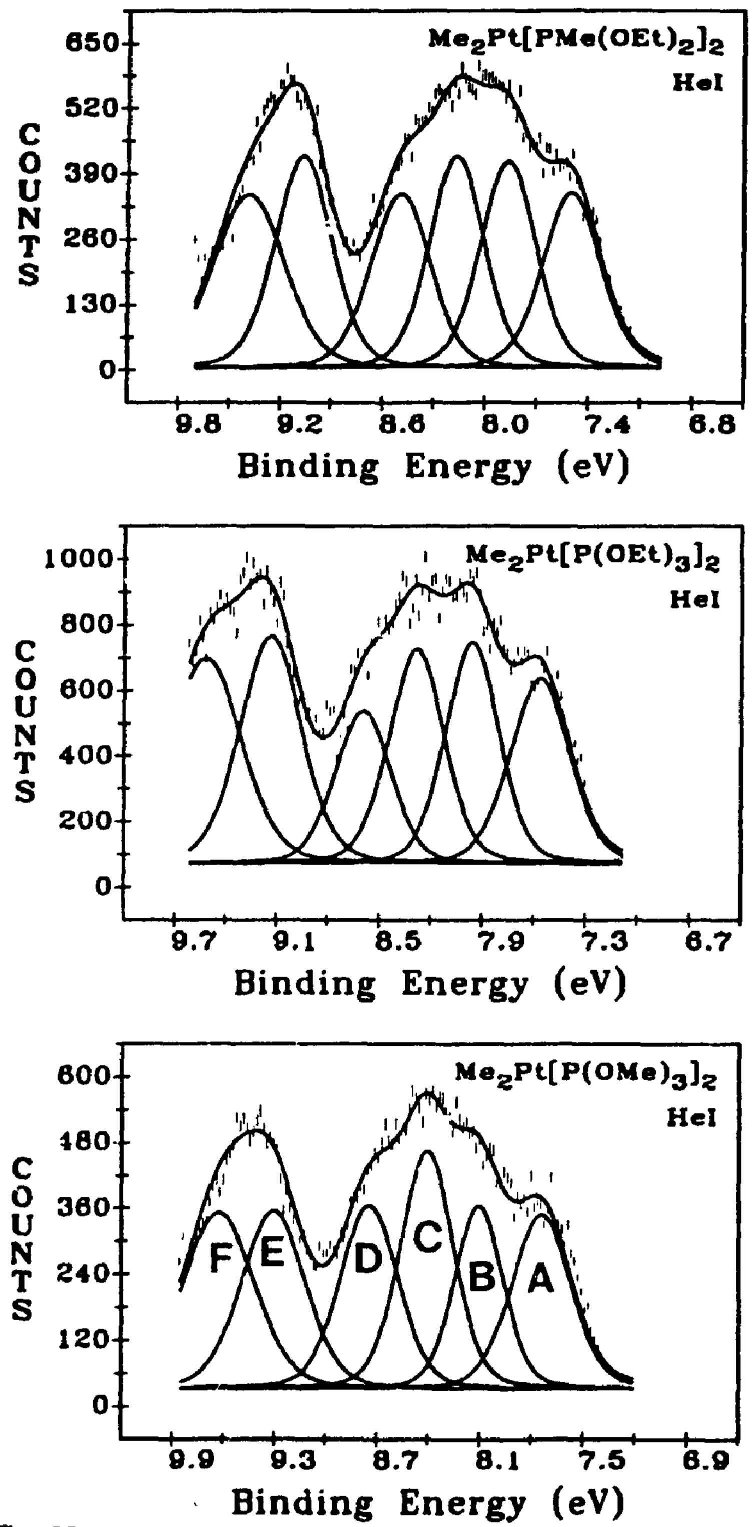

Figure 2.5. The He I spectra of cis-[$PtMe_2L_2$] where L = $P(OMe)_3$, $P(OEt)_3$, and $PMe(OEt)_2$.

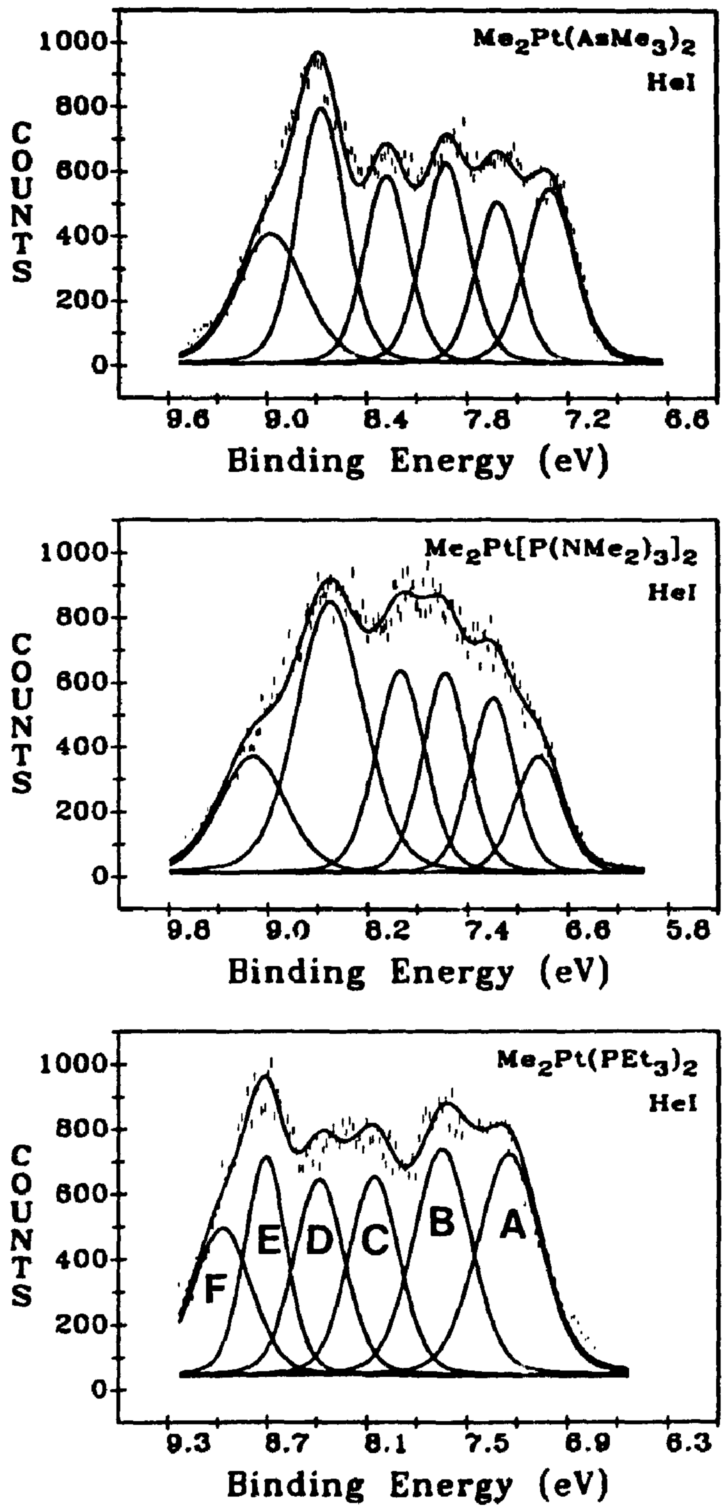

Figure 2.6. The He I spectra of cis-[$PtMe_2L_2$] where L = PEt_3, $P(NMe_2)_3$, and $AsMe_3$.

appear to be degenerate (eg. the spectra of [$PtMe_2$(TMED)] in Figure 2.3). A six-peak fit to the more poorly resolved spectra (eg. Figure 2.5) gives consistent line widths and areas and good overall fits. The ionization energy and intensity data are given in Tables 2.1-2.3. Since a platinum (II) complex should have four filled 5d orbitals, two of the six bands must be due to metal-ligand σ bond ionizations and these two ionizations are generally expected to be shifted larger in energy than the Pt 5d ionizations upon ligand replacement between the chemically or electronically related molecules. It is, however, interesting to note that the experimental observations for these complexes do not reflect the above expectation, and that the I.E.'s for all levels (Tables 2.1 and 2.2) are shifted by a similar amount from one compound to another. For example, on going from [$PtMe_2(PEt_3)_2$] to [$PtMe_2$(NBD)], peaks A, B, C, D, E, F shifted by 0.76, 0.81, 0.73, 0.78, 0.72, 0.90 eV respectively.

For transition metal complexes it is often possible to distinguish between d orbitals and σ orbitals by comparing the band intensities in the He I and He II spectra, since d orbitals frequently have a greater relative photoionization cross section for He II radiation.[22,23] However, as the data in Table 2.3 indicates, the six low I.E. bands often give very similar He II:He I band intensity ratios and so this technique is not useful for these dimethylplatinum(II) complexes.

Two methods have proved useful for band assignment. Firstly, it was observed that the lowest ionization energy band, labelled band A, was split into two peaks for the complexes cis-[$PtMe_2L_2$] with L_2 =COD, NBD and TMED (Figures 2.2 and 2.3) and the separation was 0.17 (~1400 cm^{-1}) eV for [$PtMe_2$(COD)], 0.15 eV (~1200 cm^{-1}) for [$PtMe_2$(NBD)], and 0.13 eV (~1100 cm^{-1}) for [$PtMe_2$(TMED)]. The splittings correlate well with the known C=C stretching frequencies of 1428 cm^{-1} in [$PtMe_2$(COD)] and 1174-1188 cm^{-1} in [$PtMe_2$(NBD)][24-27], and the C-N stretching frequency of ~1100 cm^{-1} in $N(CH_2R)_3$.[28] In turn, this indicates that the HOMO

Table 2.1. Ionization energies (eV) and assignments of bands for cis-[$PtMe_2L_2$]

Band	Orbital	COD	NBD	TMED	$AsMe_3$	Orbital	MeNC	PhNC
A	$4a_1$	7.76, 7.93	7.91, 8.06	6.85, 6.98	7.30	$5a_1$	7.60	
B	$2b_2$	8.47	8.45	7.67	7.60	$4a_1$	7.98	8.16
C	$3a_1$	8.76	8.77	8.03	7.91	$3b_2$	8.31	
D	$1b_1$	9.05	9.10	8.59	8.28	$2b_1$	8.70	
E	$1a_2$	9.39	9.42		8.67	$2a_2$	9.12	9.04
F	$2a_1$	9.82	9.87	9.20	8.98	$3a_1$	9.59	9.26
						Ph(π)		9.91, 10.57

Table 2.2. Ionization energies (eV) and assignments of bands for cis-[$PtMe_2(PR_3)_2$]

Band	PMe_3	PMe_2Ph	$PMePh_2$	PEt_3	$PMe(OEt)_2$	$P(OMe_3)$	$P(OEt)_3$	$P(NMe_2)_3$	Orbital
A	7.34	7.17	7.12	7.23	7.48	7.72	7.55	6.82	$4a_1$
B	7.70	7.45	7.43	7.64	7.85	8.09	7.95	7.19	$2b_2$
C	7.98	7.82	7.73	8.04	8.16	8.40	8.27	7.57	$3a_1$
D	8.38	8.18	8.02	8.32	8.49	8.74	8.59	7.93	$1b_1$
E	8.80	8.83	8.65	8.70	9.06	9.30	9.13	8.49[a]	$1a_2$
F	9.08			8.97	9.38	9.62	9.52	9.12	$2a_1$
G, H		9.14, 9.48	9.05, 9.40						Ph(π)

[a]Ligand band superimposed on this band, see text.

Table 2.3. He II:He I area ratios for cis-[$PtMe_2L_2$][a]

Compound	A	B	C	D	E	F
L_2 = COD[b]	1.00	0.82	1.05	0.90	1.05	1.01
	(1.00)	(0.64)	(1.16)	(1.19)	(1.17)	(1.13)
NBD	1.00	0.66	1.03	1.04	1.04	1.10
TMED	1.00	0.90	0.93	0.77	0.77	0.82
L[c] = PMe_3	1.00	0.81	0.87	1.08	0.83	0.89
PEt_3	1.00	0.83	0.90	0.88	0.82	1.10
$P(OMe)_3$	1.00	0.99	0.90	1.08	1.04	1.13
$P(OEt)_3$	1.00	0.84	0.96	1.14	1.18	1.10
$P(NMe_2)_3$	1.00	0.98	0.84	0.81	0.55	0.89
$AsMe_3$	1.00	1.05	1.02	1.12	1.00	0.88
CNMe	1.00	1.13	1.07	0.96	1.15	1.10

[a]The band A is used as reference in the He I and He II area calculations.

[b]The values in brackets are the He II:HeI cross section ratios from Gelius model, see text. [c]For L = PMe_2Ph, $PMePh_2$, and CNPh, reliable He II spectra could not be obtained due to the low vapour pressure of these complexes below their decomposition temperatures.

(Highest Occupied Molecular Orbitals) must have metal-ligand σ character. Secondly, Xα-SW calculations were carried out on the model compounds cis-[$PtMe_2L_2$], where L = NH_3, PH_3, AsH_3, C_2H_4 and HN≡C. These calculations, in agreement with a previous calculation for cis-[$PtMe_2(PH_3)_2$],[8] also predict that the HOMO is a metal-ligand σ orbital. Further details of the calculations and spectral assignments are given below.

2.3 Xα-SW RESULTS

2.3.1 The Complex cis-[$PtMe_2(C_2H_4)$]

In order to draw up an energy correlation diagram, the molecules cis-[$PtMe_2L_2$] (Figure 2.7, including the definition of axes) have been considered to be formed by combination of the fragments cis-[$PtMe_2$] and L_2, and calculations have been carried out separately for cis-[$PtMe_2(C_2H_4)_2$], cis-[$PtMe_2$], and L. There is a previous Xα-SW calculation by Johnson and co-workers on cis-[$PtMe_2(PH_3)_2$] in which the alternative approach was used, considering the molecule to be formed from cis-[$Pt(PH_3)_2$] and two methyl radicals; the results of the two calculations for this molecule are in good agreement.[8] In the correlation diagram of Figure 2.8 for cis-[$PtMe_2(C_2H_4)_2$], only the interactions between the outer orbitals of the fragment Me_2Pt and the ligands C_2H_4 are considered for the sake of simplicity.

Consider first the fragment cis-[$PtMe_2$]. There are two σ bonding MO's, the orbitals $1b_2$ and $1a_1$, in Figure 2.8 and in Table 2.4. Orbital $1b_2$ is formed mostly by overlap of $5d_{yz}$ on platinum with the antisymmetric combination of the two Me σ orbitals, while the orbital $1a_1$ is formed by overlap of 6s and $5d_{x^2-y^2}$ on platinum with the symmetric combination of the two Me σ orbitals. There are two virtual orbitals also, labelled $2b_2$ and $4a_1$. The orbital $2b_2$ is formed by the symmetric combination of the two CH_3 σ orbitals bonding to $6p_y$ but antibonding to $5d_{yz}$ on platinum. The net result is weakly antibonding because of its higher $5d_{yz}$ character. The orbital $4a_1$ is

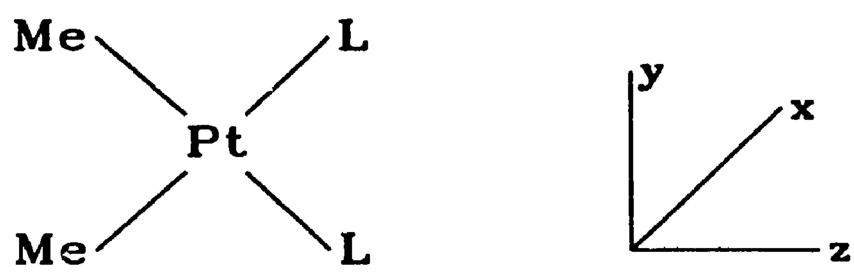

L=PMe_3, PMe_2Ph, $PMePh_2$, PEt_3, $P(NMe_2)_3$,
$PMe(OEt)_2$, $P(OEt)_3$, $P(OMe)_3$, $AsMe_3$
CNMe and CNPh

or

L_2=$Me_2NCH_2CH_2NMe_2$(TMED),
1,5−cyclooctadiene(COD) and norbornadiene(NBD)

Figure 2.7. Structure of the molecules with the axis system used in the discussion.

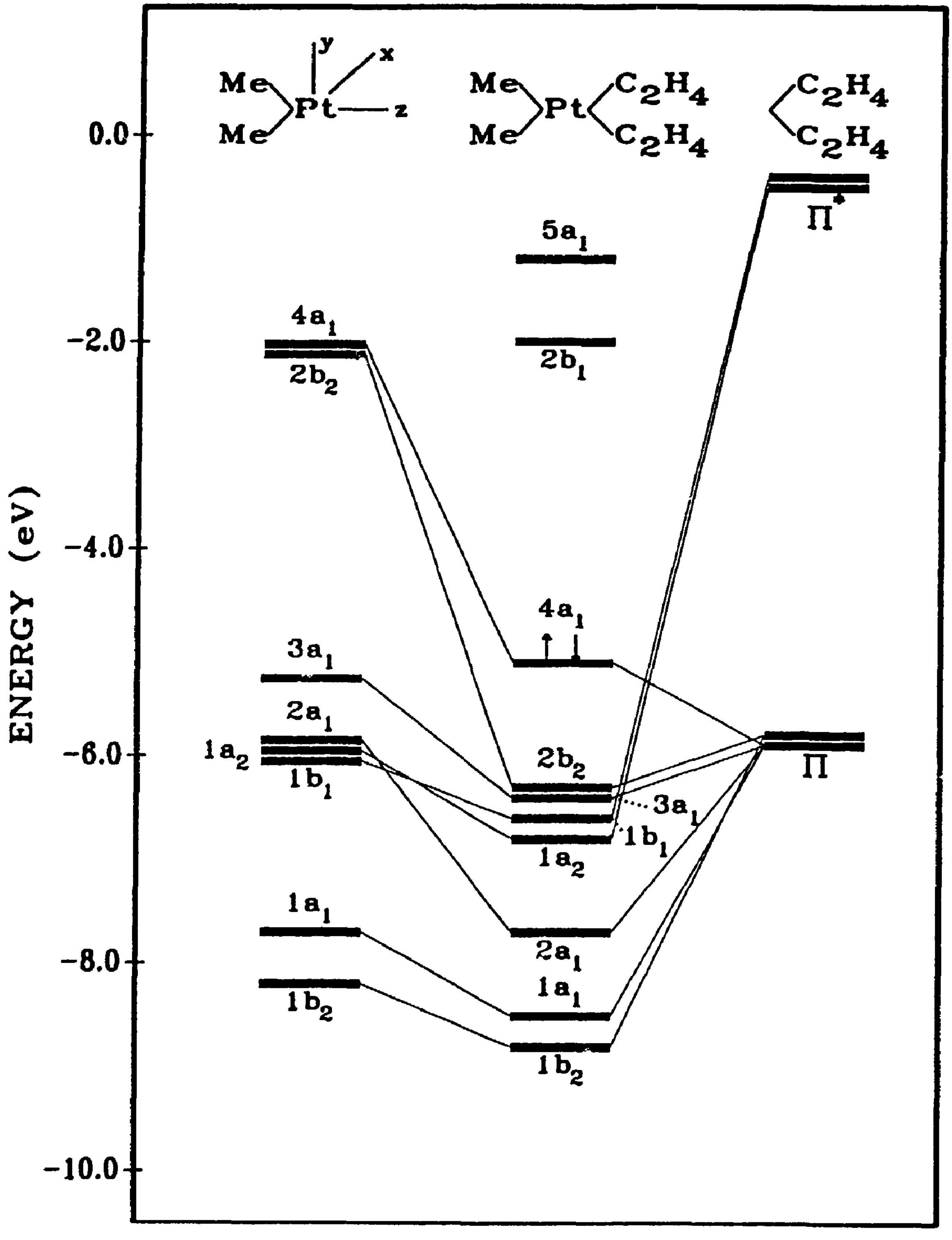

Figure 2.8. An orbital interaction diagram for cis-[$PtMe_2(C_2H_4)_2$].

Table 2.4. Xα-SW results for cis-$[PtMe_2]$ (C_{2v}) upper valence orbitals

Orbital[a]	Orbital Energy (eV)	Charge Distribution (%)[b]				
		Pt	C	H	Inter	Outer
$4a_1$	2.06	4s, $9p_z$, $5d_{z^2}$	9		41	32
$2b_2$	2.09	$11p_y$, $21d_{yz}$	23	2	32	10
$3a_1$	5.26	15s, $1p_z$, $40d_{x^2-y^2}$	11	1	29	3
$2a_1$	5.90	$85d_{z^2}$	1	3	10	1
$1a_2$	5.94	$87d_{xy}$	1	2	9	1
$1b_1$	5.98	$86d_{xz}$	1	2	10	1
$1a_1$	7.71	6s, $2p_z$, $44d_{x^2-y^2}$	30	4	12	2
$1b_2$	8.20	$1p_y$, $58d_{yz}$	27	5	7	2

[a] $3a_1$ is HOMO. [b] The contributions of carbon are essentially 2p character. For the Pt contributions, the % contribution followed by the orbital is given. For a_1 symmetry, the particular d orbital is not given by the calculation directly, and the assignment of an a_1 orbital to mostly d_{z^2} or $d_{x^2-y^2}$ is based on the orbital contour diagrams. These assignments are therefor not certain. The explanation is followed in the other tables.

very diffuse because of small atomic contributions from both the platinum atom and methyl groups (Table 2.4). Between this $PtMe_2$ σ and virtual levels, there are four orbitals having mostly platinum 5d character, as expected for a platinum(II) d^8 complex. These are identified as $3a_1$ ($5d_{x^2-y^2}$, HOMO), $2a_1$ (d_{z^2}), $1a_2$ (d_{xy}) and $1b_1$ (d_{xz}), using the axes defined in Figure 2.7. The orbital $3a_1$, the counterpart of the orbital $1a_1$, is at highest energy because of its partial σ^* character.

Now the orbitals of interest for the two cis-C_2H_4 ligands are the π orbitals (a_1 + b_2 symmetry) and the π^* orbitals (a_2 + b_1 symmetry) arising from the C=C bonds. The energies of these MO's, as calculated by the Xα-SW method, are shown in Figure 2.8. It is clear from the resulting correlation diagram that there is strong mixing of the π levels of C_2H_4 with the σ ($1a_1$ + $1b_2$) and virtual ($4a_1$ + $2b_2$) orbitals of the Me_2Pt fragment and also with the platinum d orbitals ($2a_1$ + $3a_1$) of a_1 symmetry. The $2a_1$ orbital is particularly stabilized by this interaction (Figure 2.8). It is possible to identify the σ orbitals and d orbitals in Figure 2.8 from their origins but these characters are strongly mixed in some of the MO's. The calculated orbital characters for this complex are given in Table 2.5.

There are two strongly bonding σ MO's labelled $1a_1$ and $1b_2$ and two weakly bonding σ MO's labelled $2b_2$ and $4a_1$. Contour diagrams for these orbitals are given in Figure 2.9.[29] The HOMO is $4a_1$ which is fairly evenly distributed between platinum, methyl and ethylene character (Table 2.5) but retains the Pt-Me character of the $PtMe_2$ fragment along with Pt-C_2H_4 σ character, as indicated by the contour diagram of Figure 2.9. The orbital $2b_2$ is calculated to have very largely the character of the C=C π orbital from which it is derived (Table 2.5 and Figures 2.8, 2.9).

Now considering the platinum 5d orbitals of the Me_2Pt fragment, it has been seen that the $3a_1$ and, especially, the $2a_1$ orbital are strongly stabilized by taking on C_2H_4 π character in forming the complex cis-$[PtMe_2(C_2H_4)_2]$. The orbital $1a_2$ and $1b_1$ are also

Table 2.5. Xα-SW results for cis-[$PtMe_2(C_2H_4)_2$] (C_{2v}) upper valence orbitals

Orbital	Energy(eV)[a]		Pt	Charge Distribution (%) C_{Me}	$C_{C=C}$	H_{Me}	$H_{C=C}$	Inter	Outer
$4a_1$	5.09	7.57	3s, $6p_z$, $24d_{z^2}$	16	24	1	1	23	2
$2b_2$	6.34	8.73	$8p_y$, $1d_{yz}$	10	47	2		31	1
$3a_1$	6.38	8.93	11s, $48d_{x^2-y^2}$	7	8	2	1	22	1
$1b_1$	6.56	9.22	$78d_{xz}$	2	5	3	4	8	
$1a_2$	6.78	9.41	$66d_{xy}$	2	11	3	9	8	
$2a_1$	7.73	10.30	1s, $55d_{z^2}$	4	18	4		18	
$1a_1$	8.49	11.06	4s, $45d_{x^2-y^2}$	21	11	4	1	12	1
$1b_2$	8.78	11.36	$49d_{yz}$	21	13	4	4	8	1

[a]The second column is the molecular orbital energy of the ground state, and the third column is the transition state energy, calculated by removal of a half of electron from the HOMO ($4a_1$).

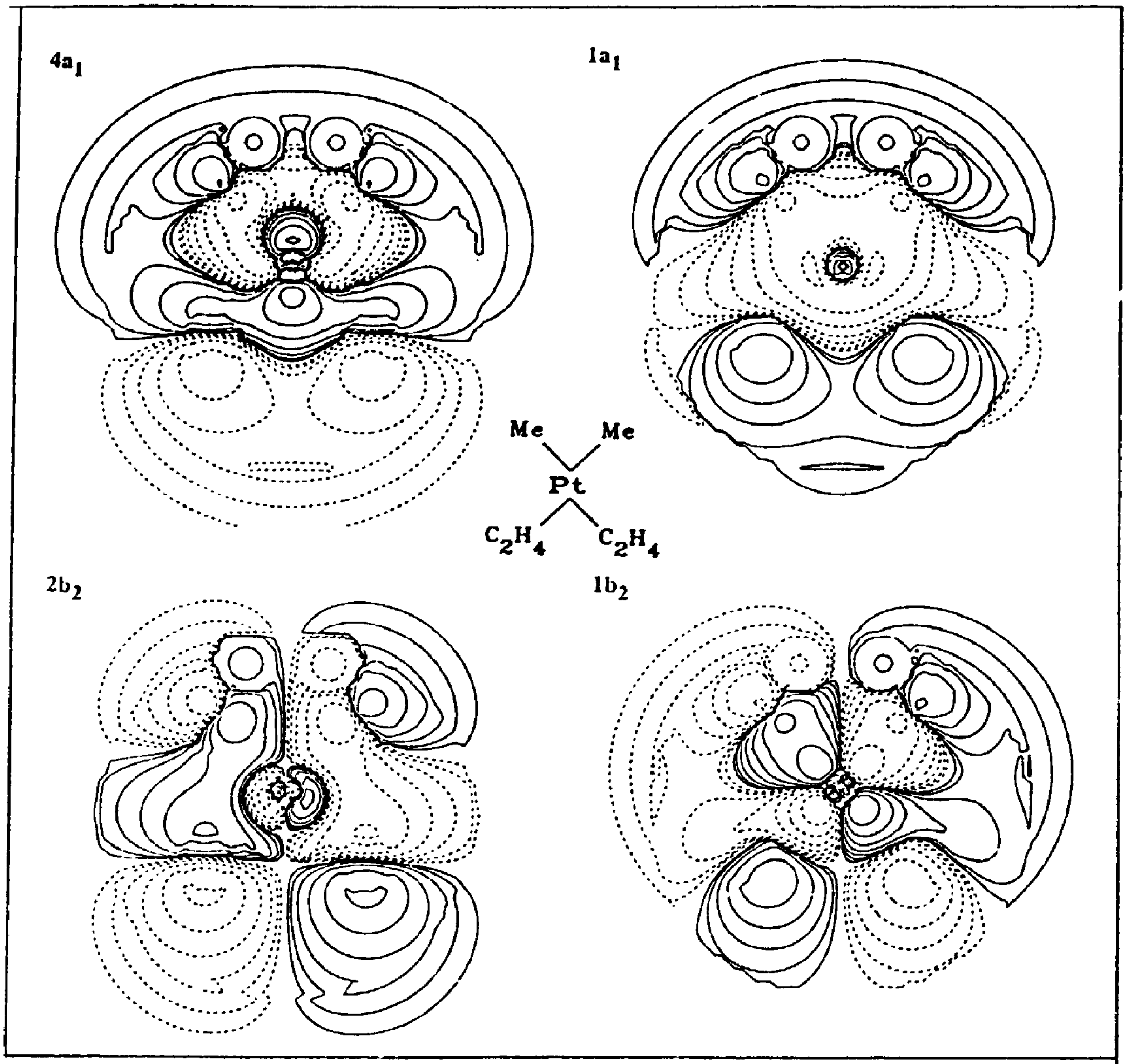

Figure 2.9. Contour diagrams of orbitals $4a_1$, $2b_2$, $1a_1$, and $1b_2$. The contours are plotted on the yz plane and at values of ±0.002, ±0.0047, ±0.0094, ±0.0188, ±0.0375, and ±0.150 e bohr^{-3}, starting from the outermost.

stabilized by interacting with the C_2H_4 π^* orbitals of appropriate symmetry. This is the backbonding expected in this type of complex, but it is relatively weak since the C_2H_4 π^* levels is at high energy.

To summarize, the calculation for cis-[$PtMe_2(C_2H_4)_2$] predicts that the upper eight occupied MO's will contain four orbitals of mostly platinum 5d character sandwiched between two strongly bonding σ MO's and two weakly bonding σ MO's.

2.3.2 The Complexes cis-[$PtMe_2(EH_3)_2$], E = N, P, or As

The results for these complexes are similar to those for cis-[$PtMe_2(C_2H_4)$] (Tables 2.6, 2.7 and 2.8) and so are treated more briefly. The calculations on the free ligands EH_3 indicate that the lone pair orbitals of symmetry a_1 + b_2 have mostly p character with s contribution of 7% in NH_3, 19% in PH_3 and 20% in AsH_3. No virtual orbital was found for NH_3 in an energy search up to -0.007 eV and the virtual orbitals for PH_3 (-0.38 eV) and AsH_3 (-0.54 eV) are contributed largely from outersphere regions and thus are not shown in the correlation diagram (Figure 2.10).

Compared to cis-[$PtMe_2(C_2H_4)_2$], the σ orbitals of EH_3 interact more strongly with the $1b_2$ and $1a_1$ levels and less strongly with the $4a_1$ and $2b_2$ levels of the cis-[$PtMe_2$] fragment. This leads to a larger calculated energy gap between $1b_2$ and $2b_2$ or $1a_1$ and $4a_1$ for the EH_3 complexes. In addition, the orbitals $3a_1$, $2a_1$, $1a_2$ and $1b_1$ of the Me_2Pt fragment, which were identified earlier as having mostly platinum 5d character, are much less strongly perturbed by the additional bonding to EH_3 groups compared to C_2H_4. This is easily seen by comparison of the correlation diagram in Figure 2.8 and 2.10. Both σ- and π-interactions with the EH_3 groups are calculated to be lower than with C_2H_4 in all cases, but both σ- and π-bonding involving these d orbitals on platinum follow the series EH_3 = AsH_3 > PH_3 > NH_3. In all cases, however, the orbitals identified as having mostly Pt 5d character are sandwiched between two strongly bonding σ MO's and two nonbonding or weakly bonding σ

Table 2.6. $X\alpha$-SW results for cis-$[PtMe_2(NH_3)_2]$ (C_{2v}) upper valence orbitals

Orbital	Energy(eV)[a]		Charge Distribution (%) Pt	C	N	H_C	H_N	Inter	Outer
$4a_1$	5.01	7.74	13s, $4p_z$, $19d_{z^2}$	26	2	3		29	3
$2b_2$	5.57	8.25	$9p_y$, $13d_{yz}$, $2f^b$	28	24	3	2	15	4
$3a_1$	5.77	8.67	$85d_{x^2-y^2}$	1	2	1	1	9	1
$1b_1$	5.90	8.83	$87d_{xz}$	1		2	1	8	
$1a_2$	5.94	8.87	$87d_{xy}$	2	1	2	1	8	
$2a_1$	6.04	8.81	$5p_z$, $44d_{z^2}$	14	16	2	1	15	2
$1a_1$	8.92	11.59	8s, $26d_{x^2-y^2}$	5	40	1	4	14	2
$1b_2$	9.41	12.15	$44d_{yz}$	8	30	4	3	10	1

[a]See the footnote of Table 2.5. [b]$f_{yz^2, y(x^2-y^2)}$.

Table 2.7. Xα-SW results for cis-[$PtMe_2(PH_3)_2$] (C_{2v}) upper valence orbitals

Orbital	Energy(eV)[a]			Charge Distribution (%)						
				Pt	C	P	H_C	H_p	Inter	Outer
$4a_1$	4.60	4.70	7.24	6s, $10p_z$, $10d_{z^2}$	34	8	3	2	22	5
$2b_2$	5.13	5.27	7.76	$11p_y$, $3d_{yz}$, $2f^b$	24	22	2	3	33	
$3a_1$	5.39	5.37	7.91	9s, $46d_{x^2-y^2}$	1	17		3	22	2
$1b_1$	6.02	5.96	8.52	$86d_{xz}$	1	1	2	2	8	
$1a_2$	6.09	5.94	8.60	$85d_{xy}$	1	2	2	2	8	
$2a_1$	6.16	6.05	8.69	$77d_{z^2}$	4	5	3	3	7	1
$1a_1$	8.28	8.40	10.94	9s, $39d_{x^2-y^2}$	8	27	1	6	7	3
$1b_2$	8.95	9.01	11.64	$52d_{yz}$	10	23	4	5	6	

[a]The second and third columns are the molecular orbital energies of the ground state without and with relativistic effect of the platinum atom, respectively. The fourth column is the transition state energy. [b]f_{yz^2}, $f_{y(3x^2-y^2)}$.

Table 2.8. Xα-SW results for cis-[$PtMe_2(AsH_3)_2$] (C_{2v}) upper valence orbitals

Orbital	Energy(eV)[a]		Charge Distribution (%)						
			Pt	C	As	H_C	H_{As}	Inter	Outer
$4a_1$	4.91	7.33	3s, $9p_z$, $16d_{z^2}$	29	12	3	3	21	4
$2b_2$	5.66	7.98	$11p_y$, $3d_{yz}$, $1f$[b]	23	30	3	6	17	6
$3a_1$	5.80	8.75	12s, $49d_{x^2-y^2}$		10		2	25	2
$1b_1$	6.36	8.92	$84d_{xz}$	1	1	3	2	9	
$1a_2$	6.39	8.95	$83d_{xy}$	1	2	3	2	9	
$2a_1$	6.68	9.21	$69d_{z^2}$	7	7	4	2	9	2
$1a_1$	8.54	11.00	9s, $36d_{x^2-y^2}$	11	22	2	6	11	3
$1b_2$	8.99	11.49	$56d_{yz}$	11	18	2	5	6	2

[a]See the footnote of Table 2.5. [b]f_{yz^2}, $y(x^2-y^2)$.

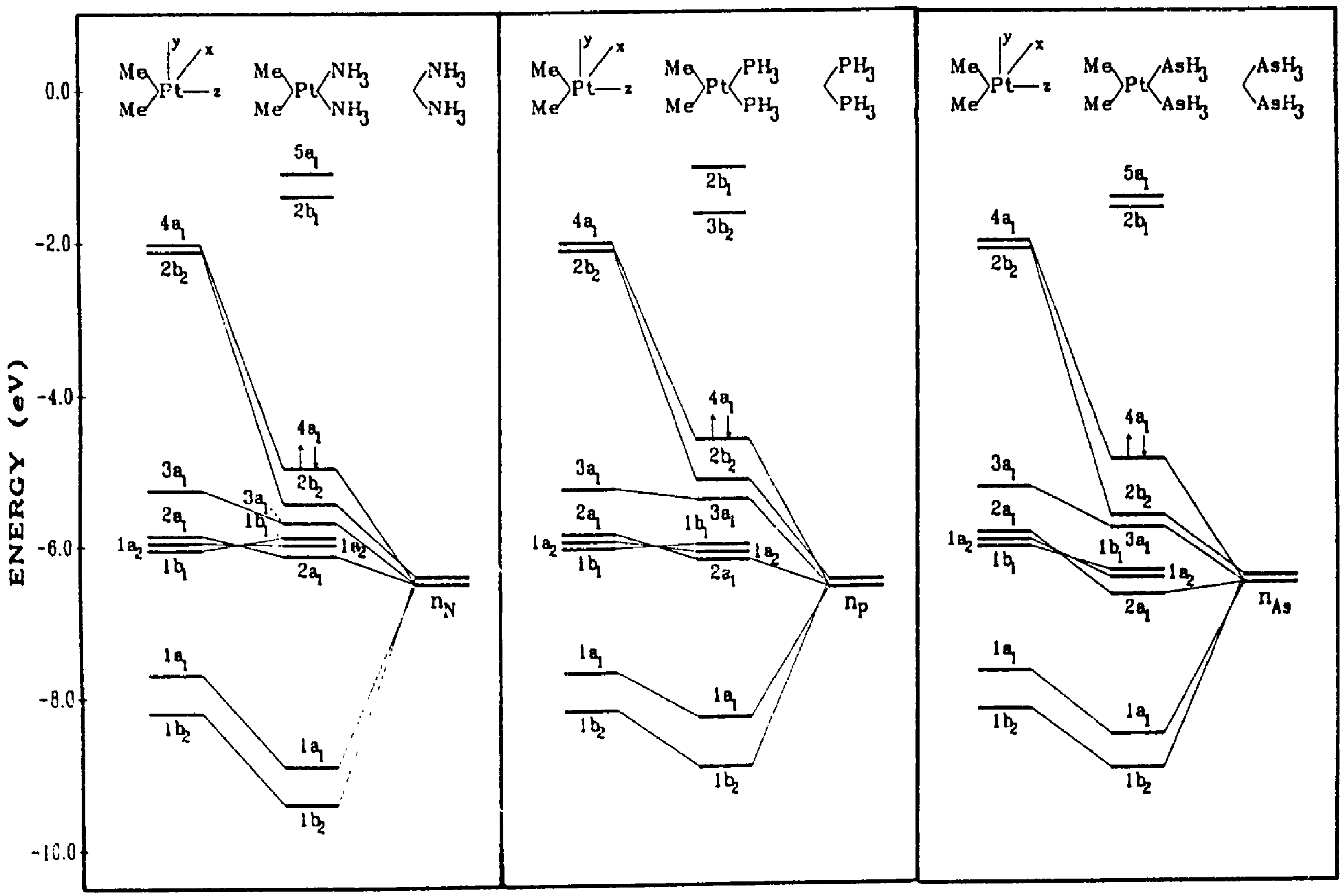

Figure 2.10. An orbital interaction diagram for cis-$[PtMe_2(EH_3)_2]$ where E = N, P, and As.

MO's, similar to the case of cis-[$PtMe_2(C_2H_4)_2$].

Finally, it should be pointed out that the relativistic and non-relativistic orbital energies are very similar indeed (Table 2.7). Thus, as has been shown for other square planar platinum(II) complexes,[17-20,31-33] relativistic corrections are very small.

2.3.3 The Complexes cis-[$PtMe_2(C\equiv NH)_2$]

The results for this complex are given in Table 2.9 and Figure 2.11. This is the most complex example studied, since the HN≡C ligands have both π_x and π_y filled orbitals and π_x^* and π_y^* empty orbitals of energy suitable for bonding, as well as the σ lone pair orbitals.

The σ lone pair orbitals of HNC are sp hybrid MO's and are of low energy, so that they interact very strongly with the $1a_1$ and $1b_2$ orbitals of the Me_2Pt fragment and only weakly with the $4a_1$ and $2b_2$ orbitals. The HNC ligands appear to act mostly as π acceptor (rather than π donor) ligands, but the π_x orbitals are stabilized to some extent on coordination of HNC and this suggests that the isocyanide can also act as a weak π donor.

Finally, we note that the σ orbital $3b_2$ in cis-[$PtMe_2(HNC)_2$], which correlates with the $2b_2$ orbital of the cis-[$PtMe_2$] fragment, is calculated to be almost degenerate with three of the platinum d orbitals. In the other complexes studied, the corresponding orbital was always calculated to lie higher in energy than the 5d orbitals.

2.4 SPECTRAL ASSIGNMENT AND INTERPRETATION

2.4.1 The Complexes [$PtMe_2(COD)$] and [$PtMe_2(NBD)$]

The low I.E. regions of the spectra for these compounds are similar and contain six well resolved bands, as shown in Figure 2.2. Five of these bands (B-F in Figure 2.2) could be fitted to single Lorentzian-Gaussian band shapes. However band A was clearly split into two peaks with separations of 0.17 eV (~1400 cm^{-1}) for [$PtMe_2(COD)$] and 0.15 eV (~1200 cm^{-1}) for [$PtMe_2(NBD)$]. The area of band A is

Table 2.9. Xα-SW results for cis-[$PtMe_2(CNH)_2$] (C_{2v}) upper valence orbitals

Orbital	Energy(eV)[a]		Charge Distribution (%)[b]						
			Pt	C_{Me}	C_{CN}	N_{CN}	H_{Me}	Inter	Outer
$5a_1$	5.81	8.27	15s, $6p_z$, $18d_{z^2}$	28	1	2	3	26	1
$4a_1$	6.83	9.35	2s, $64d_{x^2-y^2}$	1	1	16	1	15	
$3b_2$	6.90	9.41	$12p_y$, $16d_{yz}$, $4f^c$	36	9	2	5	16	
$2b_1$	7.03	9.58	$69d_{xz}$	2		15	3	11	
$2a_2$	7.04	9.51	$70d_{xy}$	2		14	3	11	
$3a_1$	7.41	9.96	$6p_z$, $51d_{z^2}$	18	5	4	3	12	1
$2b_2$	9.24	11.51		3	23	46	3	25	
$1a_2$	9.73	12.05	$9d_{xy}$	5	24	34	5	23	
$1b_1$	9.93	12.24	$12d_{xz}$	2	25	33	2	26	
$2a_1$	10.17	12.51	$15d_{x^2-y^2}$	4	25	28	5	23	
$1a_1$	14.50	17.04	13s, $7p_z$, $18d_{z^2}$	2	52	3	2		
$1b_2$	15.13	17.72	$6p_y$, $38d_{yz}$, $2f^c$	3	47	2	2		

[a]See the footnote of Table 2.5.

[b]The % of H_{CN} is always less than 1%, and therefore it is not listed in the Table.

[c]f_{z^3} [illegible]

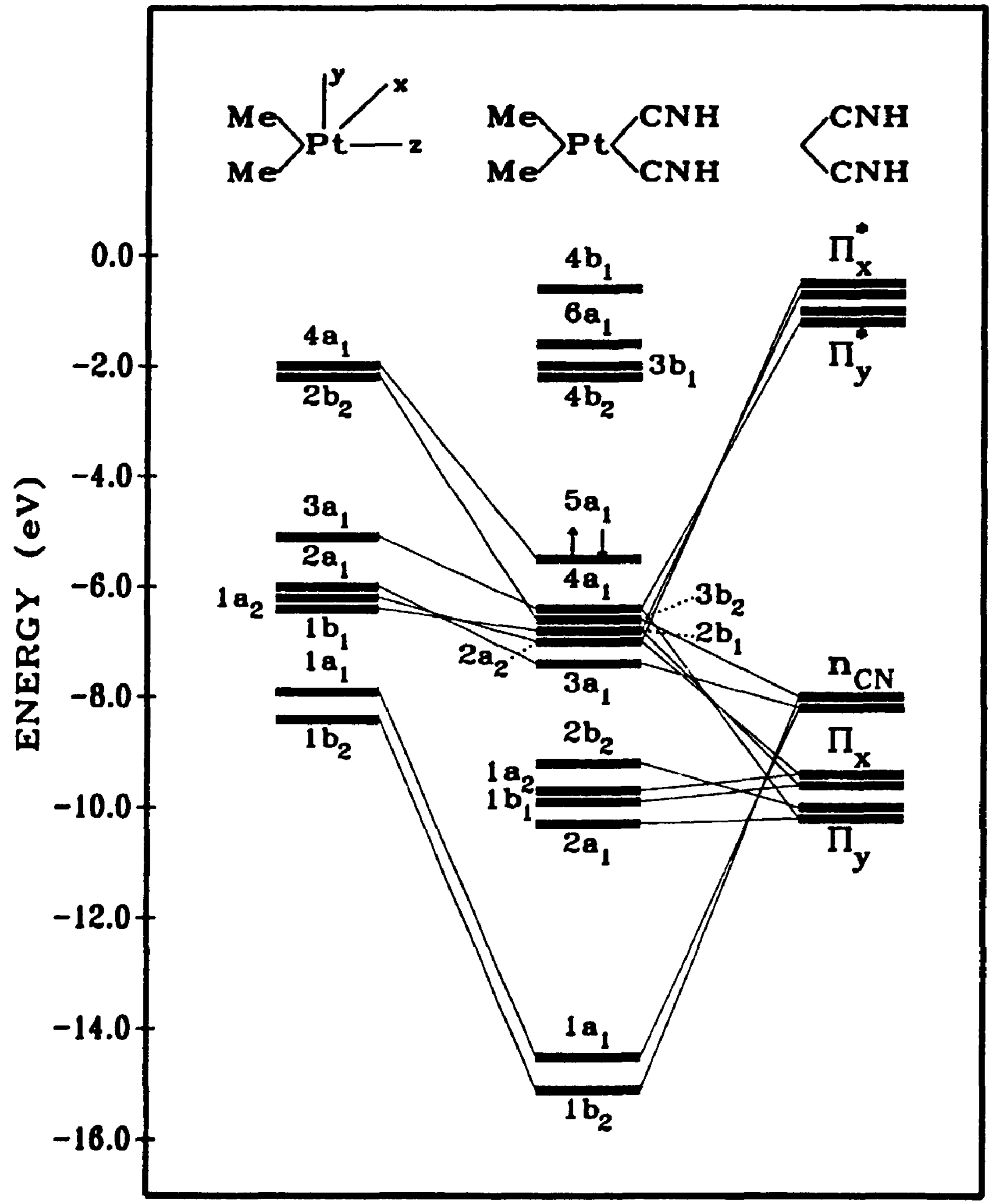

Figure 2.11. An orbital interaction diagram for cis-[$PtMe_2(CNH)_2$].

approximately equal to the areas of each of the other five bands B-F, suggesting that the splitting is not due to overlap of peaks arising from two almost degenerate MO's.[34] More importantly, the splittings correlate well with the known C=C stretching frequencies of 1428 cm^{-1} in [$PtMe_2$(COD)]and 1174-1188 cm^{-1} in [PtIMe(NBD)],[24-27] and the Xα-SW calculated transition state energies predict that the $4a_1$ and $2b_2$ orbitals should be well separated (Table 2.5). Therefore, the splitting is assigned to vibrational coupling and indicates that the HOMO has substantial platinum-alkene bonding character, as predicted by the Xα-SW calculation on the model compound cis-[$PtMe_2(C_2H_4)_2$]. Although resolution of ligand vibrational splitting is not very common, CO vibrational structure has also been seen on the bands due to metal-carbon σ MO's ionizations in [$W(CO)_6$].[35,36]

Band B is assigned to a second metal-ligand σ MO based on the Xα-SW calculation for cis-[$PtMe_2(C_2H_4)_2$], which predicts that the orbital has largely alkene π character. Vibrational splitting of the band would be expected but was not resolved, probably because of strong overlap with band C (Figure 2.2).

It is natural to assign the next four bands (C-F) to ionizations from orbitals with mostly Pt 5d character. There is no experimental evidence to aid assignment of each band to a specific d orbital and so the assignments in Table 2.1 are based only on the prediction of the Xα-SW calculation. They are therefore tentative assignments only. The Xα-SW calculation predicts that the two strongly bonding σ MO's $1a_1$ and $1b_2$ of Figure 2.8 should lie at high ionization energy and the peaks from these MO's are presumed to be hidden in the broad envelope at ~11 eV.

Consider next the energy shift of the alkene π orbitals on coordination. Free COD shows one π ionization band at 9.06 eV[17] and NBD gives two bands at 8.69 and 9.55 eV.[38] In the complex [$PtMe_2$(COD)], the σ orbitals having mostly alkene π orbital character are $4a_1$ and $2b_2$. These appear in the photoelectron spectra at 7.76/7.93 and

8.47 eV respectively. The corresponding calculated energies for cis-[$PtMe_2(C_2H_4)_2$] are 7.57 and 8.73 eV, after allowance for relaxation effects. It is important to note that Figure 2.8, and the other correlation diagrams, refer to the ground state only. The calculated and observed ionization energies for the C_2H_4 π orbitals are 9.66 and 10.51 eV,[39] respectively. Thus it appears that the π orbitals are destabilized on coordination and it is therefore tempting to suggest that the major component of the Pt-alkene bonding is the backbonding which increases the charge on the alkene.[40-44] However, this conclusion is not justified since the MO's for cis-[$PtMe_2(C_2H_4)_2$] are delocalized and there is much C_2H_4 π character calculated for the low energy MO's $1b_2$, $1a_1$ and $2a_1$. Similar considerations apply to the other complexes cis-[$PtMe_2L_2$] as described below. The best evidence for backbonding in cis-[$PtMe_2(C_2H_4)_2$] and [$PtMe_2$(COD)] from the present work is the stabilization of the dπ orbitals $1b_1$ and $1a_2$ of the Me_2Pt fragment on coordination of ethylene ligands as predicted by the Xα-SW calculation (Figure 2.8), coupled with the excellent agreement between the experimentally observed band energies for [$PtMe_2$(COD)] and the calculated band energies for cis-[$PtMe_2(C_2H_4)_2$] (Tables 2.1 and 2.5).

2.4.2 The Complex [$PtMe_2$(TMED)]

The Spectra in the low I.E. region are displayed in Figure 2.3, in which five resolved bands are observed. Band A again splits into two peaks with a separation of 0.13 eV. This corresponds to the N-C stretching frequency of ~1100 cm^{-1},[28] and the splitting is therefore attributed to vibrational coupling. In this case the assignment is tentative because the calculation on the model compound cis-[$PtMe_2(NH_3)_2$] indicates only a low contribution of N-orbital character to the HOMO $4a_1$. However, the model is a crude one and the calculations on the other molecules cis-[$PtMe_2L_2$] do indicate substantial L-orbital character in the HOMO. To see N-C vibrational coupling, the nitrogen long pair orbital must be delocalized to some extent onto the carbon atoms of the ligand TMED, which is indeed evidenced in $N(CH_3)_3$ by electron momentum spectroscopy.[45]

The fourth band in the photoelectron spectrum (labelled D, E) has about twice the area of the other bands and is therefore assigned to two almost degenerate MO's. Because TMED has no π acceptor properties, the platinum $d\pi$ orbitals d_{xz} ($1b_1$) and d_{xy} ($1a_2$) are expected to be close in energy and the calculation also predicts near degeneracy of these levels. The band D, E is therefore assigned to these orbitals, and the other bands are assigned in a similar way as for [$PtMe_2$(COD) and [$PtMe_2$(NBD)].

2.4.3 The complexes cis-[$PtMe_2(ER_3)_2$]

This is the largest group of compounds studied, with ER_3 = PMe_nPh_{3-n} (n = 1-3), PEt_3, $P(NMe_2)_3$, $PMe(OEt)_2$, $P(OMe)_3$, $P(OEt)_3$ and $AsMe_3$. The compounds were designed to give as wide a range of electronic properties of the phosphine and related ligands as possible, while accommodating the requirement of high volatility (without decomposition) needed to obtain satisfactory photoelectron spectra. The spectra are given in Figure 2.4-2.6, and data are in Table 2.2.

The spectra are less resolved than those for the complexes discussed above, but in most cases the spectra were fitted most satisfactorily to six bands. Two extra bands, G and H, were present in the spectra of the complexes with phenylphosphines, $PMePh_2$ and PMe_2Ph, and are readily assigned as due to phenyl π electron ionization.[46] In no case does band A show resolved vibrational structure, in contrast to the observations for the alkene and TMED complexes discussed above. This is because bands A and B are also close in energy and fairly broad, which would make vibrational splitting difficult to resolve.

The platinum $d\pi$ orbitals are the $5d_{xz}$ ($1b_1$) and $5d_{xy}$ ($1a_2$). These are expected to be almost degenerate and the calculations on the model compounds cis-

$[PtMe_2(PH_3)_2]$ and cis-$[PtMe_2(AsH_3)_2]$ (Tables 2.7 and 2.8, Figure 2.10) predict that they are close in energy, with $1a_2$ at slightly lower energy than $1b_1$, presumably due to slightly better backbonding to phosphorus or arsenic π acceptor orbitals by the $5d_{xy}$ orbital. Using these arguments, bands D and E are assigned to the $1b_1$ and $1a_2$ levels. To support this assignment, it is particularly interesting that the energy gap between these orbitals is greater for the phosphorus donors with more electronegative substituents RO, R_2N or Ph than with methyl or ethyl substituents.[47,48] It was noted earlier that in the TMED complex, with no backbonding ability, bands D and E are degenerate.

Finally, in the complex cis-$[PtMe_2\{P(NMe_2)_3\}_2]$ it was found that band E was about double the intensity of other bands and that its intensity was much reduced in the He II spectrum. An ionization of ligand electrons is expected in this region due to the psuedo-π orbital of a nitrogen lone pair interacting with the lone pair of phosphorus or the σ orbital of two nitrogen lone pairs interacting in an anti-symmetric fashion,[49] and is presumed to overlap with the platinum $d\pi$ band which is also expected. The assignments are given in Table 2.2.

2.4.4 The Complexes cis-$[PtMe_2(C{\equiv}NR)_2]$, R = Me or Ph

The photoelectron spectra of these two complexes were measured in these laboratories by L. Dignard-Bailey[21]. The ionization energies are compiled in Table 2.2. and the He II:He I spectral intensity ratios of cis-$[PtMe_2(C{\equiv}NMe)_2]$ are listed in Table 2.3. The spectra of cis-$[PtMe_2(C{\equiv}NMe)_2]$ are typical of the complexes cis-$[PtMe_2L_2]$, which display six ionization bands. In the absence of other useful information, the tentative band assignments given in Table 2.2 are those predicted by the calculation on the model compound cis-$[PtMe_2(C{\equiv}NH)_2]$. In this complex, HOMO $5a_1$ (Figure 2.11) is predicted to contain almost no isocyanide ligand character and so vibrational fine structure is not expected.

The spectra of cis-[$PtMe_2(C{\equiv}NPh)_2$] is different in two respects. First, there are two bands at 9.91 and 10.57 eV (see Table 2.2) which are readily assigned to phenyl π orbitals by analogy with the spectra of the free ligand and the complexes [$W(CO)_5(C{\equiv}NPh)$] and [$Fe(CO)_4(C{\equiv}NPh)$].[21,50,51] Secondly, the first band at 8.16 eV, which is narrow (fwhm = 0.5-0.6 eV) and can be fitted to only one band, appears to correspond to the first four bands of cis-[$PtMe_2(C{\equiv}NMe)_2$] which are resolved and spread over an energy range of > 1 eV. The mean energies are then similar and indicate similar overall donor strength for MeNC and PhNC as observed in other complexes.[32,50,51] Calculations on ligands RN≡C have indicated that, where R = Ph compared to alkyl, the π^* level is stabilized and the π level is destabilized, thus leading to better energy matching with metal d orbitals.[52,53] It is then likely that there are differences in the π-donor and π-acceptor behaviour of the PhN≡C compared to MeN≡C ligand, which lead to the major differences in the observed spectra. In particular the resolution of band E, due to the $5d_{xy}$ level, for cis-[$PtMe_2(C{\equiv}NPh)_2$] indicates that here backbonding ($5d_{xy}$--π_x^*) may be significant in this complex, while the overlap of other bands may be due to enhanced π-donor interactions of PhNC.

2.4.5 The He I and He II Spectral Intensity

As shown by the data in Table 2.3, the He II:HeI spectral intensity ratios are not significantly different between the Pt 5d based and Pt-ligand orbital ionizations for these dimethylplatinum(II) complexes. In contrast, it has been reported that complexes trans-[$PtCl_2L_2$] (L = NMe_3, PMe_3, PEt_3, or $AsEt_3$) display a large He II intensity decrease of the Pt-Cl orbital ionizations compared to the Pt 5d based orbitals.[17,18,20] The observed discrepancy between these two series of complexes can be qualitatively understood by the following considerations. As discussed in Chapter one, effects of cross section variations from He I to He II radiations are very different. For an electron ionized from a C 2p orbital, the cross sections are 6.128

and 1.875 Mb respectively at He I and He II photon energies (i.e. He II:He I ratio = 0.31).[54] Alternatively, for a Cl 3p electron, the cross sections are 13.84 and 0.647 Mb respectively at He I and He II photon energies (i.e. He II:He I ratio = 0.05).[54] Thus the decrease of the Cl 3p cross section is a factor of six greater than that of the C 2p. Therefore the observed differences in the He I and He II intensity ratios when chlorine is substituted by a methyl group are not surprising.

To explain the insignificant variations of the spectral intensities from He I and He II radiations in our compounds, we need to consider both the C 2p and Pt 5d cross sections (29.46 Mb at He I and 31.33 Mb at He II for Pt 5d[54]). As an example, we have performed a simple calculation of the relative HeII·He I intensity ratios for $Me_2Pt(COD)$, by using the Gelius atomic model.[55] In this model, the intensity of the jth molecular orbital I_j^{MO} is proportional to

$$I_j^{MO} \propto \sum_{A,\lambda}(2+\beta_A\lambda^{AO}/2)(P_A\lambda)\sigma_A\lambda^{AO} \qquad (2.1)$$

assuming an angle of $\pi/2$ between the beam and the emitted photoelectron. $\sigma_A\lambda^{AO}$ is the photoionization cross section of an atomic $A\lambda$ orbital, $\beta_A\lambda^{AO}$ is the corresponding atomic asymmetry parameter, and $(P_A\lambda_j^{AO})_j$ is the "probability" of finding in the jth molecular orbital an electron belonging to the atomic $A\lambda$ orbital. In the calculation, the $\sigma_A\lambda^{AO}$ and $\beta_A\lambda^{AO}$ values were taken from the tables given by Yeh and Lindau.[54] The $P_A\lambda$ values were considered to approximate the orbital character from the Xα-SW calculations (the charges in the intersphere and outersphere (see Table 2.5) were normalized to the individual atomic sphere). The calculated He II:He I intensity ratios of the upper six orbitals of $Me_2Pt(COD)$ are listed in Table 2.3 to compare with the experimental values. There is a good agreement in the intensity ratios between the simple theoretical treatment and the experimental measurements. This is apparently a combined result of the heavy mixing between the Pt 5d and ligand 2p orbitals and of the undramatic changes of the related atomic orbital photoionization cross sections (especially for the Pt 5d) at He I and He II radiations. This explanation is also applicable to the observations for the other Pt(II) and the Pt(IV) complexes studied in this thesis (see following chapters).

A detailed photoionization study of the upper valence levels of $Me_2Pt(COD)$ will be reported in Chapter 6, in which photoelectron spectra over the range of 21 to 100 eV photon energies will be discussed in terms of branching ratios.

2.5 TRENDS IN LIGAND BONDING

2.5.1 σ-Donor Ability

Figure 2.12 shows a graph of the first ionization energy of the complex cis-$[PtMe_2L_2]$ vs. the ionization energy of the ligand L. The values of the first ionization energies of the free ligands were taken from the literature,[17,18,47-49,50,56,57] except for TMED for which the ionization energy was measured in this work (8.35 eV). Most of the ligands are phosphorus or arsenic donors and for these there is an excellent correlation. Similar correlations are observed for other energy levels. This indicates that the ionization energy of such ligands is indeed a good criterion of donor strength. Interestingly, the ligand $P(NMe_2)_3$ also fits the correlation even though the ionization of the free ligand probably does not arise from the phosphorus lone pair orbitals.[49] The strong σ donor ability of $P(NMe_2)_3$ has also been observed in the derivative cis-$[Mo(CO)_4L_2]$.[58] We note also that, for the ligands PMe_nPh_{3-n}, the ionization energies of both the free ligands and the dimethylplatinum(II) complexes follow the series $PMe_3 > PMe_2Ph > PMePh_2$, the reverse of the series expected on electronegativity grounds. Similar effects have been observed previously with other metal complexes and these results suggest that, in the gas phase, the phenylphosphines are the stronger donors.[46,57,59,60] However, in solution the opposite trend appears to operate.[61-63]

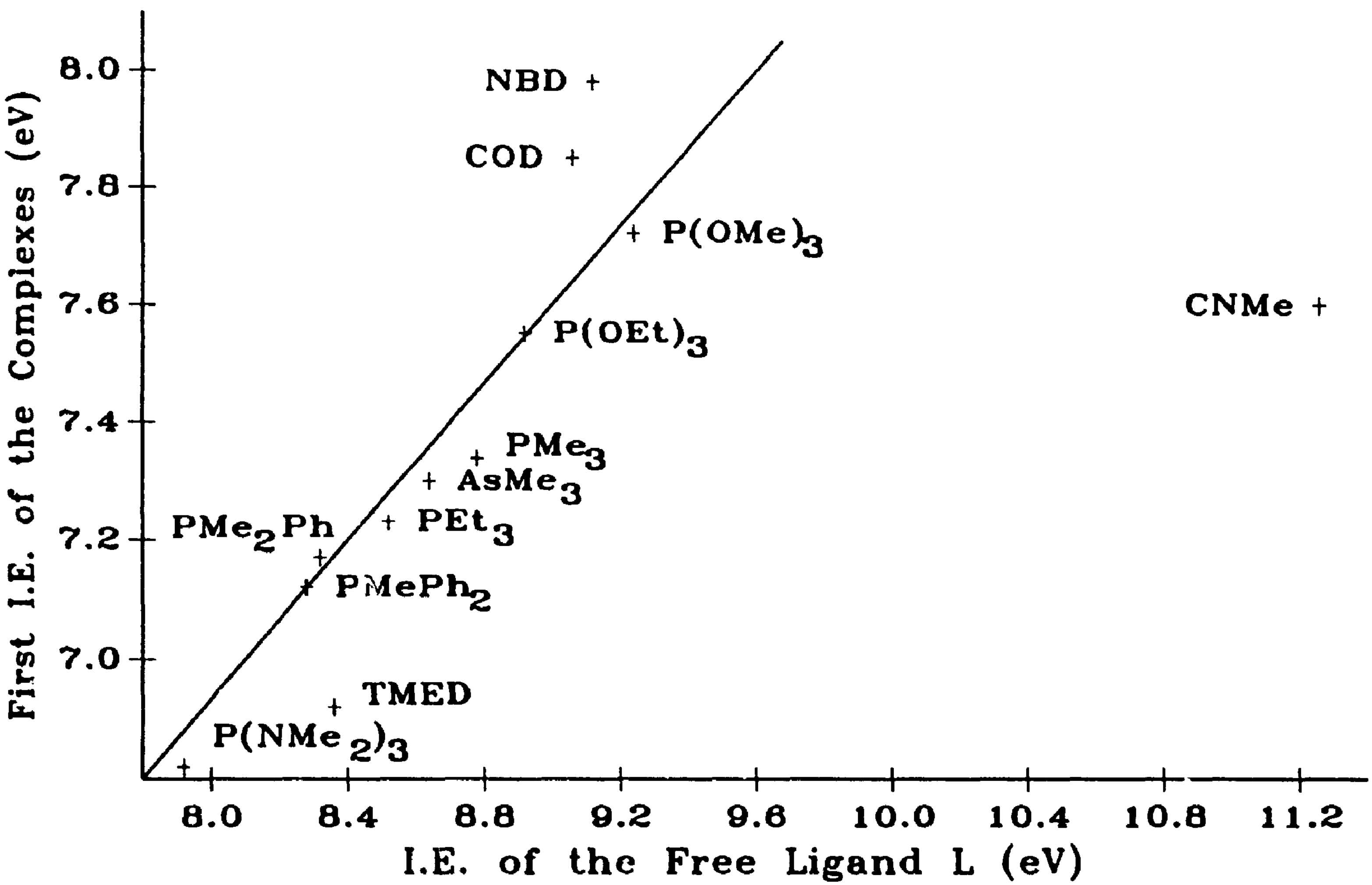

Figure 2.12. A graph of the first I.E. (eV) of the complex cis-[PtMe [illegible] vs. the I.E. (eV) of the free ligand L.

If there is a synergic σ-donor/π-acceptor type of bonding in these complexes then the ionization energies of the complexes may also be influenced to some extent by π-bonding effects. For example, TMED appears to be a stronger donor than predicted by the I. E. of the free ligand (Figure 2.12) and this may be due to the absence of π-acceptor properties for this ligand compared to the phosphorus donors. Similarly, COD and NBD appear as poorer donors than expected (Figure 2.12) and this could be due to their better π-acceptor properties compared to the phosphorus donors. Of course, these deviations from the correlation of Figure 2.12 could also be due to differences in the nature of the donor orbital of the ligand, which becomes progressively larger and more diffuse on going from nitrogen to phosphorus to alkene donors.

Finally, we note the very large deviation from the correlation of Figure 2.12 for the isocyanide ligands, which appear to be good donors though the ligand ionization energies are high. The π-donor ability of these ligands may be a factor here, but the deviation is probably too large to be explained solely by this effect.

If the ligands are arranged in order of the ionization energies for cis-$[PtMe_2L_2]$ the donor series is $P(NMe_2)_3$ > TMED > $PMePh_2$ ~ PMe_2Ph > PEt_3 > $AsMe_3$ ~ PMe_3 > $PMe(OEt)_2$ > $P(OEt)_3$ > MeNC > $P(OMe)_3$ > COD > NBD > PhNC. Generally, this order is consistent with the σ-donor series determined by other methods though, as mentioned above, there are some reversals on going from the gas phase to solution.[61-63] The position of the isocyanide ligands in this series probably results from both σ and π effects.

2.5.2 π-Acceptor Ability

As discussed earlier, the π-acceptor ability of the ligands may be measured by the splitting between the platinum $5d_{\pi}$ levels, that is the energy between bands D and E in the photoelectron spectra. There are problems in measuring this small energy difference accurately, but it is possible to arrange the ligands into three groups of decreasing π-acceptor properties on this basis. The series is $PMePh_2$, PMe_2Ph, $P(OMe)_3$, $P(OEt)_3$, $PMe(OEt)_2$, $P(NMe_2)_3$ > $AsMe_3$, PMe_3, PEt_3, COD, NBD > TMED. The series should be regarded with caution but the general trend is reasonable. Thus the alkyl phosphines or arsines appear to be weaker π-acceptors than the phosphorus donors with more electronegative substituents, and TMED has no π-acceptor properties based on this criterion. The series may underestimate the π-acceptor ability of the alkene ligands however, since both the Xα-SW calculation and the deviation of COD and NBD from the correlation of Figure 2 suggest that the alkenes are better π-acceptors than phosphines. The isocyanides are difficult to treat here because they appear to act both as π-donors and π-acceptors.

2.6 IMPLICATIONS FOR THE CHEMISTRY OF THE COMPLEXES

These complexes may be considered as models for square planar d^8 complexes generally; such complexes have a very rich chemistry and many important catalytic applications. They are able to interact with both nucleophilic (using the empty p orbital, $6p_x$ using the nomenclature of Figure 2.7, $6p_z$ using the more usual axes for square planar complexes) and electrophilic reagents (using the filled d orbital, $5d_{x^2-y^2}$ using Figure 2.7 axes, $5d_{z^2}$ using the more usual axes).

In oxidative addition chemistry of dimethylplatinum(II) compounds, it is clearly the filled d orbitals on the platinum which lead to metal-based nucleophilicity. The orbital used is $3a_1$, which is not the HOMO according to our interpretation of the spectra and the calculations, but which is close enough to act as a nucleophile. The platinum-ligand σ-bonding MO $4a_1$ is the HOMO but it is much more delocalized and inaccessible than the non-bonding platinum 5d orbital $3a_1$, and it is therefore reasonable that the more exposed orbital $3a_1$ should be the more effective nucleophile, especially in oxidative addition reactions with sterically hindered electrophiles such as alkyl halides. Thus in oxidative addition of methyl iodide, the $3a_1$ orbital of platinum would give S_N2 attack at the methyl group with displacement of iodide,[7,64] which subsequently coordinates to give octahedral $[PtIMe_3L_2]$. The reactivity depends on the donor ability of L, and the series for reactivity to oxidative addition L_2 = TMED > R_3P > $(RO)_3P$ > COD, MeNC is fully consistent with the donor ability of the ligands as deduced from the photoelectron spectra.

A more difficult problem arises in determining the mechanism of cleavage of platinum-methyl bonds by electrophilic reagents. For example, the reaction of H^+Cl^- with cis-$[PtMe_2L_2]$ gives methane and cis-$[PtClMeL_2]$. Here the reaction could occur by oxidative addition of H^+Cl^- followed by reductive elimination of methane,[65,66] or the electrophile (H^+ in this example) could attack the Pt-Me σ-MO directly[67] to give methane. The HOMO is believed to be the σ-MO $4a_1$ and this makes the direct attack plausible, especially with the reagent H^+Cl^-, which has a low steric requirement. As discussed above, bulkier reagents would almost certainly attack the d-orbital $3a_1$, and this has been shown to occur with the reagent $Ph_3PAu^+Cl^-$.[65] Since $3a_1$ and $4a_1$ are close in energy (and of the same symmetry so that mixing is predicted), it is possible that H^+ could attack the σ-MO $4a_1$ orbital, or that H^+Cl^- could attack the d-orbital $3a_1$. We note, however, that $4a_1$ is calculated to be very weakly bonding or even antibonding with respect to the Pt-Me groups and in some complexes it is localized to a greater extent on the ligands L (eg. when L = C_2H_4). Attack of H^+ at the PtL bond would not lead to productive chemistry; the orbital $1a_1$ which is much more strongly Pt-Me bonding is considerably lower in energy, and is less likely to be involved in reactions with electrophiles. To summarize, the electronic structure of the complexes cis-$[PtMe_2L_2]$, in which d-orbitals and σ-MO's are close in energy, should allow electrophilic cleavage to occur by direct attack on the M-C bond or by oxidative addition-reductive elimination. Steric or solvation factors are likely to have a considerable effects in determining which mechanism is preferred. Intermediate mechanisms are possible also.

The complexes are also susceptible to nucleophilic attack and [$PtMe_2$(COD)] is often used as a precursor to other complexes [$PtMe_2L_2$]. The NBD ligand in [$PtMe_2$(NBD) is displaced even more readily.[68,69] These reactions are probably associative, using the empty 6p orbital on platinum as acceptor. Since the calculations indicate diffuse features for the lowest virtual orbitals, and the photoelectron spectra give only small energy differences between the HOMO's, the nature of these reactions will not be discussed further.

2.7 CONCLUSION

The UV photoelectron spectra of the dimethylplatinum(II) complexes can be assigned with the help of the resolved vibrational fine structure, substitution effects and Xα-SW calculations, while the He II:He I area ratios are generally not useful. The first two molecular orbitals with low I.E. values contain contributions from both Pt and ligand orbitals and these are followed by the essentially nonbonding Pt 5d orbitals. The σ-donor ability falls in the order $P(NMe_2)_3$ > TMED > $PMePh_2$ ~ PMe_2Ph > PEt_3 > $AsMe_3$ ~ PMe_3 > $PMe(OEt)_2$ > $P(OEt)_3$ > $P(OMe)_3$ > COD > NBD and the π-acceptor ability falls in the order $PMePh_2$ ~ PMe_2Ph ~ $P(OMe)_3$ ~ $P(OEt)_3$ ~ $PMe(OEt)_2$ ~ $P(NMe_2)_3$ > $AsMe_3$ ~ PMe_3 ~ PEt_3 ~ COD ~ NBD > TMED. Both CNMe and CNPh have comparable σ-donor properties and the latter has stronger π-donor and π-acceptor abilities. Some typical chemical reactions such as oxidative addition, and electrophilic cleavage of a Pt-C bond leading to ligand replacement can be reasonably accounted for, based on the established σ/π series and the ionization features.

2.8 REFERENCES

1. R. Romeo, D. Minniti, S. Lanza, P. Uguagliati, and U. Belluco, Inorg. Chem., 17, 2813 (1978).
2. J. K. Jawad, R. J. Puddephatt, and M. A. Stalteri, Inorg. Chem., 21, 332 (1982).
3. G. Alibrandi, D. Minniti, L. M. Scolaro, and R. Romeo, Inorg. Chem., 27, 318 (1988).
4. R. Minniti, G. Alibrandi, M. L. Tobe, and R. Romeo, Inorg. Chem., 26, 3956 (1987).
5. D. L. Thorn and J. C. Calabrese, J. Organomet. Chem., 342, 269 (1988).
6. G. Alibrandi, D. Minniti, L. M. Scolaro, and R. Romeo, Inorg. Chem., 29, 1939 (1989).
7. P. K. Monaghan and R. J. Puddephatt, J. Chem. Soc. Dalton Trans., 595 (1988).
8. A. C. Balazs, K. H. Johnson, and G. M. Whitesides, Inorg. Chem., 21, 2162 (1982).
9. J. J. Low and W. A. Goddard, III, J. Am. Chem. Soc., 108, 6115 (1986).
10. J. J. Low and W. A. Goddard, III, Organometallics, 5, 609 (1986).
11. T. M. Miller, A. N. Izumi, Y. S. Shih, and G. M. Whitesides, J. Am. Chem. Soc., 110, 3146 (1988).
12. T. M. Miller, T. J. McCarthy, and G. M. Whitesides, J. Am. Chem. Soc., 110, 3156 (1988).
13. T. M. Miller and G. M. Whitesides, J. Am. Chem. Soc., 110, 3164 (1988).
14. J. M. Brown, N. A. Cooley, and D. W. Price, J. Chem. Soc. Chem. Commun., 458 (1989).
15. R. Kumar, S. Roy, M. Rashidi, and R. J. Puddephatt, Polyhedron, 8, 551 (1989).
16. J. Behan, R. A. W. Johnstone, and R. J. Puddephatt, J. Chem. Soc. Chem. Commun., 444 (1978).

17. J. N. Louwen, R. Hengelmolen, D. M. Grove, D. J. Stufkens, and Ad. Oskam, J. Chem. Soc. Dalton Trans., 141 (1986).

18. G. Zangrande, G. Granozzi, M. Casarin, and J. P. Daudy, Inorg. Chem., 25, 2872 (1986).

19. J. N. Louwen, R. Hengelmolen, D. M. Grove, Ad. Oskam, and R. L. DeKock, Organometallics, 3, 908 (1984).

20. G. Granozzi, G. Zangrande, M. Bonivento, and G. Michelon, Inorg. Chim. Acta, 77, L229 (1983).

21. For sake of systematic discussion of this type of complexes, the ionization energies of the compounds cis-[$PtMe_2L_2$] with L = PMe_3, PMe_2Ph, CNMe and CNPh are included in this chapter and taken from L. M. Dignard, Ph.D. Dissertation, University of Western Ontario, London, Ontario, Canada, 1986.

22. J. C. Green, Struct. Bonding (Berlin), 43, 37 (1981).

23. A. H. Cowley, Prog. Inorg. Chem., 26, 45 (1979).

24. C. R. Kistner, J. H. Hutchinson, J. R. Doyle, and J. C. storlie, Inorg. Chem., 2, 1255 (1963).

25. T. G. Appleton, J. R. Hall, D. W. Neale, and M. A. Williams, J. Organomet. Chem., 276, C73 (1984).

26. H. C. Clark and L. E. Manzer, J. Organomet. Chem., 59, 411 (1973).

27. M. H. Chisholm, H. C. Clark, L. E. Manzer, J. B. Stothers, and J. E. H. Ward, J. Am. Chem. Soc., 97, 721 (1975).

28. C. N. R. Rao, Chemical Applications of Infrared spectroscopy, Academic Press Inc. (London) Ltd., 1963, P.250.

29. The contour diagrams were plotted by J. S. Tse, National Research Council, Ottawa, Canada.

30. J. N. Louwen, D. M. Grove, H. J. C. Ubblels, D. J. Stufkens, and A. Oskam, Z. Naturforsch B. 38, 1657 (1983).

31. A. Oskam, D. J. Stufkens, and J. N. Louwen, J. Mol. Struct., 142, 347 (1986).

32. S. D. Bella, I. Fragalia, and G. Granozzi, Inorg. Chem., 25, 3997 (1986).

33. G. Granozzi, A. Vittadini, L. Sindellari, and D. Ajo, Inorg. Chem., 23, 702 (1984).

34. J. H. D. Eland, Photoelectron Spectroscopy, Butterworth & Co. Ltd., 2nd ed., London, 1984.

35. B. Higginson, D. R. Lloyd, P. Burroughs, D. M. Gibson, and A. F. Orchard, J. Chem. Soc. Faraday Trans. II, 69, 1659 (1973).

36. J. L. Hubbard and D. L. Lichtenberger, J. Am. Chem. Soc., 104, 2132 (1982).

37. C. Batich, O. Ermer, and E. Heilbronner, J. Electron Spectrosc. Relat. Phenom., 1, 333 (1973).

38. M. H. Plamer, J. Mol. Struct., 161, 333 (1987).

39. D. W. Turner, C. Baker, A. D. Baker, C. B. Brundle, Molecular Photoelectron Spectroscopy, whiley-Interscience, New York, 1970

40. D. C. Calabro and D. L. Lichtenberger, J. Am. Chem. Soc., 103, 6846 (1981).

41. G. Morelli, G. Polzonetti, and V. Sessa, Polyhedron, 4, 1185 (1985).

42. C. D. Cook, K. Y. Wan, U. Gelius, K. Humrin, G. Johansson, E. Olsson, H. Siegbahn, C. Nordling, and K. Siegbahn, J. Am. Chem. Soc., 93, 1904 (1971).

43. K. Kitaura, S. Sakaki, and K. Morokuma, Inorg. Chem., 20, 2292 (1981).

44. S. Sakaki, N. Kudou, and A. Ohyoshi, Inorg. Chem., 16, 202 (1977).

45. A. O. Bawagan and C. E. Brion, Chem. Phys. 123, 51 (1988).

46. R. J. Puddephatt, G. M. Bancroft, and T. Chan, Inorg. Chim. Acta, 73, 83 (1983).

47. L. W. Yarbrough, II and M. B. Hall, Inorg. Chem., 17, 2269 (1978).

48. A. Yamamato, Organotransition Metal Chemistry, John Willey & Sons, Inc., 1986, P.209.

49. D. Gonbeau, M. Sanchez, and G. P. Guillouzo, Inorg. Chem., 20, 1966 (1981) and references therein.

50. V. Y. Young and K. L. Cheng, J. Electron Spectrosc. Relat. Phenom., 9, 317 (1976).

51. D. B. Beach, R. Bertoncello, G. Granozzi and W. L. Jolly, Organometallics, 4, 311 (1985).

52. B. E. Bursten and R. F. Fenske, Inorg. Chem., 16, 963 (1977).

53. P. Fantucci, L. Naldini, F. Cariati, V. Valenti, and C. Bussetto, J. Organomet. Chem, 64, 125 (1974).

54. J. J. Yeh and I. Lindau, At. Nucl. Data Tables, 32, 1 (1985).

55. V. Gelius, J. Electron Spectrosc. Relat. Phenom., 5, 985 (1975).

56. S. Elbel, H. Bergmann and W. Enblin, J. Chem. Soc. Faraday II, 70, 555 (1974).

57. R. J. Puddephatt, L. Dignard-Bailey and G. M. B ncroft, Inorg. Chim. Acta, 96, L91 (1985).

58. M. F. Lappert, J. B. Pedley, B. T. Wilkins, O. Stelzer, and E. Unger, J. Chem. Soc. Dalton Trans., 1207 (1975).

59. G. M. Bancroft, T. C. S. Chan and R. J. Puddephatt, Inorg. Chem., 22, 2133 (1983).

60. G. M. Bancroft, L. Dignard-Bailey and R. J. Puddephatt, Inorg. Chem., 25, 3675 (1986).

61. B. L. Shaw, J. Chem. Soc., Chem. Commun., 104 (1979).

62. R. C. Bush and R. J. Angelici, Inorg. Chem., 27, 681 (1988).

63. Md. M. Rahman, H. Y. Liu, K. Eriks, A. Prock, and W. P. Giering, Organometallics, 8, 1 (1989).

64. K. T. Aye, A. J. Canty, M. Crespo, R. J. Puddephatt, J. D. Scott, and A. A. Watson, Organometallics, 8, 1518 (1989).

65. J. K. Jawad, R. J. Puddephatt, and M. A. Stalteri, Inorg. Chem., 21, 332 (1982)

66. G. J. Arsenault, C. M. Anderson, and R. J. Puddephatt, Organometallics, 7, 2094 (1988).

67. G. Alibrandi, D. Minniti, L. M. Scolaro, and R. Romeo, Inorg. Chem., 27, 318 (1988).

68. T. G. Appleton, J. R. Hall, D. W. Neale, and M. A. Willams, J. Organomet. Chem., 276, C73 (1984).

69. D. L. Thorn and J. C. Calabrese, J. Organomet. Chem., 342, 269 (1988).

CHAPTER 3

THE ELECTRONIC STRUCTURE OF SQUARE-PLANAR CIS-BIS(TRIFLUOROMETHYL)PLATINUM(II) COMPLEXES

3.1 INTRODUCTION

It has been recognized that perfluoroalkyl transition metal complexes in general have very different properties from the corresponding alkyl complexes. For example, the perfluoroalkyl compounds have enhanced thermal stability[1,2] and shorter metal-carbon bond lengths (0.04 Å) compared to their alkyl analogues.[3,4] In platinum(II) complexes, perfluoroalkyl groups have a high NMR trans influence, comparable to that of the methyl group.[5-7] Replacement of methyl groups bound to platinum(II) by trifluoromethyl groups leads to deactivation of the metal center toward oxidative addition reactions.[8-10] Thus, although the powerful oxidant X_2 will oxidize cis-$[Pt(CF_3)_2L_2]$ (L = EtNC, 1/2(bipy), and PMe_2Ph) to $[Pt(CF_3)_2X_2L_2]$ (X = halogen),[2] no reaction has been observed with the weaker oxidants MeI and CF_3I.[8] A ligand L is more readily displaced from cis-$[Pt(CF_3)_2L_2]$ than from cis-$[PtMe_2L_2]$.[2] Together these observations show that the platinum centres are more susceptible to nucleophilic attack but less susceptible to electrophilic attack when R = CF_3 rather than CH_3 in cis-$[PtR_2L_2]$ complexes. This is expected because of the greater electron withdrawing power of CF_3 than CH_3.

The unusual effects of fluorine as a substituent are normally attributed to its high electronegativity and its three non-bonding electron pairs. Based on these properties, it was suggested that the unusual chemistry of the perfluoroalkyl transition metal complexes was at least in part due to π-backbonding between filled d orbitals on the metal atom and σ* orbitals of the perfluoroalkyl group.[11,12] Later, it was suggested that the π-backbonding was not important,[13,14] and Fenske and Hall concluded from their approximate molecular orbital calculations on $MeMn(CO)_5$ and $(CF_3)Mn(CO)_5$[15] that the significant differences between the alkyl and perfluoroalkyl complexes could be understood in terms of σ-donation from an antibonding CF_3 orbital and energy stabilization due to the effects of charge on neighbouring atoms. Since a detailed study of the electronic structure of square-planar cis-dimethylplatinum(II) complexes has been discussed (see the last chapter), a further investigation of the electronic structure of the corresponding perfluoromethyl would be helpful to understand their differences in chemical properties and reactions.

This chapter will describe the photoelectron spectra of cis-$[Pt(CF_3)_2L_2]$ (L_2 = COD and TMED or L = PEt_3 and $AsMe_3$) and Xα-SW results on the model compounds cis-$[Pt(CF_3)_2(C_2H_4)_2]$ and cis-$[Pt(CF_3)_2(PH_3)_2]$. The nature of the C-F bonding, the effect of the CF_3 groups on the MO energies and on the platinum bonding to the ligands L in these molecules are then discussed.

3.2 UV PHOTOELECTRON SPECTRA

Some representative spectra are shown in Figure 3.1, along with the corresponding spectra for the dimethylplatinum(II) complexes for comparison. It is interesting to note that the ionization bands in the range > 11.5 eV (bands labelled G-J(K)) are shifted more than those in the range < 11.5 eV (bands labelled A-F) upon replacement of CH_3 by CF_3. This leads to a smaller energy separation between the two regions of the spectra when compared to the dimethylplatinum(II) complexes as indicated by the separation of the band G from the band F in Figure 3.1. In the range > 11.5 eV, the spectra contain broad envelopes, with contributions from many ligand-based MO ionizations. The highest I.E. band at ~18 eV (band K in $[Pt(CF_3)_2(COD)$ and band J in cis-$[Pt(CF_3)_2(AsMe_3)_2]$) is absent in the spectra of the dimethylplatinum(II) complexes and thus is assigned to ionizations of C-F σ

Table 3.3. Xα-SW results for cis-[$Pt(CF_3)_2(C_2H_4)_2$] (C_{2v}) upper valence orbitals

Orbital	Energy(eV)[a]		Charge Distribution (%) Pt	C^b	C^c	F	H	Inter	Outer
$4a_1$	5.89	8.36	$4p_z$, $18d_{z^2}$,	2s, 7p	39p	4p		25	
$2b_2$	6.49	8.92	$6p_y$, $1d_{yz}$	2s, 5p	49p	7p		29	1
$3a_1$	6.89	9.38	14s, $2p_z$, $36d_{x^2-y^2}$	2s, 8p	6p	12p	1	18	1
$1a_2$	7.46	10.02	$44d_{xy}$		1s, 23p	1p	24	7	
$1b_1$	7.51	10.13	$75d_{xz}$		6p	2p	9	8	
$2a_1$	8.59	11.18	2s, $70d_{z^2}$		11p	3p		14	
$1a_1$	9.29	11.79	1s, $2p_z$, $46d_{x^2-y^2}$	2s, 11p	6p	24p	1	5	2
$1b_2$	9.61	12.06	$35d_{yz}$	2s, 11p	1s, 11p	1s,25p	6	5	2

[a]The second column is the molecular orbital energy of the ground state, and the third column is the transition state energy, calculated by removal of a half of electron from the HOMO ($4a_1$). [b]carbon in CF_3; [c]carbon in C_2H_4.

orbitals.[16] The fluorine lone pairs which ionize at ~ 14 eV contribute to, for example, band H in the L = $AsMe_3$ complex, and band I in the L_2 = COD complex, as indicated by the relative area increases from the dimethylplatinum(II) to the bis(trifluoromethyl)platinum(II) compounds (Figure 3.1), as well as by the higher He II:He I intensity ratios than those of the other bands in this region, since the fluorine 2p orbital ionizations show larger He II:He I cross section ratio than those of the other ligand orbital ionizations (0.91 for F 2p, 0.31 for C 2p, 0.45 for N 2p, 0.41 for P 3p, and 0.08 for As 4p).[17] Band G in the L = $AsMe_3$ complex at least partially arises from the ionizations of As-C orbitals, since the ionization energy is approximately the same as that of As-C in the free ligand $AsMe_3$[18] and remains almost unchanged in both cis-$[PtMe_2(AsMe_3)_2]$ and cis-$[Pt(CF_3)_2(AsMe_3)_2]$. Other bands in this region contribute mostly to the non-fluorine containing orbital ionizations, but detailed assignments will not be attempted.

In the region < 11.5eV, the spectra are not resolved as well as those of the dimethylplatinum(II) complexes due to the broader inherent line width,[19-21] but typically six bands are satisfactorily fitted except for cis-$[Pt(CF_3)_2(TMED)]$ in which two of the bands appear to be degenerate. The spectra are shown in Figures 3.2 and 3.3 and the data given in Table 3.1. There are three important features in the spectra of this region. Firstly, the first band labelled A in $[Pt(CF_3)_2L_2]$ (L_2 = COD and TMED) clearly has an asymmetric shape although it is not resolved as well as the same band in $[PtMe_2L_2]$(L_2 = COD and TMED). Thus this band was fitted to two peaks with separations of 0.20±0.04 eV in $[Pt(CF_3)_2(COD)]$ and of 0.19±0.04 eV in $[Pt(CF_3)_2(TMED)]$. The band B in $[Pt(CF_3)_2(TMED)]$ was also fitted to two due to its asymmetric shape with separation of 0.20±0.04 eV. These splittings are similar to, but larger than, the splittings in the corresponding dimethylplatinum(II) complexes, and are probably vibrational in origin. Secondly, the perfluoromethyl effect causes a

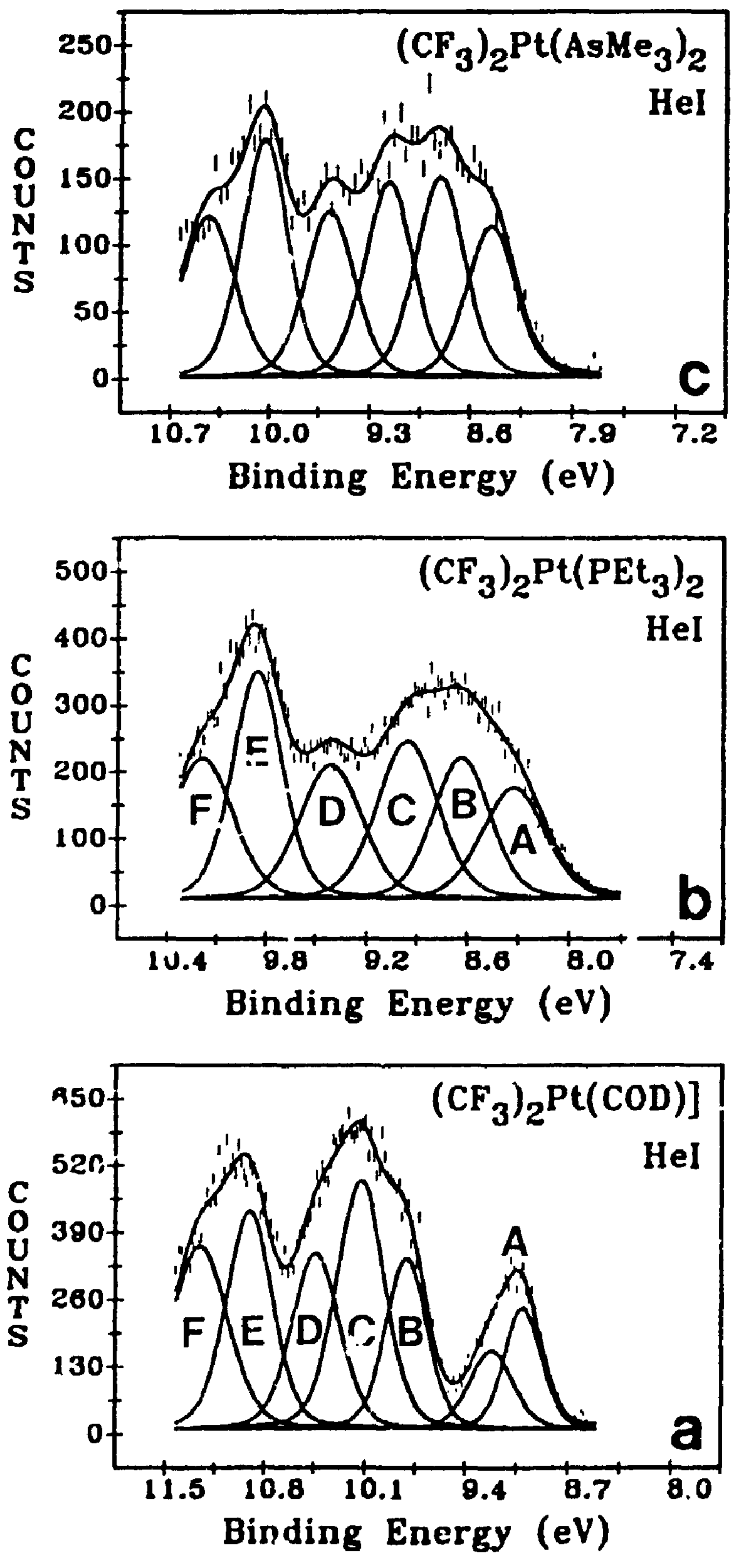

Figure 3.2. The He I spectra of $[Pt(CF_3)_2(COD)]$ (a), cis-$[Pt(CF_3)_2(PEt_3)_2]$ (b), and cis-$[Pt(CF_3)_2(AsMe_3)_2]$ (c) (expanded low I.E. region only).

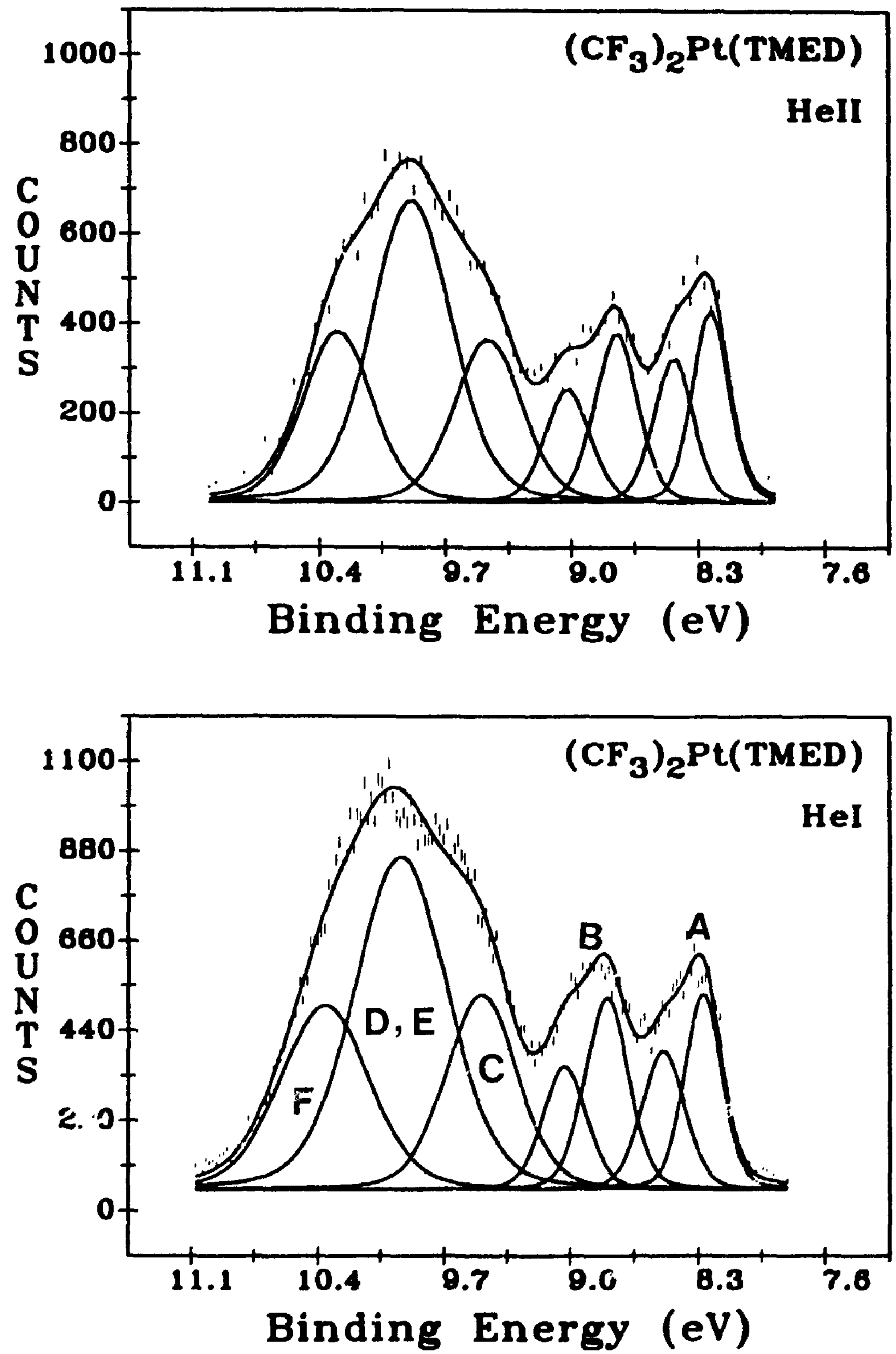

Figure 3.3. The He I and He II spectra of $[Pt(CF_3)_2(TMED)]$ (expanded low I.E. region only).

Table 3.1. Ionization energies (eV), He II:He I intensity ratios and assignments of Bands for cis-[$Pt(CF_3)_2L_2$] (L_2 = COD, TMED or L = PEt_3, $AsMe_3$)

	COD		TMED			PEt_3		$AsMe_3$	
Band	I.E.	He II:He I	I.E.	He II:He I	Orbital	I.E.	He II:He I	I.E.	Orbital
A	9.00	1.00	8.26	1.00	$4a_1$	8.33	1.00	8.42	$4a_1$
	9.20		8.45						
B	9.80	0.87	8.80	0.87	$2b_2$	8.63	1.04	8.78	$2b_2$
			9.00						
C	10.12	0.86	9.49	0.85	$3a_1$	8.95	0.97	9.15	$3a_1$
D	10.43	0.82	9.96	0.96	$1a_2$	9.41	0.95	9.56	$1b_1$
E	10.90	0.93	9.96	0.96	$1b_1$	9.85	1.02	10.03	$2a_1$
F	11.26	0.96	10.41	1.04	$2a_1$	10.19	1.01	10.43	$1a_2$

stabilization of all orbitals by ~1 eV when compared with the corresponding methyl platinum complexes. Finally, the six bands give very similar He II:He I area ratios as for the dimethylplatinum compounds. The spectra in this low I.E. region will be assigned using the Xα-SW predictions on the model compounds cis-$[Pt(CF_3)_2(C_2H_4)_2]$ and cis-$[Pt(CF_3)_2(PH_3)_2]$, and by comparison with the spectra of the corresponding dimethylplatinum(II) complexes.

3.3 Xα-SW RESULTS

3.3.1 The Complex cis-$[Pt(CF_3)_2(C_2H_4)_2$

As for cis-$[PtMe_2(C_2H_4)_2]$, the molecule cis-$[Pt(CF_3)_2(C_2H_4)_2]$ has been considered to be formed by combination of the fragment of cis-$[Pt(CF_3)_2]$ and $(C_2H_4)_2$, and calculations have been carried out separately for cis-$[Pt(CF_3)_2(C_2H_4)_2]$, cis-$[Pt(CF_3)_2]$, and C_2H_4. In the correlation diagram of Figure 3.4(b), only the interactions between the $Pt(CF_3)_2$ and the π and π^* orbitals of the ligand C_2H_4 are presented. The analysis will begin with a consideration of the fragment $Pt(CF_3)_2$ and a comparison with the fragment $PtMe_2$ which is again presented in Figure 3.4(a).

The results of Xα-SW calculations for the cis-$[Pt(CF_3)_2$ fragment are given in Table 3.2 and in Figure 3.4(b), and in many respect are similar to those for cis-$[PtMe_2]$. Thus there are two Pt-C σ-levels ($1b_2$ and $1a_1$) below four orbitals which have mostly platinum 5d character ($2a_1$, $1b_1$, $1a_2$ and $3a_1$). The orbital $1b_2$ is formed by overlap of the $5d_{yz}$ orbital on platinum with the unsymmetrical combination of CF_3 σ-orbitals, but there is also considerable fluorine 2p-character in this MO (Table 3.2). Similarly, the $1a_1$ orbital is formed from the 6s and $5d_{x^2-y^2}$ and $5d_{z^2}$ orbitals on platinum combining with the symmetric combination of CF_3 σ-orbitals, and again there is much fluorine 2p-character. Of the platinum 5d levels, three have 89-90% d-character and are assigned as $1a_2$ ($5d_{xy}$), $1b_1$ ($5d_{xz}$) and $2a_1$ ($5d_{z^2}$), while the HOMO $3a_1$ has only 33% platinum 5d-character ($5d_{x^2-y^2}$), with some 6s character and clearly

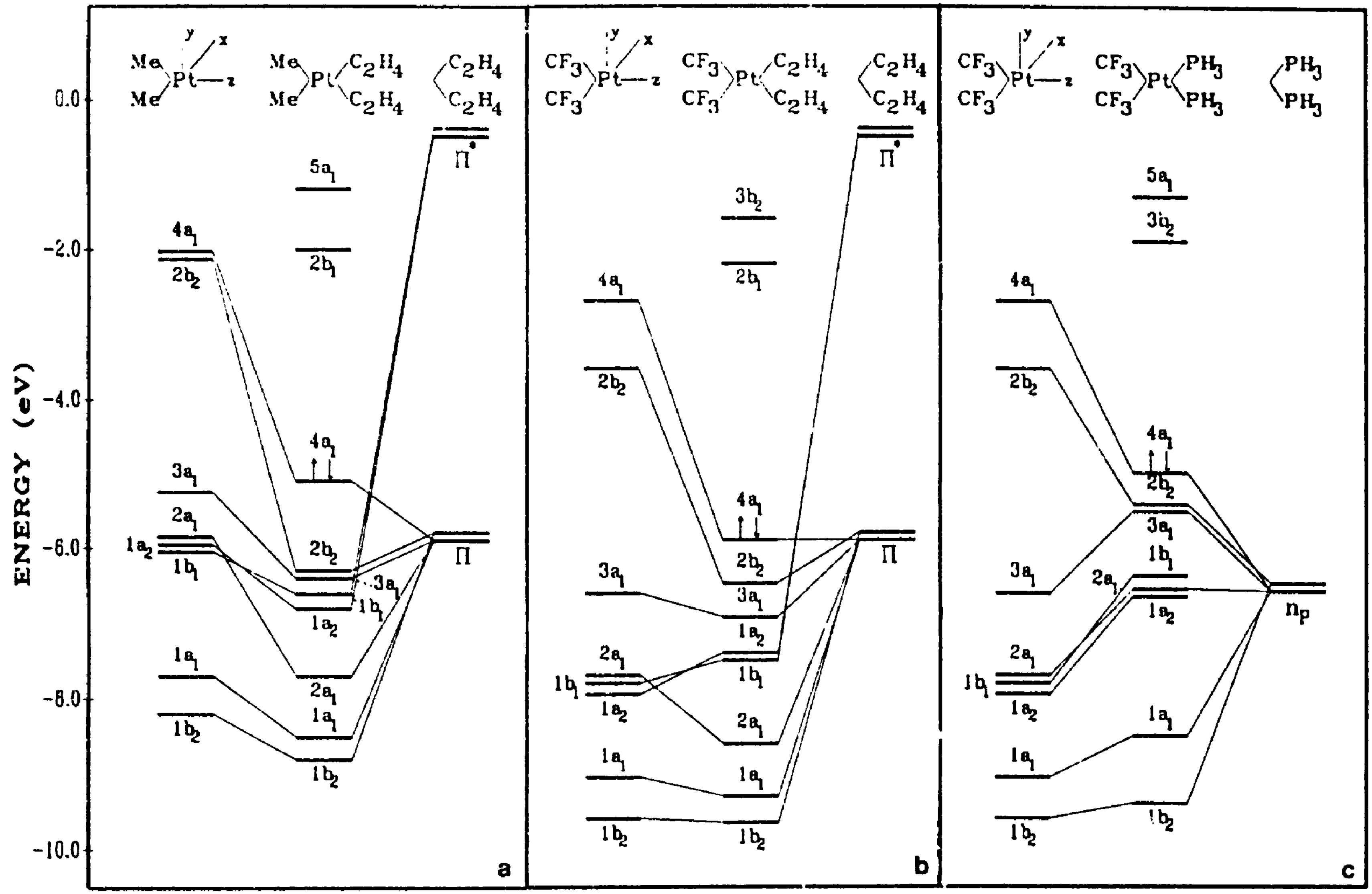

Figure 3.4. Orbital correlation diagrams for cis-[$PtMe_2(C_2H_4)_2$] (a), cis-[$Pt(CF_3)_2(C_2H_4)_2$] (b), and cis-[$Pt(CF_3)_2(PH_3)_2$] (c).

Table 3.2. Xα-SW results for cis-[$Pt(CF_3)_2$] (C_{2v}) upper valence orbitals

Orbital[a]	Orbital Energy (eV)	Charge Distribution (%)[b]				
		Pt	C	F	Inter	Outer
$4a_1$	2.71	6s, $9p_z$, $5d_{z^2}$	2s, 7p	2p	46	20
$2b_2$	3.62	$11p_y$, $30d_{yz}$	7s, 19p	10p	20	3
$3a_1$	6.56	16s, $1p_z$, $33d_{x^2-y^2}$	3s, 11p	14p	21	1
$2a_1$	7.79	$89d_{z^2}$		3p	8	
$1b_1$	7.84	$90d_{xz}$		2p	8	
$1a_2$	7.93	$89d_{xy}$		2p	9	
$1a_1$	9.07	2s, $1p_z$, $50d_{x^2-y^2}$	2s, 12p	25p	8	
$1b_2$	9.62	$46d_{xz}$	2s,10p	34p	7	1

[a] $3a_1$ is HOMO. [b] For the Pt contributions, the % contribution followed by the orbital is given. For a_1 symmetry, the particular d orbital is not given by the calculation directly, and the assignment of an a_1 orbital to mostly d_{z^2} or $d_{x^2-y^2}$ is based on the orbital contour diagrams. These assignments are therefore not certain. The explanation is followed in the other tables.

some σ*-character. Orbitals $2b_2$ and $4a_1$ are the virtual ones, with obvious σ*-character in the orbital $2b_2$ because of considerable $5d_{yz}$ contribution.

It is interesting to note that the non-bonding platinum 5d orbitals $1a_2$, $1b_1$, and $2a_1$ are calculated to be about 1.9 eV lower in energy than in the dimethylplatinum fragment, while the Pt-C σ-orbitals $1b_2$ and $1a_1$ are lower in energy compared to the $PtMe_2$ fragment by only about 1.4 eV. The general stabilization is clearly due to the inductive effects of the electronegative fluorine atoms, but the predicted smaller stabilization of the σ-orbitals is probably a result of the poor energy matching and overlap between the Pt 5d orbitals and the CF_3 σ-orbitals, since the CF_3 fragment is more electronegative than that of CH_3.

In considering the interaction of the cis-[$Pt(CF_3)_2$] fragment with ethylene, the orbitals of interest with respect to the two cis-C_2H_4 ligands are the π-orbitals (a_1 + b_2) and the π*-orbitals (a_2 + b_1) arising from the C=C bonds. The energies as calculated are shown in Figure 3.4(b). It is clear from the resulting diagram and from the orbital characters in Table 3.3, that the two σ-orbitals ($1b_2$ + $1a_1$) of the fragment $Pt(CF_3)_2$ are perturbed only slightly and the molecular orbitals labelled $1a_1$ and $1b_2$ retain their large Pt-CF_3 σ-character. As for the dimethylplatinum analogue, cis-[$PtMe_2$], the two empty orbitals ($4a_1$ + $2b_2$) of the fragment $Pt(CF_3)_2$ mix strongly with the π electrons of the ethylene ligands, and this interaction produces molecular orbitals $4a_1$ and $2b_2$ of much lower energy. The orbital $2b_2$ is calculated to have mostly C=C π character (Table 3.3), and it has the smallest energy shift (~0.15 eV) compared to the orbital $2b_2$ in cis-[$PtMe_2(C_2H_4)_2$], whereas the other orbitals in the upper valence region are stabilized by 0.70±0.20 eV, compared to the corresponding orbitals in cis-[$PtMe_2(C_2H_4)_2$]. The HOMO is $4a_1$ which has mainly Pt-C_2H_4 character, along with some Pt-CF_3 σ* character as indicated by the contour diagram in Figure 3.5. The contours were plotted on the molecular plane with the CF_3 groups on the

Table 3.3. Xα-SW results for cis-[$Pt(CF_3)_2(C_2H_4)_2$] (C_{2v}) upper valence orbitals

Orbital	Energy(eV)[a]		Charge Distribution (%)						
			Pt	C[b]	C[c]	F	H	Inter	Outer
$4a_1$	5.89	8.36	$4p_z$, $18d_{z^2}$,	2s, 7p	39p	4p		25	
$2b_2$	6.49	8.92	$6p_y$, $1d_{yz}$	2s, 5p	49p	7p		29	1
$3a_1$	6.89	9.38	14s, $2p_z$, $36d_{x^2-y^2}$	2s, 8p	6p	12p	1	18	1
$1a_2$	7.46	10.02	$44d_{xy}$		1s, 23p	1p	24	7	
$1b_1$	7.51	10.13	$75d_{xz}$		6p	2p	9	8	
$2a_1$	8.59	11.18	2s, $70d_{z^2}$		11p	3p		14	
$1a_1$	9.29	11.79	1s, $2p_z$, $46d_{x^2-y^2}$	2s, 11p	6p	24p	1	5	2
$1b_2$	9.61	12.06	$35d_{yz}$	2s, 11p	1s, 11p	1s,25p	6	5	2

[a]The second column is the molecular orbital energy of the ground state, and the third column is the transition state energy, calculated by removal of a half of electron from the HOMO ($4a_1$). [b]carbon in CF_3; [c]carbon in C_2H_4.

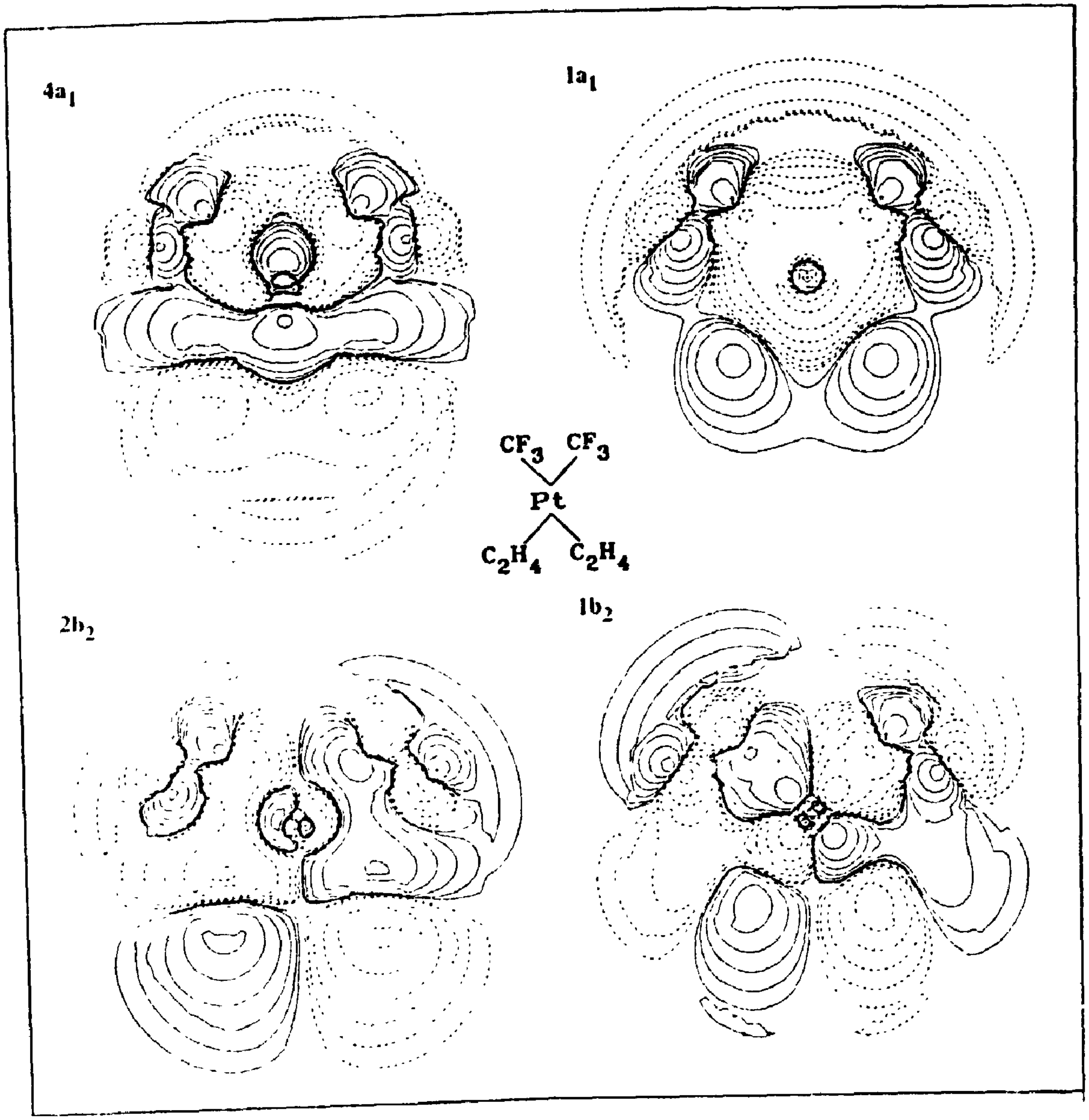

Figure 3.5. The contour maps of $1a_1$, $1b_2$, $2b_2$ and $4a_1$ orbitals for cis-$[Pt(CF_3)_2(C_2H_4)_2]$. The contours were plotted at values ±0.002, ±0.0047, ±0.0094, ±0.0188, ±0.0375, and ±0.15, starting from the outermost.

upper side and the C_2H_4 groups on the lower side with respect to the platinum atom. It is very obvious from the contours that the contribution of the CF_3 groups to each MO always has some C-F σ^* character instead of the carbon 2p orbital character alone.

As for the middle four levels ($3a_1$ + $2a_1$ +$1b_1$ +$1a_2$) of the fragment $Pt(CF_3)_2$, it can be seen from the correlation diagram that the $2a_1$ orbital and, to a less extent, the $3a_1$ orbital are stabilized by the symmetric mixing with the a_1 combination of C_2H_4 π-orbitals. On this basis the $3a_1$ orbital can be considered as having largely non-bonding Pt 5d character though it is involved in σ-bonding to C_2H_4 and σ^*-antibonding to CF_3. The orbitals $1a_2$ and $1b_1$ of the fragment $Pt(CF_3)_2$ are predicted to be stabilized on formation of cis-$[Pt(CF_3)_2(C_2H_4)_2]$, which is perhaps surprising since both the $1b_1$ and $1a_2$ orbitals are expected to be stabilized by back-bonding to the C_2H_4 π^*-orbitals, as calculated for cis-$[PtMe_2(C_2H_4)_2]$ (Figure 3.4(a)). This "unexpected" result could be understood by the following considerations. On the one hand, the energy gap between the filled platinum $5d\pi$ ($1a_2$ +$1b_1$) orbitals and the empty C_2H_4 π^* orbitals is greater in the fragment $Pt(CF_3)_2$ than in the fragment $PtMe_2$ (see Figure 3.4 (a) and (b)), which leads to weaker back-bonding between the $Pt(CF_3)_2$ and $(C_2H_4)_2$ groups; on the other hand, low energy Pt $5d\pi$ orbitals will have better energy matching with the filled C-H orbitals of the ligand C_2H_4, and thus there is stronger filled-filled orbital interaction in a pseudo-π manner between them. This filled-filled orbital interaction then will stabilize the C-H based orbitals but destabilize the platinum $5d\pi$ orbitals since the C-H orbitals are expected to be located at lower energy than the $5d\pi$ orbitals. Indeed the Xα-SW calculations for cis-$[Pt(CF_3)_2(C_2H_4)]_2$ show considerable H-character in the orbital $1a_2$ and $1b_1$, especially in $1a_2$ (see Table 3.3), consistent with C_2H_4 acting also as a pseudo π-donor in this molecule. The destabilization of the Pt $5d\pi$ orbitals apparently is the overall result of both the π-acceptor and π-donor properties of C_2H_4 displayed in this case.

3.3.2 The Complex cis-[Pt(CF_3)$_2$(PH_3)$_2$]

The results for this molecule are similar to those for cis-[Pt(CF_3)$_2$(C_2H_4)$_2$] and so are treated more briefly (Figure 3.4(c) and Table 3.4).

Compared to cis-(C_2H_4)$_2$, the lone pair orbitals of the two PH_3 interact more strongly with the $1b_2$ and $1a_1$ levels of the fragment Pt(CF_3)$_2$, leading to both CF_3 and PH_3 having comparable contributions to the MO's $1b_2$ and $1a_1$. In contrast, the PH_3 lone pairs interact less strongly with the $4a_1$ and $2b_2$ levels, resulting in the $4a_1$ MO having largely Pt-CF_3 character and the $2b_2$ MO being fairly evenly distributed among Pt, CF_3 and PH_3 groups (Table 3.4). In addition, the orbitals $3a_1$, $2a_1$, $1a_2$ and $1b_1$, which were identified earlier as having mostly Pt 5d character, are less strongly perturbed by additional mixing with PH_3 compared with C_2H_4. It is also interesting to note that all of the upper valence occupied orbitals of the fragment Pt(CF_3)$_2$ increase in energy by taking on cis-(PH_3)$_2$. This is a reflection of the significant charge transfer to the fragment Pt(CF_3)$_2$ from the ligand PH_3.

Compared to cis-[PtMe$_2$(PH_3)$_2$], the orbital interactions between the fragments PtMe$_2$ and (PH_3)$_2$ are rather similar to those between the fragments Pt(CF_3)$_2$ and (PH_3)$_2$. But more charge transfer to Pt(CF_3)$_2$ from the PH_3 is implied by the relative energy shifts of the Pt(CF_3)$_2$ and PtMe$_2$ orbitals, especially for the non-bonding Pt 5d orbitals, upon PH_3 attachment (see Figure 3.4 (c) and Figure 2.10 of chapter 2).

3.4 SPECTRAL ASSIGNMENT AND INTERPRETATION

3.4.1 The complex [Pt(CF_3)$_2$(COD)]

The low I.E. region of the fitted spectrum is given in Figure 3.2(a). Five of the six bands (B-F) could be fitted to single Lorentzian-Gaussian shapes. Band A is clearly asymmetric and thus was fitted to two peaks with a separation of 0.20±0.04 eV (~1600±320 cm^{-1}), comparable to the separation of 0.17±0.02 eV (~1400±160

Table 3.4. Xα-SW results for cis-[$Pt(CF_3)_2(PH_3)_2$] (C_{2v}) upper valence orbitals

Orbital	Energy(eV)[a]		Charge Distribution (%)						
			Pt	C	P	F	H	Inter	Outer
$4a_1$	5.13	7.65	10s, $6p_z$, $25d_{z^2}$	5s, 17p	3p	17p		16	1
$2b_2$	5.56	8.05	$13p_y$, $3d_{yz}$	5s, 17p	3s, 25p	15p	4	15	
$3a_1$	5.63	8.10	8s, $7p_z$, $23d_{x^2-y^2}$	1s, 5p	1s, 27p	2p	5	19	2
$1b_1$	6.38	9.11	$86d_{xz}$		2d	2p	3	7	
$2a_1$	6.51	9.22	$79d_{z^2}$	1p	2p, 3d	3p	5	7	
$1a_2$	6.55	9.27	$83d_{xy}$		3d	1p	4	9	
$1a_1$	8.53	11.08	6s, $36d_{x^2-y^2}$	1s, 4p	18p, 2d	20p	7	4	2
$1b_2$	9.40	11.97	$41d_{yz}$	1s, 4p	19p, 2d	20p	10	3	

[a]See the footnote of the Table 3.3.

cm-1) of the band A in [$PtMe_2$(COD)] which was assigned due to vibrational splitting of the C=C bond. Therefore, this splitting is also assigned to vibrational coupling and indicates that the HOMO has substantial platinum-alkene bonding character, as is predicted by the Xα-SW calculation on the model compound cis-[$Pt(CF_3)_2(C_2H_4)_2$]. The relatively large error in energy is due to the poor resolution of the vibrational splitting in this band. Band B is assigned to the orbital $2b_2$ based on the Xα-SW calculation. Vibrational splitting of this band would be expected, since much C=C ligand character in this MO was predicted theoretically (Table 3.3), but was not resolved because of overlap with band C (Figure 3.2(a)). It is then natural to assign the next four bands (C-F) to ionizations of four orbitals with mostly Pt 5d character. There is no experimental evidence to aid assignment of each band to a specific d-orbital and so the assignments in Table 3.1 are based on the Xα-SW predictions only.

Consider next the energy shift of the alkene π-orbitals on coordination. Free COD shows one π ionization band at 9.06 eV,[22] while the σ-orbitals in cis-[$Pt(CF_3)_2(C_2H_4)_2$] having most character of the alkene π-orbitals are $4a_1$ and $2b_2$, which appear in the spectrum at 9.00/9.20 eV (vibrational coupling) and 9.80 eV respectively. This indicates that the π-orbitals are stabilized on coordination, suggesting that the alkene σ-donation is more important than its π-acceptance, in agreement with the theoretical prediction of Figure 3.4(b).

3.4.2 The complex [$Pt(CF_3)_2$(TMED)]

The He I and He II spectra in the low I.E. region are displayed in Figure 3.3 and they are very similar to the spectra of [$PtMe_2$(TMED)]. By comparison, bands (A-B) are assigned to platinum-ligand σ-MO's and bands (C-F) to four MO's having mostly Pt 5d character as given in Table 3.1.

In [$PtMe_2$(TMED)], band A was split into two peaks with a separation of 0.13±0.02 eV and this splitting was assigned to the C-N vibrational coupling. The C-N vibrational splitting of the band B was also expected on the basis of an Xα-SW calculation on cis-[$PtMe_2(NH_3)_2$] but was not resolved because of its closeness to band C. In the complex [$Pt(CF_3)_2$(TMED)], bands A and B are both asymmetric and they were fitted as two peaks with separations of 0.19±0.04 eV and 0.20±0.04 eV respectively. These splittings could be assigned to the C-N vibrational coupling although the separations here are somewhat larger than that observed in [$PtMe_2$(TMED)]. There are two reasons causing the larger separations. First is the relatively large error in the energy determinations due to the poor resolution of the vibrational splittings of the bands A and B. The theoretical calculation has predicted that the first two MO's with higher energies in cis-[$PtMe_2(NH_3)_2$] contain a large contribution from the methyl groups. Although we did not perform the calculation for cis-[$Pt(CF_3)_2(NH_3)_2$], the first two MO's are expected to have significant CF_3 character, since CF_3 substitution does not change the general MO sequence, as calculated for phosphine and ethylene compounds. Therefore the second possible reason may be due to both C-N and C-F stretching vibrational modes of the same symmetry being excited upon molecular ionization. In this case, frequency comparisons between molecule and ion become meaningless, as pointed out by Eland.[23] As in the spectrum of [$PtMe_2$(TMED)], the fourth band labelled D, E has about twice the area of the other bands and is thus assigned as due to two almost degenerate Pt d_π orbitals, d_{xz} ($1b_1$) and d_{xy} ($1a_2$). The assignments for the other bands are made in a similar way as for [$PtMe_2$(TMED)].

3.4.3 The Complexes cis-[$Pt(CF_3)_2(PEt_3)_2$] and cis-[$Pt(CF_3)_2(AsMe_3)_2$]

The low I.E. regions of the spectra for these complexes are similar, as shown in Figure 3.2(b) and (c). The spectra are less resolved than those for the complexes discussed above, but the spectra were fitted mostly satisfactorily with six bands. In no case band A or B show resolved vibrational structure, in contrast to the observations for the COD and TMED complexes. The responsible reasons for the unresolved vibrational couplings in these complexes have been discussed in chapter 2.

The spectra give very similar He II:He I intensity ratios (Table 3.1) and ionization energies of all bands shift by a similar amount when compared to the corresponding methylplatinum complexes. Thus it is again not possible to distinguish between the metal orbitals and the metal-ligand σ-MO's on an experimental basis. Therefore the spectral assignments given in Table 3.1 are based on the predictions of the Xα-SW calculations on cis-$[Pt(CF_3)_2(PH_3)_2]$, and are similar to those for the corresponding dimethylplatinum(II) complexes.

3.5 Pt-CF_3 BONDING AND THE CF_3 LIGAND EFFECT

From the preceding discussions, at least two features of Pt-CF_3 bonding in these complexes can be summarized as follows: (a) There is considerable C-F antibonding character with significant carbon 2s character in the Pt-CF_3 bonds. In contrast, there is essentially only the carbon 2p contribution to the σ-donor orbital of the methyl group in the Pt-CF_3 bonding. (b) π interactions between the filled d_π orbitals on platinum and σ* orbitals of perfluoromethyl group are very weak as evidenced by the very small fluorine character present in the MO's $1b_1$ and $1a_2$. Since similar platinum 6s character is predicted in both Pt-CF_3 and Pt-CH_3 bonds by Xα-SW calculations, in agreement with their comparable NMR trans influence,[5-7] the observed Pt-C shortening (0.04-0.06 Å)[4,24] in bis(trifluoromethyl)platinum(II) complexes compared to dimethylplatinum(II) complexes could only be explained in terms of the different carbon 2s contributions. In forming a bond with platinum, the perfluoromethyl group will naturally approach closer than the methyl group to Pt atom because of its greater

2 OF/DE 2

discussed above, but the spectra were fitted mostly satisfactorily with six bands. In no case band A or B show resolved vibrational structure, in contrast to the observations for the COD and TMED complexes. The responsible reasons for the unresolved vibrational couplings in these complexes have been discussed in chapter 2.

The spectra give very similar He II:He I intensity ratios (Table 3.1) and ionization energies of all bands shift by a similar amount when compared to the corresponding methylplatinum complexes. Thus it is again not possible to distinguish between the metal orbitals and the metal-ligand σ-MO's on an experimental basis. Therefore the spectral assignments given in Table 3.1 are based on the predictions of the Xα-SW calculations on cis-[$Pt(CF_3)_2(PH_3)_2$], and are similar to those for the corresponding dimethylplatinum(II) complexes.

3.5 Pt-CF_3 BONDING AND THE CF_3 LIGAND EFFECT

From the preceding discussions, at least two features of Pt-CF_3 bonding in these complexes can be summarized as follows: (a) There is considerable C-F antibonding character with significant carbon 2s character in the Pt-CF_3 bonds. In contrast, there is essentially only the carbon 2p contribution to the σ-donor orbital of the methyl group in the Pt-CF_3 bonding. (b) π interactions between the filled d_π orbitals on platinum and σ* orbitals of perfluoromethyl group are very weak as evidenced by the very small fluorine character present in the MO's $1b_1$ and $1a_2$. Since similar platinum 6s character is predicted in both Pt-CF_3 and Pt-CH_3 bonds by Xα-SW calculations, in agreement with their comparable NMR trans influence,[5-7] the observed Pt-C shortening (0.04-0.06 Å)[4,24] in bis(trifluoromethyl)platinum(II) complexes compared to dimethylplatinum(II) complexes could only be explained in terms of the different carbon 2s contributions. In forming a bond with platinum, the perfluoromethyl group will naturally approach closer than the methyl group to Pt atom because of its greater carbon 2s contribution. This interpretation is in accord with Fenske-Hall calculations on $(CF_3)Mn(CO)_5$ and $(CH_3)Mn(CO)_5$.[15]

The combined results of this study on bis(trifluoromethyl)platinum(II) complexes with that on the corresponding dimethylplatinum(II) complexes suggest that the CF_3 substituent, R = CF_3, causes greater σ-donation from the ligand L to platinum, as in the phosphine complexes cis-[PtR_2L_2] (Figure 3.4 (c)), and less π back-donating from platinum to the ligand L, as in the alkene complex (Figure 3.4(b)), compared to their derivatives with R = CH_3. The overall effect still results in more positive charge on platinum as shown experimentally by the higher ionization energies of the Pt 5d orbitals when R = CF_3. The greater positive charge on platinum will naturally lead to the deactivation of the metal center toward oxidative addition, in agreement with the chemical observations. In addition, the higher ionization energies of the platinum 5d as well as the σ orbitals account at least in part for the higher thermal stability of the perfluoromethyl complexes.

3.6 CONCLUSIONS

The UV photoelectron spectra of the cis-bis(trifluoromethyl)platinum(II) complexes can be assigned by comparison with the Xα-SW predictions based on the model compounds cis-[$Pt(CF_3)_2(C_2H_4)_2$] and cis-[$Pt(CF_3)_2(PH_3)_2$], and by comparison with the spectra of the corresponding dimethylplatinum(II) complexes. The first two ionization energies are assigned to the platinum-ligand σ orbitals followed by the essentially non-bonding platinum 5d orbitals. The nature of the Pt-CF_3 σ bonding has been discussed using Xα-SW results. The CF_3 contribution to the Pt-CF_3 σ bonds arises from the C-F antibonding orbitals with considerable carbon 2s character, rather than pure carbon 2p character.

3.7 REFERENCES

1. R. B. King and M. B. Bisnette, J. Organomet. Chem., 2, 15 (1964).
2. H. C. Clark and L. E. Manzer, J. Organomet. Chem., 59, 411 (1973).
3. M. A. Bennett, H. K. Chee, J. C. Jeffrey, and G. B. Robertson, Inorg. Chem., 18, 1071 (1979).
4. L. Manojlovic-Muir, K. W. Muir, T. Solomun, D. W. Meek, and J. L. Peterson, J. Organomet. Chem., 146, C26 (1978).
5. T. G. Appleton, M. H. Chisholm, H. C. Clark, and L. E. Manzer, Inorg. Chem., 11, 1786 (1972).
6. T. G. Appleton and M. A. Bennett, Inorg. Chem., 17, 738 (1978).
7. M. A. Bennett, H. K. Chee, and G. B. Roberston, Inorg. Chem., 18, 1061 (1979).
8. T. G. Appleton, H. C. Clark, and L. E. Manzer, J. Organomet. Chem., 65, 275 (1974).
9. T. G. Appleton, J. R. Hall, D. W. Neale, and M. A. Williams, J. Organomet. Chem., 276, C73 (1984).
10. T. G. Appleton, R. D. Berry, J. R. Hall, and D. W. Neale, J. Organomet. Chem., 342, 399 (1988).
11. F. A. Cotton and J. A. McCleverty, J. Organomet. Chem., 2, 15 (1964).
12. H. C. Clark and J. H. Tsai, J. Organomet. Chem., 7, 515 (1967).
13. W. A. G. Graham, Inorg. Chem., 7, 315 (1968).
14. M. P. Johnson, Inorg. Chim. Acta, 3, 232 (1969).
15. M. B. Hall and R. F. Fenske, Inorg. Chem., 11, 768 (1972).
16. J. E. Drake, R. Eujen, and K. Gorzelska, Inorg. Chem., 21, 1784 (1982).
17. I. Lindau and J. J. Yeu. At. Nucl. Data. Tables, 32, 1 (1985).
18. S. Elbel, H. Bergmann, and W. Enblin, J. Chem. Soc. Faraday Trans.(II), 70, 555 (1974).

19. D. L. Bristow and G. M. Bancroft, J. Am. Chem. Soc., 105, 5634 (1983).

20. B. W. Yates, K. H. Tan, G. M. Bancroft, L. L. Coatsworth, and J. S. Tse, J. Chem. Phys., 83, 4906 (1985).

21. B. W. Yates, K. H. Tan, G. M. Bancroft, and J. S. Tse, J. Chem. Phys., 85, 3840 (1986).

22. C. Batich, O. Ermer, and E. Heibronner, J. Electron Spectrosc. Relat. Phenom., 1, 333 (1973).

23. J. H. D. Eland, Photoelectron Spectroscopy, 2nd., Butterworth & Co (publishers) Ltd, London, 1984, p.138.

24. J. M. Wisner, T. J. Bartczak, and J. A. Ibers, Organometallics, 5, 2044 (1986).

CHAPTER 4

ELECTRONIC STRUCTURE OF (η^5-CYCLOPENTADIENYL)TRIMETHYLPLATINUM(IV) COMPLEXES

4.1 INTRODUCTION

Gas-phase UV photoelectron spectroscopy (PES) has been useful for understanding the electronic structure of "sandwich" compounds[1-3] and more recently has been extended to include "half-sandwich" or piano-stool compounds.[4-12] In this second class of compounds, the metal is bound to a single carbocyclic ring, with the other ligands (either inorganic or organic) bound to the metal and comprising the "legs" of the stool. The ubiquitous η^5-cyclopentadienyl (Cp) ligand is the most common "bench" in these systems, and thus most of these studies have been devoted to metal cyclopentadienyl carbonyls and their derivatives. In contrast to metal cyclopentadienyl carbonyl compounds, metal cyclopentadienyl alkyls have not been examined in great detail.[3] Because of differences in bonding characteristics of carbonyl (a neutral π-acceptor) versus alkyl (an anionic σ-only donor), significant changes between the electronic structure of these complexes may be expected.

There has been little activity regarding the chemistry of cyclopentadienyl platinum(IV) complexes. Robinson and Shaw first reported the synthesis of $CpPtMe_3$ and deduced from IR and NMR results that the compound was indeed a π complex,[13] a point later substantiated by X-ray structure analysis.[14] Maitlis has reported the synthesis of $[Cp^*PtBr_3PtCp^*]Br_2$ ($Cp^*=\eta^5$-pentamethylcyclopentadienyl), the structure of which was suggested to be an ionic triply bridged binuclear π complex.[15] Interest in chiral organometallic complexes prompted Shaver and coworkers to prepare $[CpPt(CH_3)(CH_2CH_3)(C(O)CH_3)]$, in addition to several polyfunctionalized CpPt(IV) complexes.[16-18] Photolysis of $CpPtMe_3$ in a variety of hydrocarbon solvents indicates the cleavage of the Pt-Me bond to form methyl radicals and an unidentified platinum species.[19] Decomposition of $CpPtMe_3$ in hydrogen and a noble gas over silicon or glass substrates produces impurity-free, polycrystalline films of platinum.[20] It has been reported that η^5-cyclopentadienyl trialkyl platinum(IV) complexes are catalysts in the actinic radiation-activated hydrosilation of alkenes.[21] This reaction is applicable both to the formation of low molecular weight compounds and in the curing of high molecular weight polymers containing unsaturated groups.

Fundamental studies of the electronic structure of these complexes should be important to understand the chemical properties exhibited. This chapter will present a photoelectron study of the upper valence orbitals of $CpPtMe_3$ and Cp^*PtMe_3. The Substitution of Cp by Cp* is expected to have a effect on the ionization energies of the metal and ligand orbitals, because the methyl groups on the Cp* ring have greater electron-releasing or inductive effect than the hydrogen atoms and because one combination of the methyl carbon-hydrogen orbitals has the correct symmetry to interact with the outmost Cp π orbital.[5] The energy effect should be of use in discussing the interaction between Cp and Pt.

4.2 UV PHOTOELECTRON SPECTRA

UV photoelectron spectra for $CpPtMe_3$ and Cp^*PtMe_3 are illustrated in Figures 4.1 and 4.2, respectively. The curve-fitting analysis for the valence bands in the low ionization energy region are reported in Table 4.1. In the region from 11.5 to 16 eV, the spectra show complex unresolved bands which are assigned as arising from ionizations of the cyclopentadienyl ring σ and π a_2'' orbitals, as reported in the spectra of bis(cyclopentadienyl) complexes,[22] and from the ionizations of methyl $\sigma_{C\text{-}H}$

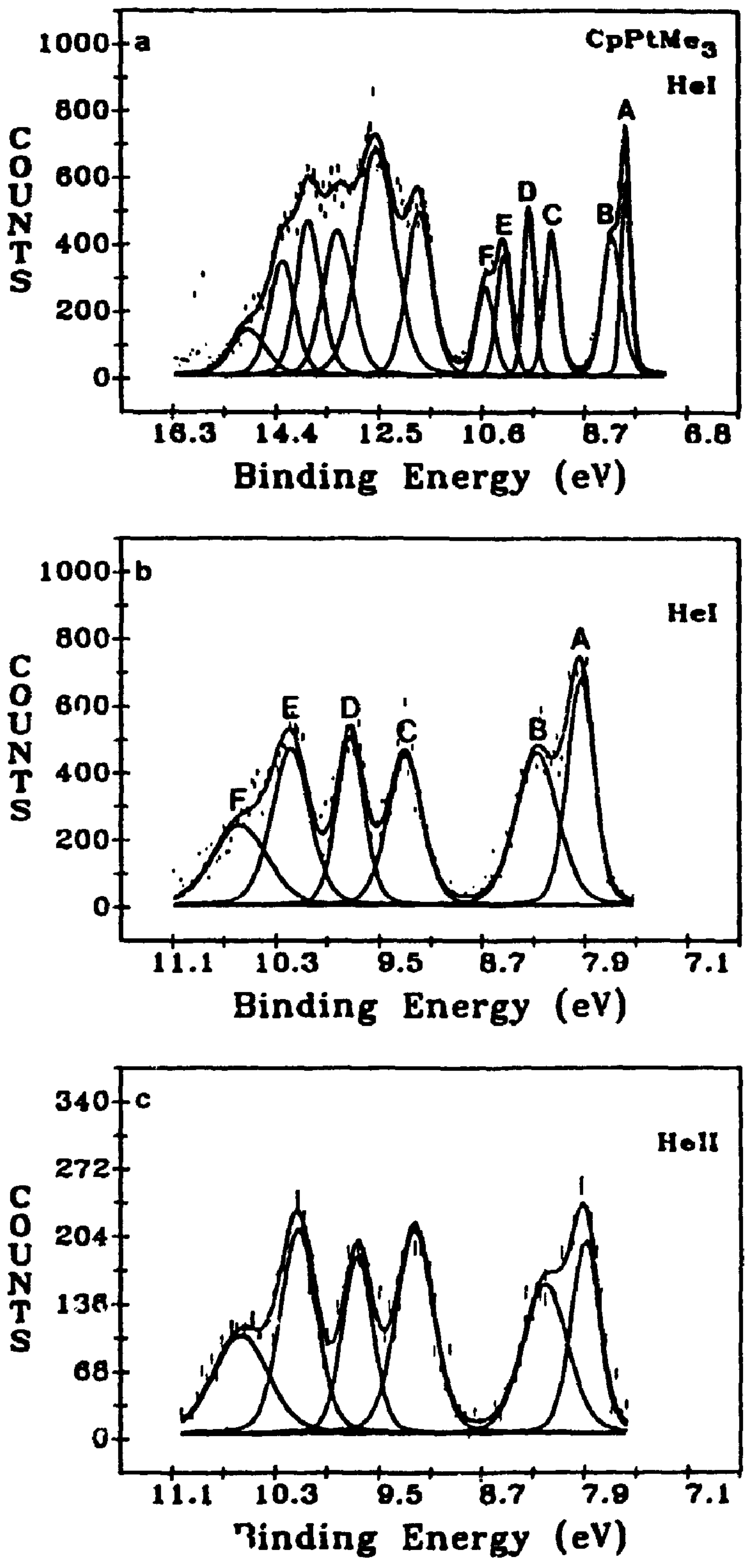

Figure 4.1. Full He I spectrum (a) and expansions of the low-energy region of He I (b) and He II (c) spectra of $CpPtMe_3$

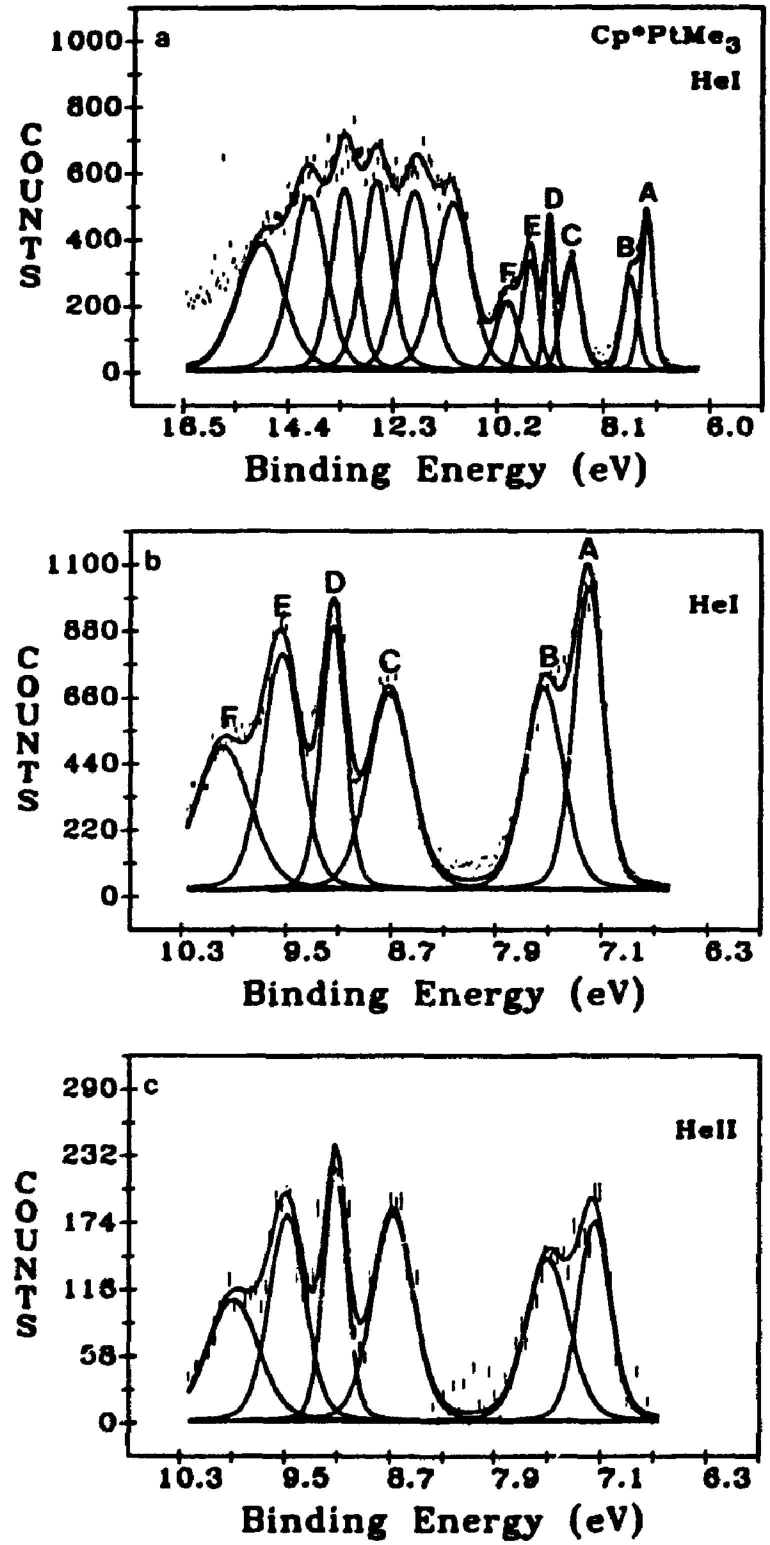

Figure 4.2. Full He I spectrum (a) and expansions of the low-energy region of He I (b) and He II (c) spectra of $Cp^{*}PtMe_3$

Table 4.1. Ionization energies, HeII:HeI intensity ratios, and assignments of the photoelectron spectra of $CpPtMe_3$ and Cp^*PtMe_3

Compound	Band	IE, eV	HeII:HeI Area Ratio[a]			Assignment
$CpPtMe_3$	A	7.90	0.88[b]	0.78[c]	1.68[d]	Cp-Pt-Me
	B	8.20	0.92	0.66	1.69	Cp-Pt-Me
	C	9.29	1.18	0.79	1.39	Cp-Pt-Me
	D	9.71	1.00	1.00	1.00	Pt 5dπ
	E	10.20	1.05	1.01	1.00	Pt 5dπ
	F	10.60	1.03	0.87	1.00	Cp-Pt-Me
Cp^*PtMe_3	A	7.19	0.85			Cp*-Pt-Me
	B	7.53	0.92			Cp*-Pt-Me
	C	8.71	1.10			Cp*-Pt-Me
	D	9.14	1.00			Pt 5dπ
	E	9.53	0.99			Pt 5dπ
	F	9.98	0.96			Cp*-Pt-Me

[a]The HeII:HeI area ratios are referenced to band D.

[b]experiment results; [c]from Xα-SW assignment; [d]from Fenske-Hall assignment.

bonding orbitals in metal alkyls.[23] A minimum number of peaks to adequately simulate this region have been fitted. These ionizations are not of significance to the valence electronic structure and will not be discussed further. Cp*PtMe$_3$ (Figure 4.2) displays an additional band at 11.08 eV which is associated with the ring methyl groups.[24] Ionization bands in the range of 7-10.5 eV are well resolved compared to those at higher energy. The first set of bands (A-B) is well separated from the subsequent bands (C-F). It is also evident that all of the bands in the 7-10.5 eV region are shifted by approximately 0.65±0.05 eV to lower energy upon ring permethylation. The energy shifts due to the Cp ring methylation were also observed in the previous photoelectron studies of cyclopentadienyl metal complexes.[5,7] This is evidence for a largely inductive and hyperconjugative influence of the methyl groups on the electronic structure of the entire molecule. Finally it is noted in the low ionization energy region that the He II:He I area ratios for all of the bands are not significantly different. These bands (A-F) will receive primary attention in the subsequent discussion.

4.3 THEORETICAL RESULTS AND SPECTRAL INTERPRETATION

Since the spectra of both complexes in the low ionization energy region are very similar (see Figures 4.1 and 4.2 and Table 4.1), the discussion that follows is applicable to both.

As mentioned above, all the ionization bands have similar energy shifts upon the ring permethylation and similar He II/He I intensity ratios. This means that the experimental information does not give evidence for a definite assignment of the bands A-C, E and F. Therefore molecular orbital results from Fenske-Hall and Xα-SW methods will be correlated with the experimental observations in the following discussion.

Fenske-Hall calculations for the molecule $CpPtMe_3$ have been performed by Bursten and McKee.[25] Molecular energies and character of the eight upper occupied MO's are presented in Table 4.2. The Fenske-Hall calculations predict that the three Pt 5dπ orbitals (5a′, 3a″ and 4a′ in Table 4.2) have the lowest binding energy and non-bonding character. This quantitative MO result for $CpPtMe_3$ is in accord with the well established, qualitative MO descriptions for $CpML_3$ molecules, where M is a transition metal and L is an arbitrary ligand with only σ-donor capability.[26] Qualitative MO analysis of $CpML_3$ assumes that the ML_3 fragment is a fac-ML_3 fragment of an octahedral ML_6 complex and that capping the ML_3 fragment with a Cp ligand preserves the octahedral geometry about the metal.[26-28] Therefore, a d^6 $CpML_3$ molecule remembers its octahedral parentage, six electrons filling in the three non-bonding, nearly degenerate dπ orbitals ("t_{2g}"),[29-35] although it has only C_s symmetry! The Pt 5dπ orbitals are followed by three Pt-Me σ MO's. Two of three Me σ combinations interact strongly with the 5dσ ("e_g") set orbitals on Pt to generate 2a″ and 3a′ MO's, while the other Me σ combination interacts almost exclusively with the Pt 6s and 6p orbitals to give 2a′ MO (Table 4.2). What remains are the two Pt-Cp bonding orbitals (1a″ and 1a′ in Table 4.2), formed by the Cp e_1'' π orbitals (e_1'' under D_{5h}; a′ + a″ under C_s) interacting with the Pt 5dσ orbitals.

Based on this Fenske-Hall prediction, the bands A and B were assigned as the ionizations of the three non-bonding Pt 5dπ orbitals (5a′, 3a″ and 4a′ orbitals in Table 4.2), the bands C and D as the Pt-Me orbitals (2a″, 3a′ and 2a′), and the bands E and F as the Pt-Cp (or Pt-Cp*) orbitals (1a″ and 1a′). This assignment of the metal and metal-ligand ionizations for $CpPtMe_3$ and Cp^*PtMe_3 (Pt 5dπ < Pt-Me < Pt-Cp, in the ordering of the ionization energy) shows agreement with the previous photoelectron studies of cyclopentadienylmetal alkyls[16,17] and

Table 4.2. Fenske-Hall results for CpPtMe$_3$ (C_s) upper valence orbitals[a]

			Charge Distribution (%)			
MO(Cs)	Energy(eV)	Pt 5d	Pt 6s	Pt 6p	Me	Cp
5a'	10.643	94.8	0.05	1.3	1.0	1.6
3a"	10.644	94.1	0.0	1.5	1.2	1.9
4a'	10.649	97.9	0.35	0.3	0.2	0.6
2a"	13.905	40.6	0.0	7.1	50.8	1.5
3a'	13.917	40.6	0.0	7.1	50.8	1.5
2a'	14.996	1.2	12.1	6.7	73.5	7.0
1a"	15.002	13.2	1.0	5.5	6.1	73.7
1a'	15.006	14.0	0.2	5.5	1.1	78.5

[a]From reference 25.

bis(cyclopentadienyl)metal alkyls,[38] but disagreement with the photoelectron studies of Cp^*IrMe_4 and $Cp^*IrMe_2(OSMe_2)$.[9] Furthermore, assigning the bands A and B to the pure Pt $5d\pi$ non-bonding orbitals, and the bands C and D to the Pt-Me σ orbitals does not appear to be consistent with the observation that their energy shifts are as large as for the bands E and F, since the non-bonding Pt 5d and the Pt-Me σ orbitals are expected to be shifted less in energy than the cyclopentadienyl-based orbitals on going from $CpPtMe_3$ to Cp^*PtMe_3. This expectation was previously proved in the photoelectron studies of other metal cyclopentadienyl complexes.[5,7] For example, from $CpMn(CO)_3$ to $Cp^*Mn(CO)_3$, the ionization energy of the non-bonding Mn 3d orbitals decreases by 0.59 eV, while that of the Cp π orbital decreases by 1.19 eV.[5]

Attempting to obtain a better correlation between theoretical calculations and experimental observations, we performed Xα-SW calculations for the molecule $CpPtMe_3$ under C_s symmetry, choosing the xz plane as the symmetry plane and the axis z along the left-right direction. The Xα-SW results for the upper eight occupied MO's are presented in Table 4.3. Apparently, the Xα-SW results are quite different from those of the Fenske-hall method (see Tables 4.2 and 4.3). According to the Xα-SW calculations, the three Pt $5d\pi$-based MO's split into two sets: one consists of two nearly degenerate orbitals 1a" and 2a', formed by two of the Pt $5d\pi$ orbitals backdonating their electrons into the e_2" orbitals (e_2" under D_{5h}; a' + a" under C_s) (see Table 4.3); the other is the 3a' orbital, formed by the filled-filled orbital interactions between one of the Pt $5d\pi$ orbitals and the Cp a_2" orbital (a_2" under D_{5h}; a' under C_s) in an antibonding way. This results in an energy gap of 1.3 eV between the two sets of the Pt $5d\pi$ based MO's (see Table 4.3). It is also noted that significant Me character is mixed into the Pt $5d\pi$ orbitals, presumably due to the ground-state distortion of the $PtMe_3^+$ fragment from a fac-ML_3 structure of an octahedral ML_6 molecule. The crystal structure of $CpPtMe_3$[14] indeed shows that the

Table 4.3. Xα-SW results for $CpPtMe_3$ (C_s) upper valence orbitals

		Charge Distribution (%)[a]				
MO(Cs)	Energy(eV)[b]	Pt 5d	Pt 6s	Pt 6p	Me	Cp
5a′	6.16	27.3	3.6	1.6	43.7	23.8
3a″	7.07	19.1	0.0	2.1	54.5	24.2
4a′	8.24	5.6	4.7	11.2	37.0	41.4
2a″	8.73	46.0	0.0	4.6	28.2	21.2
3a′	9.14	71.9	0.7	1.5	18.8	7.0
2a′	10.40	78.5	0.0	0.0	14.7	6.9
1a″	10.43	63.0	0.0	0.6	14.9	21.5
1a′	10.75	35.4	5.7	3.1	42.4	13.4

[a]In order to compare with the Fenske-Hall results (Table 4.2), the charge distributions are not usual atomic sphere charge contributions, but rather normalized atomic charges which approximately take into account the intersphere and outersphere charge densities by reproportioning them back onto the appropriate atomic spheres.
[b]Calculated by the removal of a half of an electron from the HOMO (5a′).

mean Me-Pt-Me angle is 85.4°, a 4.6° deviation from a ideal fac-ML_3 type of structure. The Pt $5d_\pi$-based orbitals are calculated to be unevenly sandwiched between the Pt-ligand σ orbitals. Above the Pt $5d_\pi$-based MO's, there are four Pt-ligand orbitals (2a", 4a′, 3a" and 5a′) (see Table 4.3). Three MO's (2a", 3a" and 5a′) are formed by the Pt $5d_\sigma$ orbitals probably bonding to the Me σ orbitals but anti-bonding to the Cp e_1" orbital, while the 4a′ orbital is formed by predominantly Pt $6p_x$ orbital mixed into both Me and Cp ligand orbitals. Underneath the Pt $5d_\pi$ based MO's, there is the 1a′ MO consisting of the Pt $5d_\sigma$ (a′) orbital bonding to the Me σ and the Cp e_1" orbitals.

On the basis of the Xα-SW calculations for $CpPtMe_3$, we propose the spectral assignment as shown in Table 4.1, i.e., the Bands A (corresponding to the ionization of MO 5a′ in Table 4.3), B (3a"), C (4a′+2a") and F (1a′) arise from the ionizations of the Pt-ligand σ orbitals, while the bands D (3a′)and E (2a′+1a") arise from the ionizations of the Pt $5d_\pi$-based orbitals, with some Cp character in the ionization band E. This assignment gives a good correlation of the theoretical MO results with the experimental ionization shifts. For example, the similar ionization energy shifts of all bands upon ring permethylation can be explained in terms of extensive mixing between the platinum and the ligand orbitals in all upper valence MO's.

Finally, to compare the Xα-SW and Fenske-Hall assignments, the theoretical He II:He I ratios of the upper eight orbitals of $CpPtMe_3$ were also calculated by using the Gelius atomic model[39], as discussed in Chapter 2. The calculated ratios are presented in Table 4.1. There is a satisfactory agreement between the experimental and Xα-SW intensity ratios, with a maximum error of about 30% in band C. But there is an error of about a factor of two in bands A and B between the experimental intensity ratios and the Fenske-Hall values. This comparison in turn gives a better support to the Xα-SW assignment. A detailed photoionization behaviour regarding the cross sections of $CpPtMe_3$ will be discussed in Chapter 6, by using synchrotron radiation photoelectron results.

4.4 CONCLUSIONS

The photoelectron spectra of $CpPtMe_3$ and Cp^*PtMe_3 can be interpreted well using $X\alpha$-SW calculations. The eight upper filled valence MO's of the complexes are composed of three Pt 5d-based MO's being unevenly sandwiched between the Pt-ligand orbitals, i.e., four at the top and one at the bottom. There are strong interactions between the Pt $5d_{\sigma}$ orbitals with both the Cp e_1'' π and the Me σ sets and significant backdonation from the Pt $5d_{\pi}$ to the empty Cp e_2'' orbitals. The extensive mixing of the platinum orbitals and coordinated ligand orbitals indicates that very effective covalent bonding is present in the high oxidation states of the heavy-transition-metal complexes.

4.5 REFERENCES

1. C. Cauletti and C. Furlani, Struct. Bonding (Berlin), 35, 119 (1978).
2. A. H. Cowley, Prog. Inorg. Chem., 26, 46 (1979).
3. J. C. Green, Struct. Bonding (Berlin), 43, 37 (1981).
4. D. L. Lichtenberger and G. E. Kellogg, Acc. Chem. Res., 20, 379 (1987).
5. D. C. Calabro, J. L. Hubbard, C. H. Blevins, A. C. Campbell and D. L. Lichtenberger, J. Am. Chem. Soc., 103, 6839 (1981).
6. D. C. Calabro and D. L. Lichtenberger, J. Am. Chem. Soc., 103, 1846 (1981).
7. D. L. Lichtenberger, D. C. Calabro and G. E. Kellog, Organometallics, 3, 1623 (1984).
8. N. Dudeney, O. N. Kirchner and J. C. Green, J. Chem. Soc., Dalton Trans., 1877 (1984).
9. D. L. Lichtenberger and J. L. Habbard, Inorg. Chem., 24, 3835 (1985).
10. C. Cauletti, C. Furlani, C. Pauliti and H. Werner, J. Organomet. Chem., 289, 417 (1985).
11. A. Terpstra, J. N. Louwen, A. Oskam and J. H. Teuben, J. Organomet. Chem., 260, 207 (1984).
12. M. T. Ashby, J. H. Enemark, and D. L. Lichtenberger, Inorg. Chem., 27, 191 (1988).
13. S. D. Robinson and B. L. Shaw, J. Chem. Soc., 1529 (1965).
14. G. W. Adamson, J. C. J. Bart and J. J Daly, J. Chem. Soc., (A) 2616 (1971).
15. S. H. Taylor and P. M. Maitlis, J. Organomet. Chem., 139, 121 (1977).
16. A. Shaver, Can. J. Chem., 56, 2281 (1978).
17. G. Hamer and A. Shaver, Can. J. Chem., 58, 2011 (1980).
18. A. Eisenberg, A. Shaver and T. Tsutaui, J. Am. Chem. Soc., 102, 1416 (1980).
19. O. Hackelberg and A. Wojcicki, Inorg. Chim. Acta 44, L63 (1980).

20. Y. J. Chen, H. D. Kaesz, H. Thridandam and R. F. Hicks, Appl. Phys. Lett., 53, 1591 (1988).

21. T. J. Drahnak, U. S. Pat. 4,510,094, (1985).

22. J. W. Rabalais, L. O. Werme, T. Bergmark, L. Karlsson, M. Hussain and K. J. Seigbahn, J. Chem. Phys., 57, 1185 (1972).

23. J. C. Green, D. R. Lloyd, L. Galyer, K. Mertis and G. Wilkinson, J. Chem. Soc., Dalton Trans., 1403 (1978).

24. C. Cauletti, J. C. Green, M. R. Kelly, P. Powell, J. Van Tiborg, J. Robbins and J. Smart, J. Electron Spectrosc. Relat. Phenom., 19, 327 (1980).

25. D. S. Yang, G. M. Bancroft, R. J. Puddephatt, B. E. Bursten and S. D. McKee, Inorg. Chem., 28, 872 (1989).

26. T. A. Albright, J. K. Burdett and M. H. Whangbo, Orbital Interactions in Chemistry; John Wiley and Sons: New York, 1985; Chapter 20 and references therein.

27. P. Kubacek, R. Hoffmann and Z. Havlas, Organometallics 1, 180 (1982).

28. S. D. McKee, R. H. Cayton and B. E. Bursten, Presented at the 19th Central Regional Meeting of the American Chemical Society, Columbus, OH, June 1987; paper 258.

29. M. Elian and R. Hoffmann, Inorg. Chem., 14, 1058 (1975).

30. D. L. Lichtenberg and R. F. Fenske, J. Am. Chem. Soc., 98, 50 (1976).

31. B. E. R. Schilling, R. Hoffmann and D. L. Lichtenberg, J. Am. Chem. Soc., 101, 585 (1979).

32. B. E. R. Schilling, R. Hoffmann and J. W. Faller, J. Am. Chem. Soc., 101, 592 (1979).

33. T. A. Albright, Tetrahedron, 18, 1339 (1982).

34. B. E. Bursten, D. J. Darensbourg, G. E. Kellog and D. L. Lichtenberg, Inorg. Chem., 23, 4361 (1984).

35. T. A. Albright, P. Hoffmann and R. Hoffmann, J. Am. Chem. Soc., 99, 7546 (1977).

36. J. C. Green and S. E. Jackson, J. Chem. Soc., Dalton Trans., 1698 (1976).

37. D. A. Symon and T. C. Waddington, J. Chem. Soc., Dalton Trans., 2140 (1975).

38. J. C. Green, S. E. Jackson and B. J. Higginson, J. Chem. Soc., Dalton Trans., 403 (1975).

39. V. J. Gelius, J. Electron Spectrosc. Relat. Phenom., 4, 985 (1974).

CHAPTER 5

ELECTRONIC STRUCTURE OF (ß-DIKETONATO)TRIMETHYLPLATINUM(IV) COMPLEXES

5.1 INTRODUCTION

Since the discovery of the compound $[PtMe_3(acac)]_2$ (acac = acetylacetonate, $(MeCO.CH.COMe)^-$) in 1928,[1] interest has been shown in the ß-diketone complexes of trimethylplatinum (IV) due to the variety of bonding modes found for these ligands. Complexes $[PtMe_3(RCO.CH.COR')]_x$ (where both R and R' are alkyls) have been found to be dimeric in solution.[2,3] The complexes were initially assumed to have bridging oxygen atoms,[2] but X-ray structure determinations[4-6] have showed that the ß-diketone functions as a tridentate ligand, bonding through both oxygen atoms to one platinum atom and through the central carbon atom to the second platinum atom. These compounds reacted readily with a number of nitrogen donor lignds[7] giving species of the type $[PtMe_3(RCO.CH.COR')L]$ (L=unidentate neutral nitrogen donor ligand) and $[PtMe_3(RCO.CH.COR')L]_2$ (L=bridging bidentate nitrogen donor ligand).[8] In these compounds the ß-diketone acts as a bidentate ligand, coordinating via the oxygen atoms. The compound $[PtMe_3(MeCO.CH.COMe)bipy]$ (bipy=2,2'-bipyridine), however, was shown to contain a unidentate acetylacetonate group bound only through the central carbon atom.[9,10] If the alkyl (R or/and R') group(s) in the complexes $[PtMe_3(RCO.CH.COR')]_x$ is/are replaced by trifluoromethyl group(s), the resulting complexes have been shown to be monomers, with an additional ligand on the sixth coordination site of the platinum atom, such as $[PtMe_3(MeCO.CH.COCF_3)H_2O]$.[11,12]

Previous studies on the ß-diketone complexes of trimethylplatinum(IV) include chemical reactions,[7] thermoanalysis,[12] X-ray diffraction,[5,6,12] NMR,[13-16] IR, UV and mass spectrometry.[10,15] None of them can provide direct information about the relative energies of the upper occupied valence orbitals, in particular the σ Pt-ligand and Pt 5d orbitals in these molecules. This chapter will discuss the electronic structure, in terms of the orbital ionization energy and electron distribution, of molecules $[PtMe_3(acac)]_2$, $[Me_3Pt(tfa)H_2O]$ (tfa = trifluoroacetylacetonate), $[PtMe_3(tfa)Me_2S]$ and $[PtMe_3(hfa)H_2O]$ (hfa = hexafluoroacetylacetonate), using UV photoelectron spectroscopy, as well as Xα-SW calculation on the model molecule $[PtMe_3(HCO.CH.COH)]$. The electronic structure of this type of molecule would be different from that of the (η^5-cyclopentadienyl)trimethylplatinum(IV) (discussed in Chapter 4), since the cyclopentadienyl ligand is a "soft" ligand, while the diketone is a "hard" ligand.

5.2 UV PHOTOELECTRON SPECTRA

Representative UV photoelectron spectra are presented in Figures 5.1-5.5. For the compound $[PtMe_3(acac)]_2$, we started collecting the spectrum at 90°C and ended at 185°C. The unique, reproducible He I spectrum (Figure 5.2) could only be obtained above 125°C. This implies that the compound is a monomer ($[PtMe_3(acac)]$) at temperatures above 125°C. The curve-fitting analyses for the valence bands in the low ionization energy region are reported in Table 5.1.

In the region >11 eV , the spectra show broad envelopes, and a minimum number of bands to adequately simulate this region has been fitted (Figure 5.1). Band J (~17 eV) in Figure 5.1(b-d) is absent in Figure 5.1(a). This band is assigned to the ionizations of C-F σ orbitals.[17] Band I (~15 eV) shows a great He II intensity enhancement (Figure 5.1(d)) and thus it is associated with fluorine 2p lone pair ionizations.[17-19] Bands G and H show reduced He II intensities and they probably arise from a large number of non-fluorine ligand orbital ionizations, as well as low

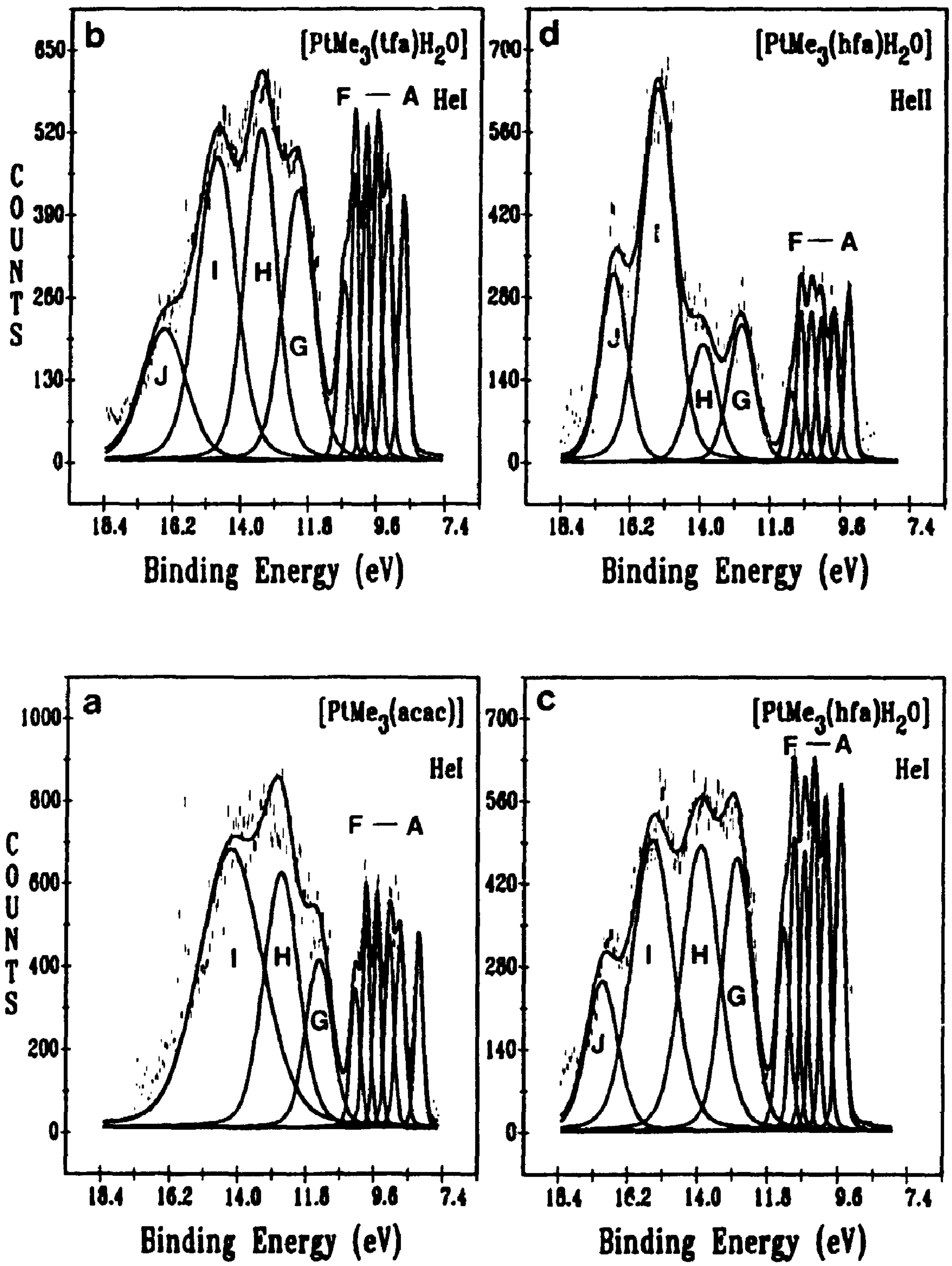

Figure 5.1. He I spectra of (a) [PtMe$_3$(acac)] and (b) [PtMe$_3$(tfa)H$_2$O] and He I (c) and He II (d) spectra of [PtMe$_3$(hfa)H$_2$O].

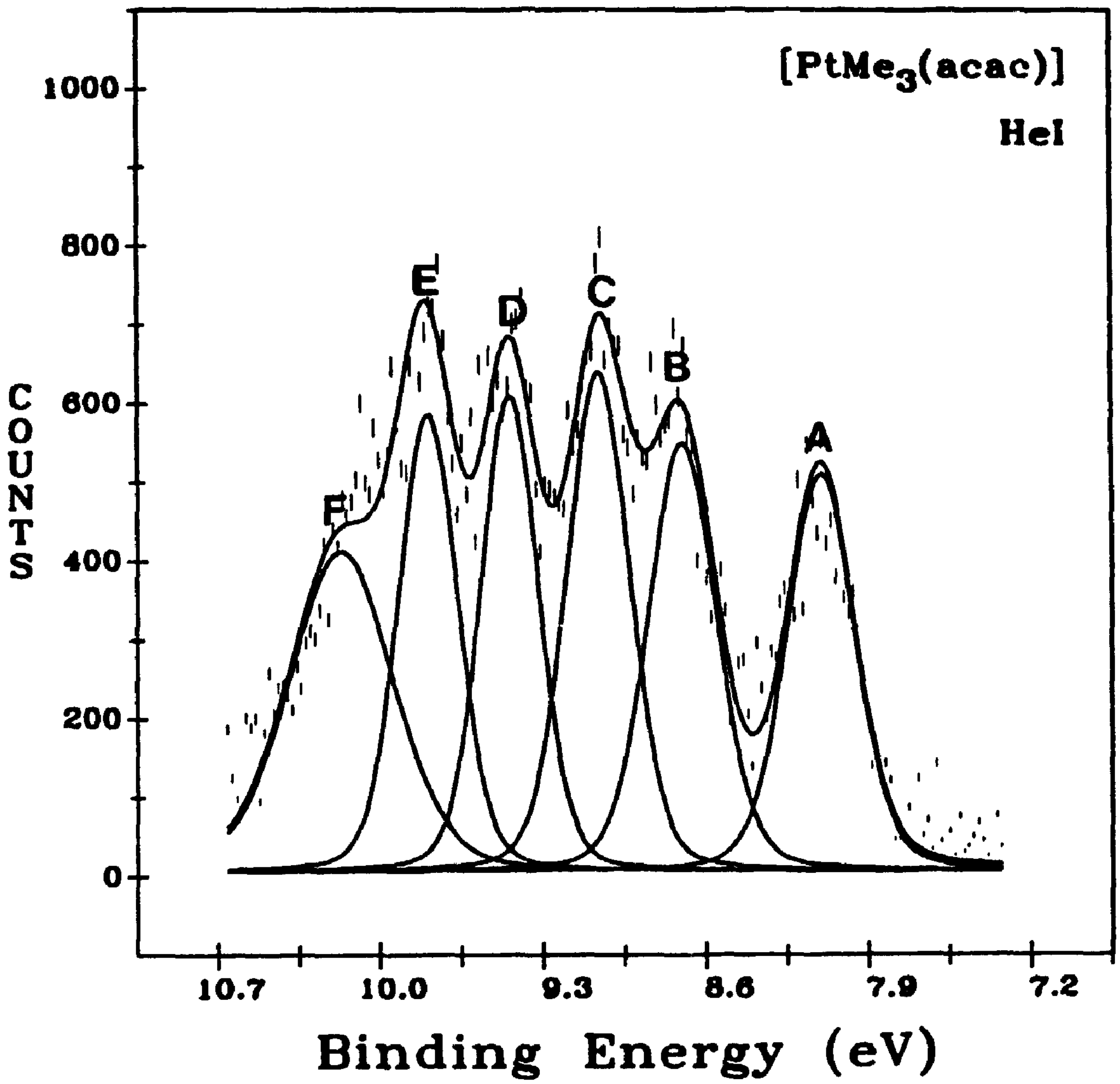

Figure 5.2. Expansion of the low-energy region of the He I spectrum of $[PtMe_3(acac)]$.

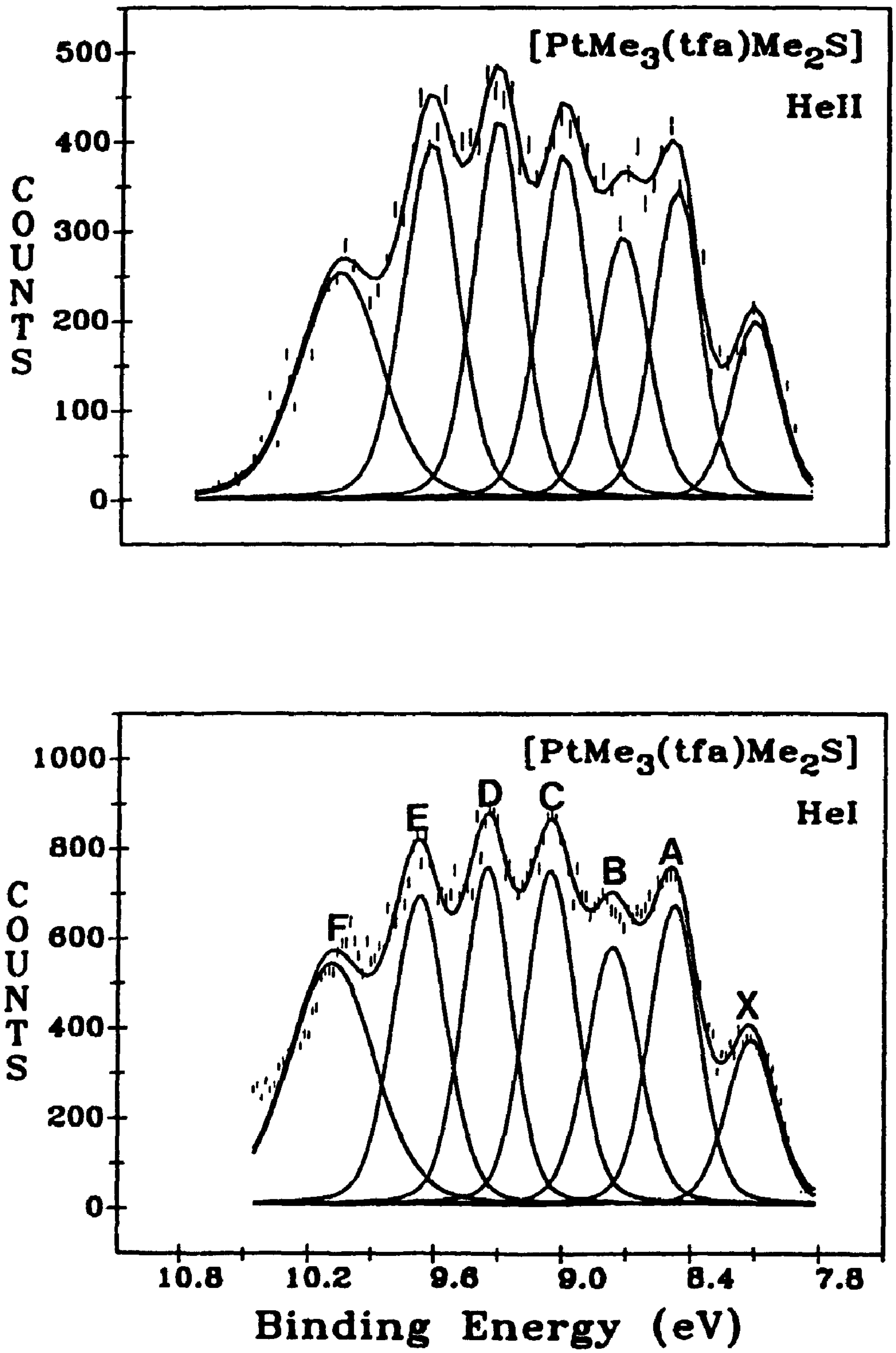

Figure 5.3. Expansions of the low-energy region of the He I and He II spectra of $[PtMe_3(tfa)Me_2S]$.

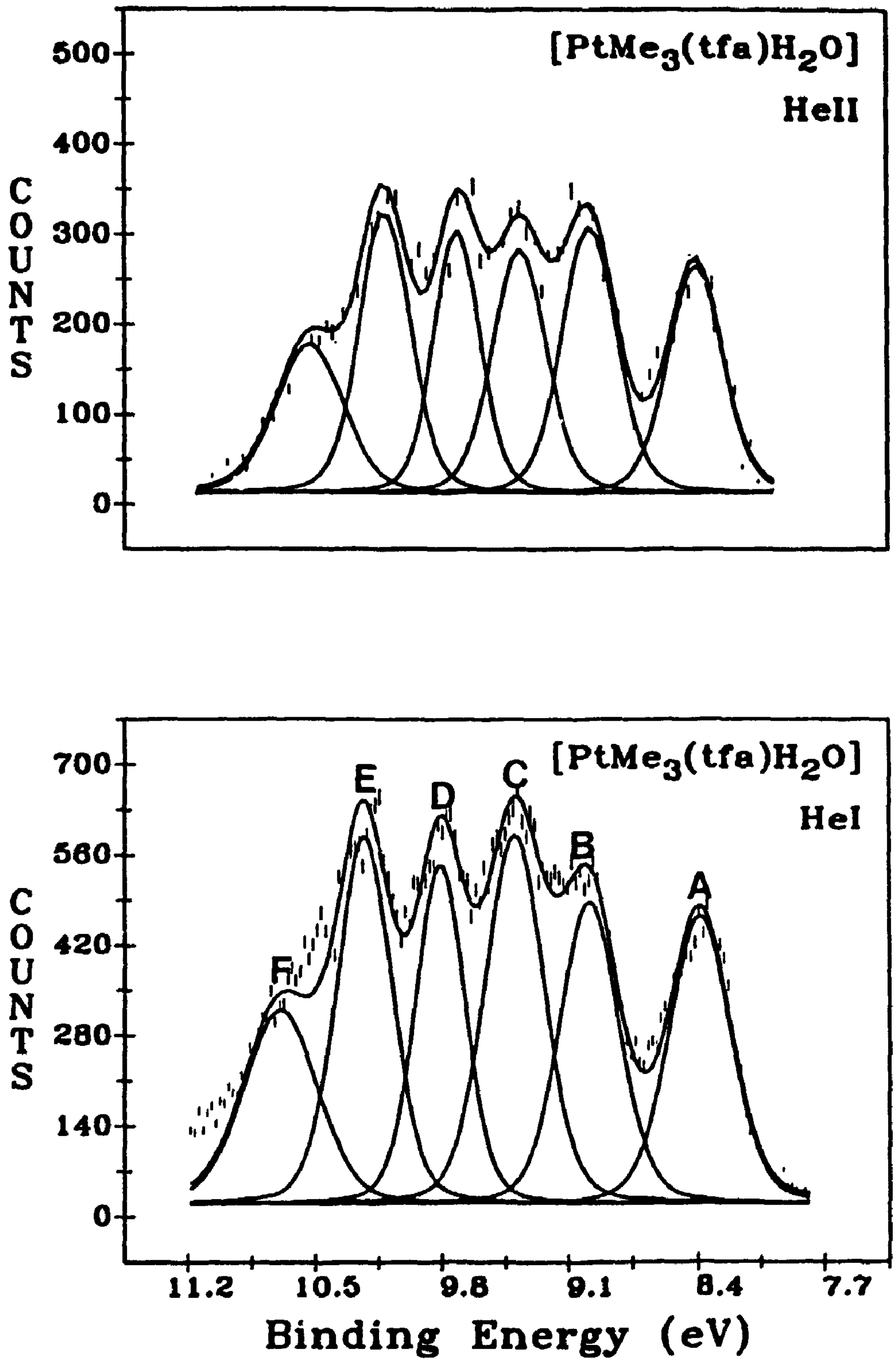

Figure 5.4. Expansions of the low-energy region of the He I and He II spectra of [PtMe$_3$(tfa)H$_2$O)].

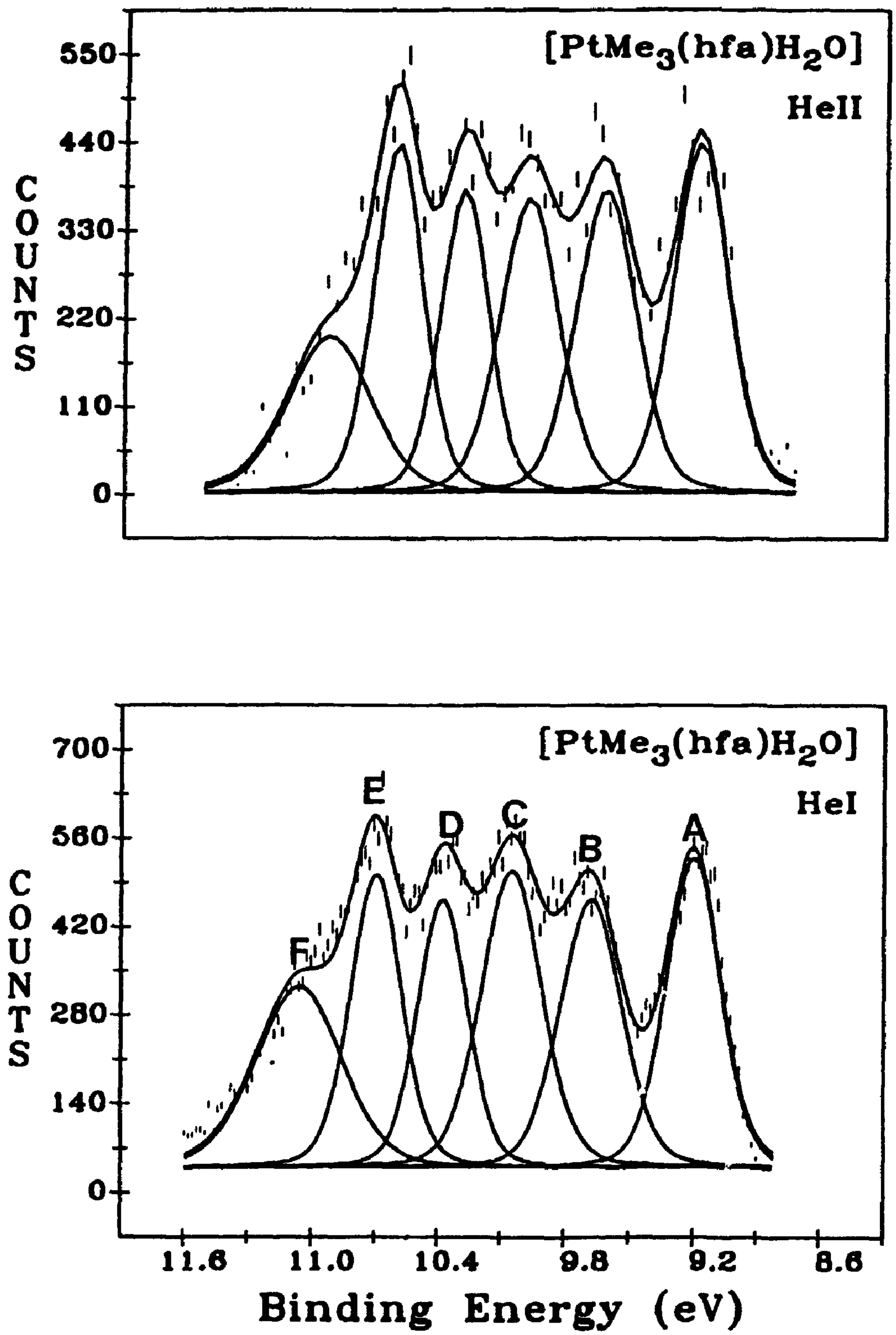

Figure 5.5. Expansions of the low-energy region of the He I and He II spectra of [$PtMe_3$(hfa)H_2O)].

Table 5.1. Vertical ionization energies, He II:He I band area ratios, and assignments of the photoelectron spectra of (ß-diketonato)trimethylplatinum(IV) complexes

compound	band	IE,eV	He II:He I area ratio[a]	assgnt
[PtMe$_3$(acac)]	A	8.10		π_3
	B	8.68		n_-
	C	9.05		d_{z^2}, n_+
	D	9.45		d_{xz}, Me
	E	9.81		d_{xy}
	F	10.19		d_{z^2}, Me
[PtMe$_3$(tfa)Me$_2$S]	X	8.30	1.00	$d_{x^2-y^2}$,Me$_2$S
	A	8.65	0.95	π_3
	B	8.95	0.96	n_-
	C	9.25	0.96	d_{z^2}, n_+
	D	9.53	1.07	d_{xz}, Me
	E	9.87	1.13	d_{xy}
	F	10.29	~0.96	d_{z^2}, Me
[PtMe$_3$(tfa)H$_2$O]	A	8.67	1.00	π_3
	B	9.20	1.05	n_-
	C	9.55	0.85	d_{z^2}, n_+
	D	9.90	1.01	d_{xz}, Me
	E	10.25	1.00	d_{xy}
	F	10.63	1.01	d_{z^2}, Me
[PtMe$_3$(hfa)H$_2$O]	A	9.16	1.00	π_3
	B	9.66	1.01	n_-
	C	10.02	0.83	d_{z^2}, n_+
	D	10.32	0.97	d_{xz}, Me
	E	10.66	0.94	d_{xy}
	F	11.04	0.83	d_{z^2}, Me

[a]Referenced to band A.

energy Pt-Me σ orbitals.

In the region <11 eV, ionization bands are narrow and well resolved compared to those at higher ionization energy. Six bands are present in all spectra (Figures 5.2 ,5.4 and 5.5) except for the spectrum of the compound [$PtMe_3$(tfa)Me_2S] in which an additional band (X) is displayed (Figure 5.3). It is evident that all of the bands (A-F) in this region are shifted to higher ionization energy from the compound [$PtMe_3$(acac)] to the compounds [$PtMe_3$(tfa)H_2O] and [$PtMe_3$(hfa)H_2O]. For example, three bands(D-F) are shifted by about 0.85 eV from [$PtMe_3$(acac)] to [$PtMe_3$(hfa)H_2O] with bands (A-C) shifted to a larger extent (1 eV) (Table 5.2). Similar features have been observed for other ß-diketonate metal complexes and explained in terms of the fluorine inductive effect.[17,20-23] It is also interesting to note that the bands D, E and F of the compound [$PtMe_3$(tfa)Me_2S] have almost the same energies as the corresponding bands of the compound [$PtMe_3$(acac)] (Table 5.1), implying that the fluorine effect on these bands (D-F) is almost cancelled with the strong σ-donor Me_2S replacing the weak donor H_2O. Finally, all bands (A-F) show no significant differences in He II:He I area ratios (Table 5.1), as observed in square-planar platinum(II) and (η^5-cyclopentadienyl)trimethylplatinum(IV) complexes.

5.3 Xα-SW RESULTS

As mentioned above, (ß-acetylacetonato)trimethylplatinum(IV) is known to be binuclear in the solid state, with each platinum being octahedrally coordinated to three methyl groups in a cis configuration, to two oxygens of one ß-diketone and to the central carbon atom of the other diketone.[5,6] In the gas phase at temperatures from 125°C to 180°C, however, this complex is a monomer. In the monomeric form of this compound, the bond between platinum and the central carbon is broken and the platinum atom is five coordinate. Therefore, the molecular orbital calculation was performed on this monomer structure as shown in Figure 5.6. Although the

Table 5.2. Ionization Energy Shift of Each Band in (ß-diketonato)trimethylplatinum(IV) Complexes

	A	B	C	D	E	F
$[PtMe_3(tfa)Me_2S]$-$[PtMe_3(acac)]$	0.55	0.27	0.20	0.08	0.06	0.10
$[PtMe_3(hfa)H_2O]$-$[PtMe_3(acac)]$	1.06	0.98	0.97	0.87	0.85	0.84
$[PtMe_3(tfa)H_2O]$-$[PtMe_3(tfa)Me_2S]$	0.02	0.25	0.30	0.37	0.38	0.35

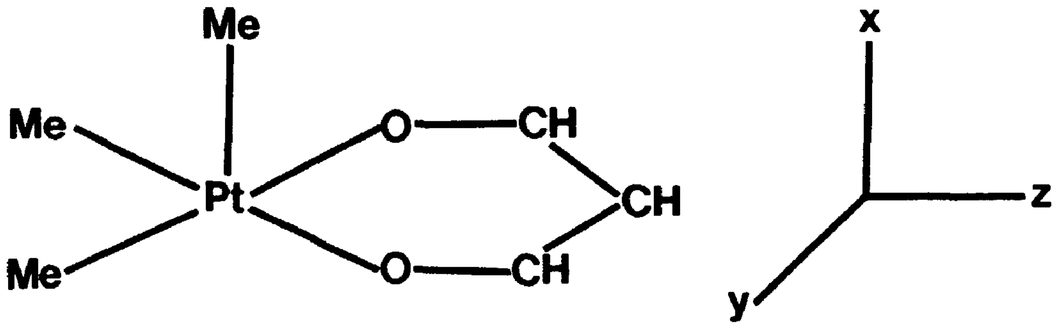

Figure 5.6. Geometry adopted for the model compound $[PtMe_3(HCO.CH.COH)]$ in the Xα-SW calculation.

molecules [$PtMe_3(tfa)H_2O$] and [$PtMe_3(hfa)H_2O$] have octahedral structures with H_2O on the sixth coordination site of the platinum atom, we believe that their valence electronic structures are similar with that of the parent acetylacetonate platinum molecule, as evidenced by their similar photoelectron spectra. The valence electronic structure of the molecule [$PtMe_3(hfa)Me_2S$] is slightly different as revealed by the additional band (X) in its photoelectron spectrum (Figure 5.3), but the origin of this additional peak is readily rationalized without a theoretical calculation (see section 5.4)

The molecular orbital results for the nine valence orbitals of the model compound [$PtMe_3$(HCO.CH.COH)] (C_s) are reported in Table 5.3. These nine MO's are all related mainly with the Pt 5d orbitals and ligand lone pairs (as [illegible] as the outermost π (π_3) orbital of the acac ligand). To discuss these data, it is helpful to mention first the relevant valence orbitals of the free acac ligand that are mainly responsible for the bonding with the central Pt atom. These are the combinations of two in-plane oxygen 2p lone pairs n_+ and n_- (a′ and a″ in C_s, respectively) and π_3 (a′) orbital formed from the symmetric combination of two π_{co} orbitals and the pπ (p_x in the coordinate system of Figure 5.6) orbital of the unique central carbon atom.[24] The energy ordering of the above MO's was previously calculated as $\pi_3 > n_- > n_+$.[24] The symmetric combination n_+ orbital interacts strongly with the hydrogen 1s orbital to form an O-H bond in the enol form of the free acacH ligand.[24] In the molecule [$PtMe_3$(acac)], the hydrogen of the ligand acacH is replaced by the platinum atom and thus the n_+ orbital is expected to be the major source for the Pt-O σ-interaction.

The highest molecular orbital (HOMO), 6a′, is essentially a π_3 contribution of the ligand acac, with the electrons largely on the unique central carbon atom (Table 5.3). The 6a′ orbital is followed by the 3a″ MO with predominant n_- character of

Table 5.3. MS-Xα Results for [$PtMe_3$(HCO.CH.COH)] Upper Valence Orbitals

MO	Energy (eV)[b]		Pt s	Pt p	Pt d	C_1	C_2	O	C_3	C_4	H_1	H_2	H_3	Int	Out	Dominant Character
						Charge Distribution (%)[a]										
6a'	5.85	8.40			1			16	8	40				33	2	π_3
3a"	7.65	10.08		6	1		6	47	6	10			6	18		n.
5a'	7.93	10.21		4	23	1	11	33	1	7	2	2	2	13	1	d_{z^2}, n_+
4a'	8.50	10.67	5		46	9	7	4	1	1	9	2		15	1	d_{xz}, Me
2a"	8.73	10.91			76	3	3	1	1		4	4		8		d_{xy}
3a'	8.82	10.96	7	2	48	5	18	1	1		2	4		11	1	d_{z^2}, Me
2a'	9.47	11.73	4		45	3	4	14	2	7		5	3	12	1	d_{xz}, π_3
1a"	10.75	12.95		1	44		24	6	6	4		7		8		d_{yz}, Me
1a'	11.35	13.54	1	1	46	21	3	7	4	2	5	1	1	8		$d_{x^2-y^2}$, Me

[a]The atoms C_1 and H_1 are the carbon and hydrogen atoms of the axial methyl group (see Figure 6). The atoms C_2 and H_2 are the carbon and hydrogen atoms of the two equatorial methyl groups. The atoms C_3 represents the two ß-carbons of the model acac ligand and C_4 represents the central carbon atom. H_3 represents the three hydrogen atoms of the model acac ligand. [b]the energies in the second column are the molecular orbital energies of the ground state and those in the third column are the transition state energies.

the acac ligand and only a small Pt contribution. The 5a′ orbital has a heavy σ mixing between the Pt 5d (mainly $5d_{z^2}$) and the n_+ orbital, as expected by the above qualitative considerations. Although the Pt $5d_{x^2-y^2}$ and $5d_{xz}$ orbitals also have the a′ representation, they are not in the same plane as that of the n_+ orbital. Therefore we assume no significant interactions with the n_+ orbital. Similar assumptions are followed below. Next, there are six MO's which all contain largely Pt 5d character. Three of them are σ type orbitals and the other three are π type orbitals. Among the σ MO's are the 3a′, 1a" and 1a′ orbitals. The 3a′ MO consists of the Pt $5d_{z^2}$ orbital mixed with the symmetric combination of the two carbon lone pairs of the equatorial methyl groups. The 1a" and 1a′ MO's, located at low energy, are the strong Pt-Me σ-bonding orbitals. The 1a" orbital is the Pt $5d_{yz}$ orbital mixed with the anti-symmetric combination of the carbon lone pairs of the two equatorial methyl groups, while the 1a′ orbital is the Pt $5d_{x^2-y^2}$ orbital mixed with the carbon lone pair of the axial methyl group. Three π type MO's are the 4a′, 2a" and 2a′ orbitals. The 4a′ and 2a′ MO's have much Pt $5d_{xz}$ character, mixed with a C-H σ orbital of the axial methyl group and the π_3 orbital of the acac ligand respectively, while the 2a" orbital has essentially Pt $5d_{xy}$ character.

It is noted from this theoretical result that there is extensive delocalization of the Pt 5d electrons to the ligand orbitals in the (ß-diketonato)trimethylplatinum(IV) molecules. As a result, simple formal oxidation state and d-electron count descriptions are not suitable in these cases. For example, the simple formal state and d-electron count give six Pt 5d electrons in these molecules, but only the molecular orbital 2a" contains the "pure" Pt $5d_{xy}$ electrons. Similar features in the cyclopentadienyl d^8 metal carbonyls have also been discussed by Lichtenberger and Green et al..[25-27] In their photoelectron spectroscopic studies on $CpM(CO)_2$ (M=Co and Rh), they found that only three ionizations could clearly be assigned to the metal d orbitals, even though these complexes have d^8 configuration based on the d-electron count description.

In comparison with the cyclopentadienylplatinum(IV) complexes discussed in Chapter 4, Both cyclopentadienyl and diketonate complexes share a common feature that there are strong interactions between the platinum 5d orbitals and the ligands. But there are major differences in the HOMO. The former has a large Me-Pt-Cp character, while the latter is essentially a diketonate orbital.

5.4 SPECTRAL ASSIGNMENT AND INTERPRETATION

Since the spectra of the four compounds are very similar (see Figures 5.2-5.5), the discussion that follows is applicable to all cases. The additional band (X) (Figure 5.3) of the compound [$PtMe_3$(tfa)Me_2S] will be assigned separately in the course of the discussion.

In the transition metal complexes containing methyl[28-30] and ß-diketonate groups,[23,31-34] the He II:He I intensity difference has been used to distinguish the metal d orbital ionizations from the ligand orbital ionizations. However, as the data in Table 5.1 indicates, the low energy bands in the photoelectron spectra give very similar He II:He I band area ratios and so this technique is not useful for these (ß-diketonato)trimethylplatinum(IV) complexes, as for square-planar platinum(II) (Chapters 2 and 3) and cyclopentadienylplatinum(IV) (Chapter 4) complexes. Therefore, the spectra will be assigned using the ionization energy shifts and the Xα-SW result for the model compound [$PtMe_3$(HCO.CH.COH)].

Regarding the ionization energy shifts (Table 5.2), we naturally expect that the ionizations of the ß-diketonate ligand orbitals will have larger energy shifts than the Pt atom and Pt-Me orbitals with fluorine substitutions in the ß-diketonate ligands. In contrast, we expect that the ligand based orbitals will have smaller shifts than the Pt

5d and Pt-Me orbitals between the compounds $[PtMe_3(tfa)H_2O]$ and $[PtMe_3(tfa)Me_2S]$. The energy shifts for these compounds are summarized in Table 5.2. It is clear from Table 5.2 that band A has the largest energy shift from the parent acac compound to the fluorinated compounds, but little shift from the compound $[PtMe_3(tfa)Me_2S]$ to $[PtMe_3(tfa)H_2O]$. This is strong evidence for band A arising from the π_3 ionization of the ß-diketonate ligand, remembering that the I.E. ordering of the outermost orbitals in the free ß-diketones is $\pi_3 < n_- < n_+$.[24] This assignment, which is based on the experimental observations, is in excellent agreement with the Xα-SW prediction in which the HOMO is calculated to be the π_3 orbital (see Table 5.3). The π_3 orbital also gives rise to the lowest I. E. band in the compound $[Pt(acac)_2]$.[31]

The bands D, E and F, on the other hand, show the least energy shifts with fluorine substitution (Table 5.2) of all the bands in the low I. E. region. This indicates that the three bands (D, E and F) contain largely Pt 5d character. Assuming that each ionization band corresponds to a single MO, the three bands D, E and F are assigned to the MO's 4a′ (d_{xz}, $Me_{(ax)}$), 2a" (d_{xy}) and 3a′ (d_{z^2}, $Me_{(eq)}$) respectively, for which predominant Pt 5d contributions are calculated (see Table 5.3). The near degeneracy of the MO's 2a" and 3a′, as predicted by the Xα-SW calculation (Table 5.3), is also in accord with the poorer resolution of the bands E and F, compared to other bands (A-D) (see Figures 5.2-5.5).

The ionization energy shifts of the bands B and C are greater than those of the bands D, E and F, but less than the band A, upon fluorine substitution (see Table 5.2). Using the same argument as above, this is an indication that the bands B and C must contain ionizations arising from the ß-diketonate ligand orbitals as well as from the Pt atom orbitals. The Xα-SW calculation indeed predicts that the second and third highest occupied MO's (3a" and 5a′) consist of the ß-diketonate ligand orbitals (n_- and n_+ respectively) mixed with some Pt character, especially a heavy mixing of the Pt $5d_{z^2}$ orbital in the MO 5a′ (see Table 5.3). The assignments for the bands B and C are shown in Table 5.1, in which only major contributions are indicated.

Finally, there is an additional band (X) in the spectrum of the compound [$PtMe_3$(tfa)Me_2S] (see Figure 5.3). This band has an ionization energy of 8.3 eV, which is similar to the lone pair ionization energy (8.7 eV) of free Me_2S.[35] The slightly lower I. E. of the band X than the lone pair of free Me_2S might imply the Pt $5d_{x^2-y^2}$ orbital being mixed with the lone pair electrons in an antibonding σ way, as indicated by the similar He I and He II intensity, since previous studies have provided evidence that, compared to carbon and oxygen 2p AO's, sulfur 3p AO's have lower photoionization cross sections for He II than for He I radiation.[36,37] Therefore, the band X is assigned to the ionization of the Pt-Me_2S orbital.

5.5 CONCLUSIONS

The ionization energy of the first six valence MO's falls in the order $\pi_3 < n_- <$ Pt-$n_+ <$ Pt 5d, Pt-Me in the complexes [$PtMe_3$(acac)], [$PtMe_3$(tfa)H_2O] and [$PtMe_3$(hfa)H_2O], while the ionization energy of the first seven valence MO's in the compound [$PtMe_3$(tfa)Me_2S] falls in the order Pt-Me_2S<π_3<n_-<Pt-n_+<Pt 5d. There is strong interaction between the platinum 5d orbitals with both the ß-diketonate n_+ and the methyl σ orbitals.

5.6 REFERENCES

1. R. C. Menzies, J. Chem. Soc., 565 (1928).
2. R. C. Menzies and E. R. Wiltshire, J. Chem. Soc., 21 (1933).
3. A. K. Chatterjee, R. C. Menzies, J. R. Steel and F. N. Youdale, J. Chem. Soc., 1706 (1958).
4. A. C. Hazell, A. G. Swallow and M. R. Truter, Chem. Ind.(London), 564 (1959).
5. A. G. Swallow and M. R. Truter, Proc. Roy. Soc. Ser. A, 254, 205 (1960).
6. A. C. Hazell and M. R. Truter, Proc. Roy. Soc. Ser. A, 254, 218 (1960).
7. K. Kite and M. R. Truter, J. Chem. Soc. A, 934 (1968).
8. M. R. Truter and E. G. Cox, J. Chem. Soc., 948 (1956).
9. A. G. Swallow and M. R. Truter, Proc. Chem. Soc., 166 (1961).
10. A. G. Swallow and M. R. Truter, Proc. Roy. Soc. Ser. A, 256, 527 (1962).
11. G. I. Zharkova, I. K. Igumenov and S. V. Zemskov, Sov. J. Coord. Chem. (Russian translation), 5, 586 (1979).
12. G. I. Zharkova, I. K. Igumenov, S. V. Zemskov and V. B. Durasov, Sov. J. Coord. Chem. (Russian translation), 5, 1073 (1979).
13. J. R. Hall and G. A. Swile, J. Organomet. Chem., 21, 237 (1970).
14. D. E. Clegg, J. R. Hall and N. S. Ham, Aust. J. Chem., 23, 1981 (1970).
15. J. R. Hall and G. A. Swile, J. Organomet. Chem., 47, 195 (1973).
16. N. S. Ham, J. R. Hall and G. A. Swile, Aust. J. Chem., 28, 759 (1974).
17. J. E. Drake, R. Eujen and K. Gorzelska, Inorg. Chem., 21, 1784 (1982).
18. A. W. Coleman, J. C. Green, A. J. Hayes, E. A. Seddon, D. R. Lloyd and Y. Nowa, J. Chem. Soc. Dalton Trans., 1057 (1979).
19. C. Cauletti, J. P. Clark, J. C. Green, S. E. Jackson, I. L. Fragalà, E. Ciliberto and A. W. Coleman, J. Electron Spectrosc. Relat. Phenom., 18,61 (1980).
20. D. R. Lloyd, Chem. Commun., 868 (1970).

21. S. Evans, H. Hamnett and A. F. Orchard, J. Coord. Chem., 2, 57 (1972).

22. C. Cauletti and C. Furlani, J. Electron Spectrosc. Relat. Phenom., 6, 465 (1975).

23. H. van Dam, A. Terpstra, D. J. Stufkens and A. Oskam, Inorg. Chem., 19, 3448 (1980).

24. S. Evans, H. Hamnett, A. F. Orchard and D. R. Lloyd, Faraday Discuss. Chem. Soc., 54, 227 (1972).

25. D. L. Lichtenberger and G. E. Kellogg, Acc. Chem. Res., 20, 379 (1987).

26. D. L. Lichtenberger, D. C. Calabro and G. E. Kellog, Organometallics, 3, 1623 (1984).

27. N. Dudeney, J. C. Green, P. Grebenik and O. N. Kirchner, J. Organomet. Chem., 252, 221 (1983).

28. G. M. Bancroft, T. Chan, R. J. Puddephatt and J. S. Tse, Inorg. Chem., 21, 2946 (1982).

29. G. M. Bancroft, L. L. Coatsworth, D. K. Creber and J. S. Tse, Physica Scripta, 16, 217 (1977).

30. N. Dudeney, O. N. Kirchner, J. C. Green and P. M. Maitlis, J. Chem. Soc. Dalton Trans. 1877 (1984).

31. S. Di. Bella, I. Fragalà and G. Granozzi, Inorg. Chem., 25, 3997 (1986).

32. M. Casarin, A. Vittadini, G. Granozzi, I. Fragalà and S. Di. Bella, Chem. Phys. Lett., 141, 193 (1987).

33. I. Fragalà, L. L. Costanzo, E. Ciliberto, G. Condorelli and C. D'arrigo, Inorg. Chim. Acta, 40, 15 (1980).

34. C. Cauletti, C. Furlani and G. Storto, J. Electron. Spectrosc. Relat. Phenom., 18, 329 (1980).

35. K. Kimura, S. Katsumata, Y. Achiba, T. Yamazki and S.Iwata, Handbook of He I Photoelectron Spectra of Fundamental Organic Molecules, Jap. Sci. Press,

Tokyo, 126 (1981).

36. A. Schweig and W. Thiel, Molec. Phys., 27, 265 (1974).

37. G. Granozzi, A. Vittadini, L. Sindellari and D. Ajò, Inorg. Chem., 23, 702 (1984).

CHAPTER 6

A PHOTOELECTRON STUDY OF THE VALENCE LEVELS OF $CpPtMe_3$ AND $Me_2Pt(COD)$ AS A FUNCTION OF PHOTON ENERGY

6.1. INTRODUCTION

In the interpretation of molecular photoelectron spectra, it is generally assumed that the molecular orbital photoionization cross sections are determined by the summation of the constituent atomic terms, and that contributions from the atomic orbital interactions, together with possible photoionization mechanisms such as resonance enhancements, can be neglected. This is known as the Gelius model.[1] Consequently, spectral assignments have been largely reliant on an empirical analysis of intensity changes between spectra taken with conventional He I and He II radiations. Usually this empirical rule has been successful in the interpretation of photoionization bands. But it has also been challenged by inconsistent observations between ionization energy shifts and intensity variations, or by theoretical predictions. This is especially evident in the cases of XeF_2,[2] $Ni(C_3H_5)_2$,[3,4] and $CpPtMe_3$ (Chapter 4). The use of synchrotron radiation allows the energy dependence of ionization cross sections and/or branching ratios to be examined in detail. Such studies should enable the problems encountered in the conventional photoelectron studies to be clarified, as evidenced for XeF_2.[2] In this case, ab initio and Xα-SW calculations gave a different ordering of molecular orbitals, and the cross sections and branching ratios were only consistent with the Xα-SW assignment.

Gas phase synchrotron radiation photoelectron experiments on organotransition metal complexes were started just two or three years ago. Among the studied compounds are metal hexacarbonyls $M(CO)_6$ (M=Cr, Mo, and W),[5] metallocenes $M(C_5H_5)_2$ (M=Fe, Ru, and Os),[6] and uranocene $U(C_8H_8)_2$.[7] In this chapter, the photoelectron studies of the upper valence levels of $CpPtMe_3$ and $Me_2Pt(COD)$ from 21 to 100 eV photon energy are reported together with the experimental and theoretical branching ratios. The primary intention of this study was to clarify the disagreements between the Fenske-Hall and Xα-SW methods on the spectral assignments of the compound $CpPtMe_3$ and to establish how the differences in orbital character are reflected in the branching ratios for the valence MO's of both compounds. The compound $Me_2Pt(COD)$ was chosen because it is representative of the Pt(II) complexes discussed in this thesis, and because it gives a better resolved spectrum than those of the other Pt(II) compounds. These are preliminary results, especially in terms of the theoretical interpretation. More work on related compounds is needed, but the preliminary results are significant.

6.2. RESULTS AND DISCUSSION

6.2.1. $CpPtMe_3$

Photoelectron spectra of $CpPtMe_3$ at 23, 39, 55, and 90 eV photon energies are presented in Figure 6.1. These are of very similar quality as the He I spectrum shown earlier (Figure 4.1). It is immediately obvious from the spectra and the branching ratios that bands A and B display a relative intensity reduction as the photon energy increases from 23 to 90 eV. The observations here are generally in accord with those from the conventional He I and He II experiments (Chapter 4). However, the conclusion about this reduction was uncertain from the He I and He II radiations, because the intensity changes were not dramatic and because there were only two observations.

On the basis of the Xα-SW and Fenske-Hall calculations, there appeared to be two different possible spectral assignments for this compound, as discussed in

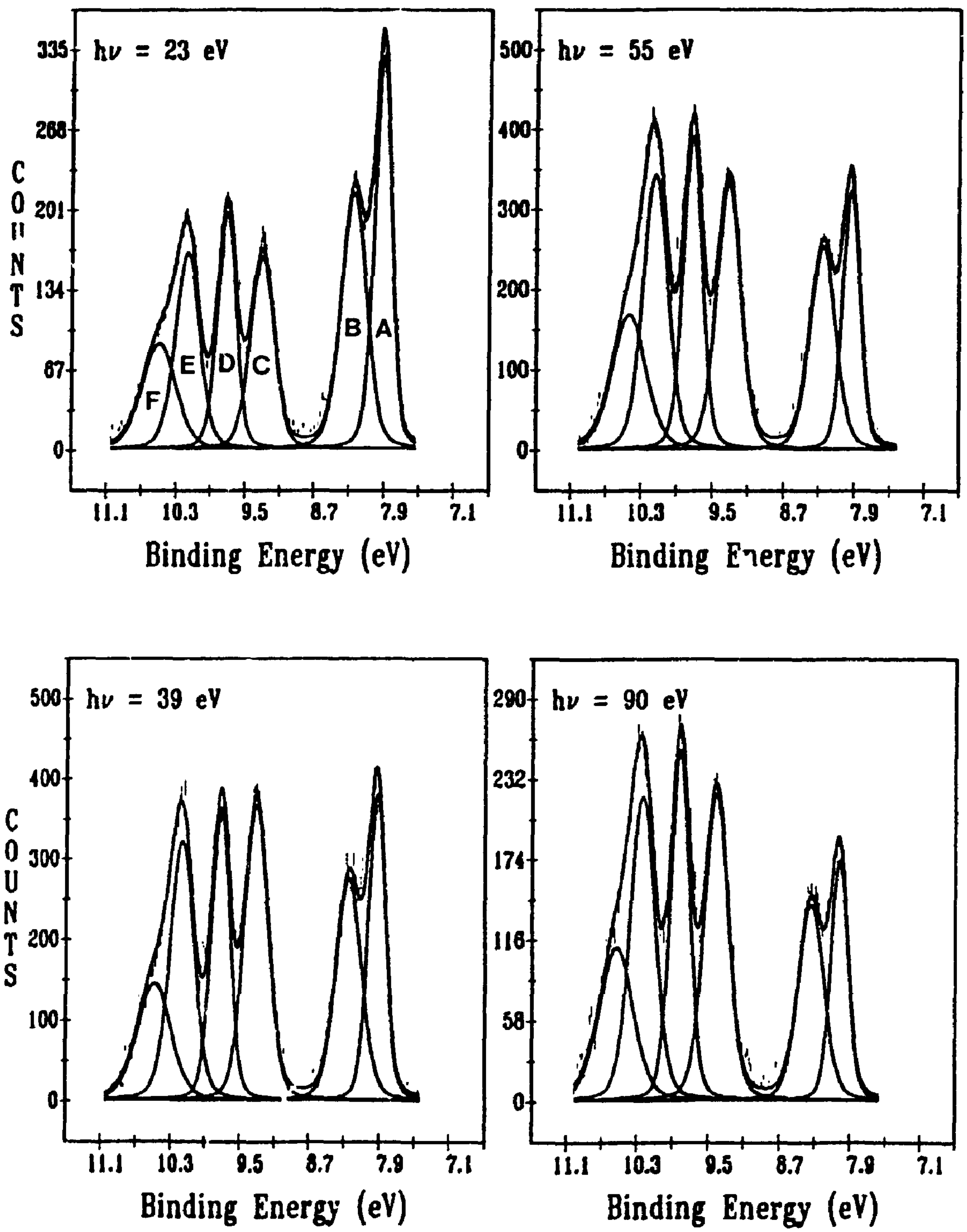

Figure 6.1. Photoelectron spectra of the upper valence orbitals of $CpPtMe_3$ at 23, 39, 55, and 90 eV photon energies.

Chapter 4. Their differences are presented in Figure 6.2. From the Fenske-Hall calculations (see also Table 4.2), Bands A (corresponding to the MO's 5a′ and 3a″ on the left side of Figure 6.2) and B (4a′) correspond to ionizations of Pt 5d orbitals (95% of Pt 5d). Bands C (2a″+3a′), D (2a′), E (1a″) and F (1a′) are assigned to the ligand-based orbitals (>70%), but with 40% of Pt 5d mixed in the band C. From the Xα-SW calculations (see also Table 4.3), on the other hand, the ionizations of the Pt 5d based orbitals (~70% Pt 5d) (3a′, 2a′+1a″ on the right side of Figure 6.2) give rise to bands D and E. The rest of the bands (A, B, C, F) are assigned to the Pt-ligand orbitals, with mostly ligand character (70-80%) in bands A and B.

To clarify this disagreement, experimental and theoretical branching ratios (or intensity ratios) over the photon energy range of 21 to 100 eV were calculated and are plotted in Figure 6.3 for comparison. The experimental branching ratios were corrected by dividing by the kinetic energy of the band and represent the individual band areas normalized with respect to the total valence band area. The theoretical values of the branching ratios were calculated using the Xα-SW partial cross sections of the upper eight valence orbitals and the Xα-SW partial cross sections were calculated with the program developed by Davenport.[8] As shown in Figure 6.3, there is a satisfactory agreement between the Xα-SW and experimental branching ratios, in the general trends and/or in the quantitative values for all of the six ionization bands. With the Fenske-Hall assignments, although a reasonable agreement between the theory and experiment is obtained for bands D and F, the agreement is very poor for bands A, C and E. For example, there is an error of more than a factor of two between the theory and experiment in the cases of bands A and E. The theory predicts a decrease in branching ratios up to photon energy of ~ 40 eV for band C, whereas the opposite trend was observed experimentally. A contradiction between the Fenske-Hall prediction and the experimental measurement also exists in the

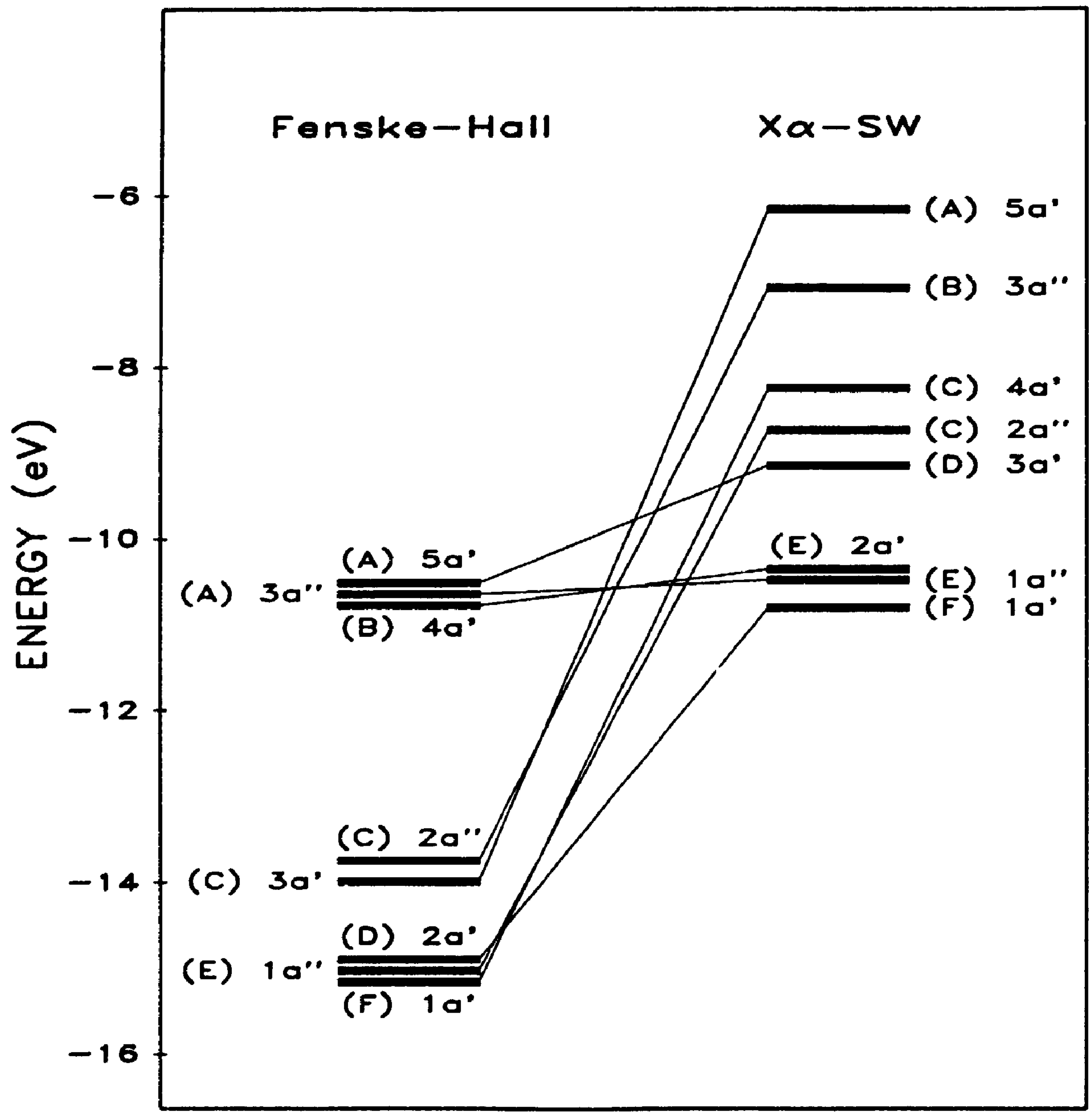

Figure 6.2. Upper valence molecular orbital diagram of $CpPtMe_3$ from the Xα-SW and Fenske-Hall calculations and the spectral assignments from the theoretical methods. (A), (B), (C), (D), (E), and (F) correspond to the band labels in Figure 6.1.

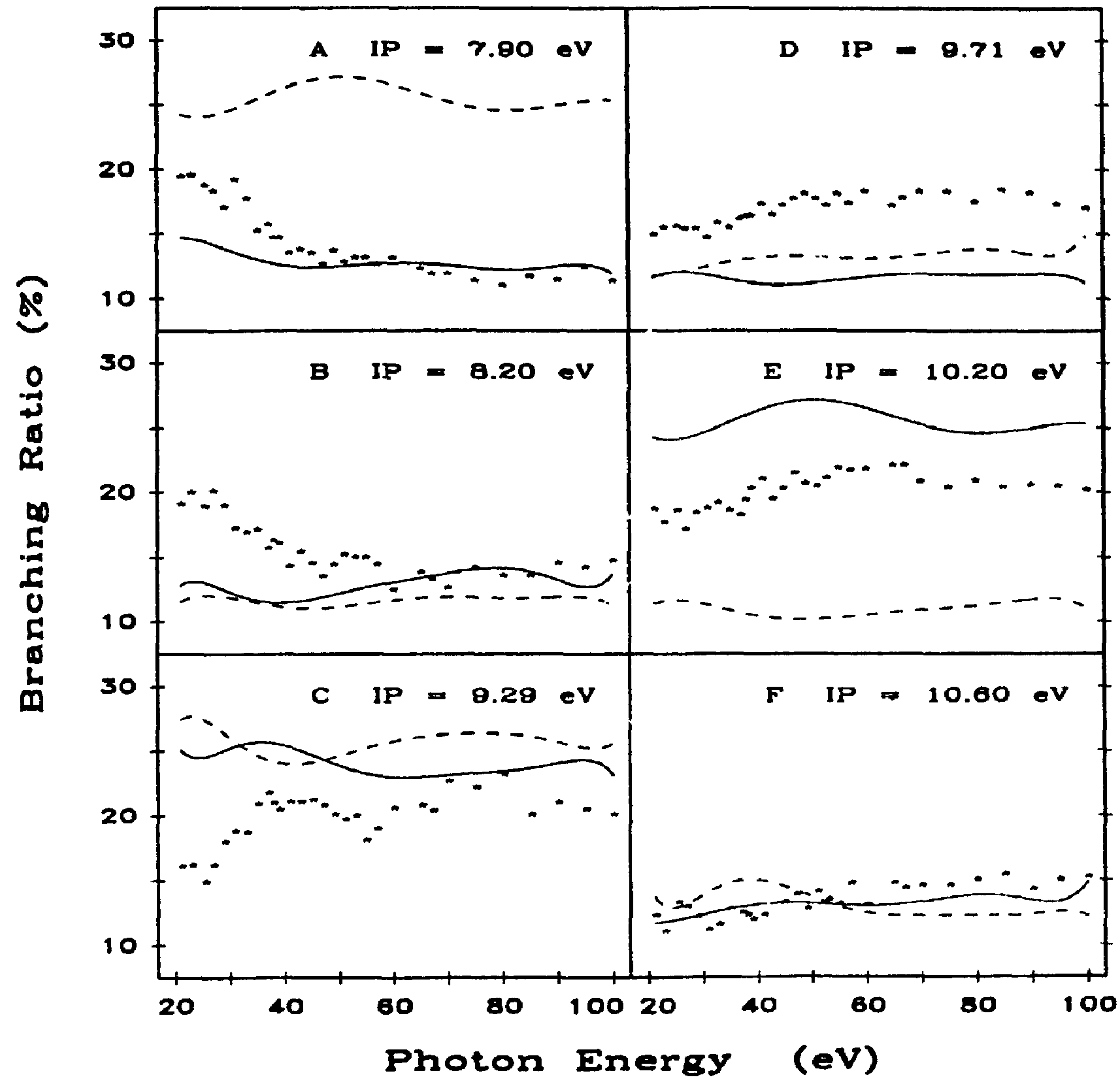

Figure 6.3. Branching ratios of the upper valence orbitals of $CpPtMe_3$ from experiment measurements (***), Xα-SW assignments (solid lines), and Fenske-Hall assignments (---).

general trend of the branching ratios below the energy of ~50 eV for band A. Therefore, this study supports the Xα-SW spectral assignments for the upper valence levels of $CpPtMe_3$.

After the settlement of the spectral assignments, it seems reasonable to discuss how the differences in orbital character are reflected in the experimental branching ratios. As the photon energy increases, the kinetic energy of an electron ejected from a level at given binding energy will increase. This in turn will change the final state wave function by decreasing the photoelectron wavelength. As discussed in Chapter one, the photoionization cross section is proportional to the integral of the electronic dipole transition moment and the dipole moment is dependent on the final state as well as the initial state, which is determined by the orbital from which the electron is ejected. Thus the intensity dependence with input photon energy will be significantly different for C 2p and Pt 5d. For an electron ionized from a C 2p orbital, the intensity of an ionization band is at a maximum near the ionization threshold (~10 eV binding energy) and decreases with increasing photon energy.[9] Alternatively, for a Pt 5d ionization, the intensity of an ionization band increases with increasing photon energy reaching a delayed maximum at ~ 35 eV and then decreases at higher photon energies.[9] As shown in Figure 6.3, there are different features for the branching ratios in the six ionization bands. Bands A and B show a large decrease of the branching ratios below ~45 eV photon energies. In contrast to bands A and B, there is a large increase in branching ratios in band C up to about 40 eV and then only a small change with the branching ratios (20±2%) up to 100 eV. For bands D, E, and F, there are small increases in branching ratios with increasing photon energy (even smaller for band F). Using the ionization behaviour of the atomic C 2p and Pt 5d orbitals and the Gelius treatment,[1] it is readily apparent that bands A and B can be attributed to the ionizations of MO's with more C 2p character, while the bands D, E, and F are attributed to the MO's with more Pt character. This is in accord with the Xα-SW predictions in which the bands A and B are assigned to the MO's with mostly C 2p (70-80%) character, while the bands D and E are assigned to the MO's with mostly Pt 5d (~70%) contributions and F to the MO with ~40% Pt character. It is interesting to note that the subtle differences of the branching ratios between the bands D, E and the F are also reflected in the orbital character (see Figure 6.3).

However, for the band C, there is a disagreement between the experimental and Xα-SW prediction, using the Gelius treatment based just on orbital character. The band C is predicted theoretically to arise from ionizations of the MO's with less Pt 5d character than the MO's responsible for bands D and E. In contrast, the experimental branching ratios would suggest that band C arise from ionization of an MO with more Pt 5d character, under the Gelius treatment, since this band has a greater increase in the branching ratio from 21 to ~40 eV photon energies (Figure 6.3). To explain this disagreement, we need to search for other contributions to the band intensity changes with variation in photon energy. For partially filled 5d transition metal complexes, there are at least two possible resonances contributing to the intensity enhancements: a d-like electron excitation to a f-like antibonding level (shape resonance)[10,11] and a 5p electron excitation to a 5d orbital.[5] In the first case, a d-like electron is firstly excited to a f-like antibonding orbital which is located in the inner well of the effective potential of the molecules. The excited electron is temporarily trapped by the molecular barrier. Eventually the electron tunnels the barrier and escapes due to the interaction with the remaining electrons. Because the f-like antibonding orbital in the inner well has a large overlap with the originating orbital, this inner well transition will result in a cross section enhancement. In the second case, the resonance mechanism can be qualitatively expressed as follows:

$5p^x5d^y \rightarrow 5p^{x-1}5d^{y+1} \rightarrow 5p^x5d^{y-1} + e$. At a photon energy corresponding to the 5p absorption edge, a metal 5p electron is excited to a metal 5d orbital. This intermediate state then undergoes a decay in which a 5d electron fills the 5p hole and a second 5d electron is ejected. The kinetic energy of the ejected 5d electron is the same as that obtained by the direct ionization process ($5p^x5d^y \rightarrow 5p^x5d^{y-1} + e$). But the second mechanism is unlikely to be the case here since the maximum position ($h\nu = 40$ eV) of the branching ratios is not around the ionization thresholds of the free Pt atomic 5p orbitals which are 51.7 and 65.3 eV.[12] Thus if a resonance exists in the band C at the photon energy around 40 eV, we feel that a Pt-ligand electron transition to a f-like antibonding orbital is a possible cause. The Xα-SW results also show a maximum in the branching ratio at about 40 eV, although the maximum is not as marked as in the experimental branching ratio. It should be pointed out, however, that branching ratios are not ideal for discussing resonance effects in detail, because the branching ratio for a particular ionization process is dependent on the ratio for other ionization processes at a particular photon energy. Therefore, the conclusion about the resonance effect here is tentative.

6.2.2. $Me_2Pt(COD)$

Photoelectron spectra of the upper valence MO's of this compound are shown in Figure 6.4 at photon energies 25, 35, 49 and 95 eV. The spectra at low photon energies are very similar to those obtained with HeI and He II radiations (Chapter 2). At high energies ($h\nu$ >~ 55 eV), however, band A shows a relative intensity reduction. The experimental branching ratios are presented in Figure 6.5 along with the Xα-SW theoretical values. There is good agreement. Considering the observed similarity with $CpPtMe_3$ especially above 50 eV photon energy, theoretical branching ratios were calculated up to 61 eV photon energy only. Since the experimental branching ratios are similar in many aspects to those of $CpPtMe_3$, only a brief

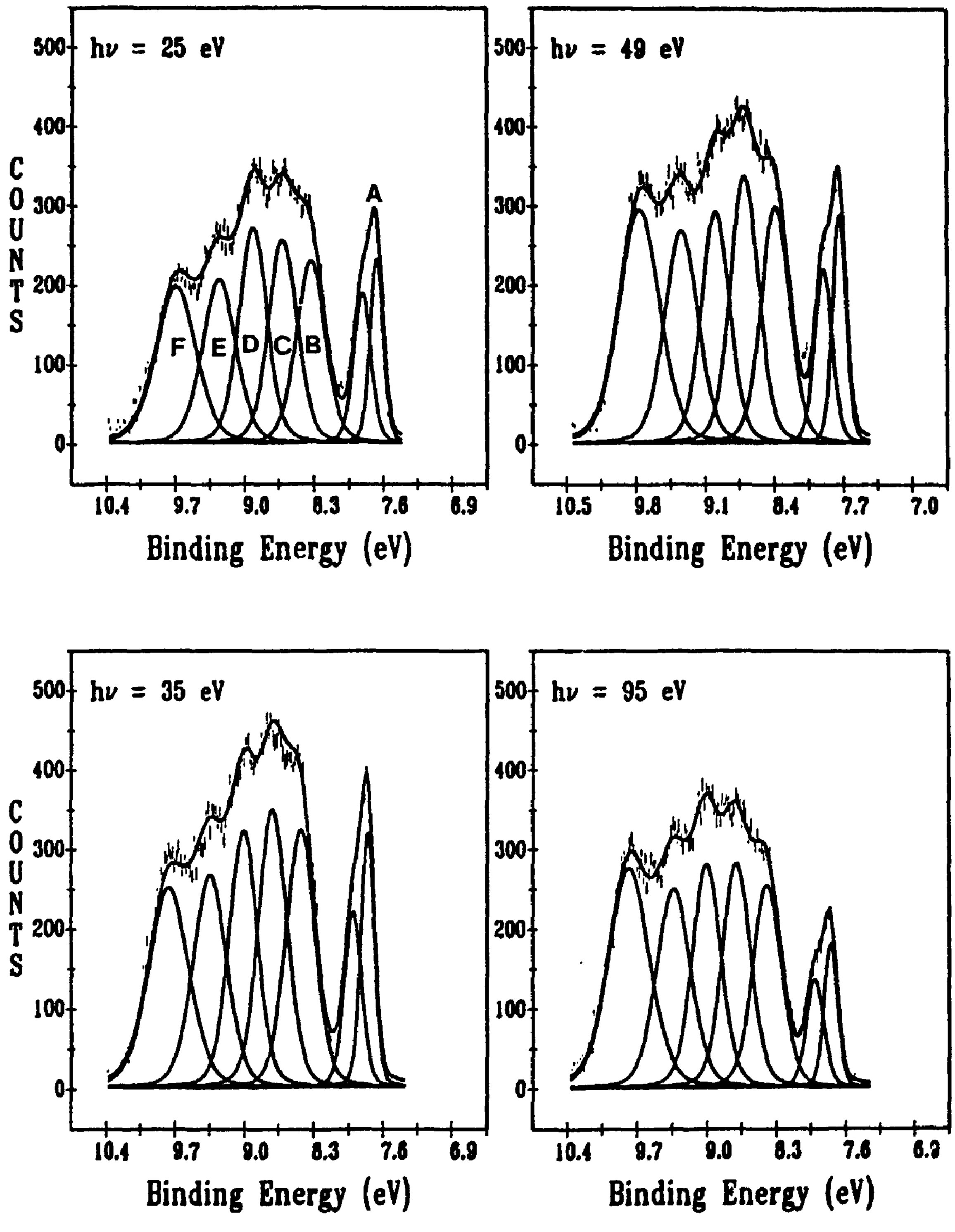

Figure 6.4. Photoelectron spectra of the upper valence orbitals of $Me_2Pt(COD)$ at 25, 35, 49, and 95 eV photon energies.

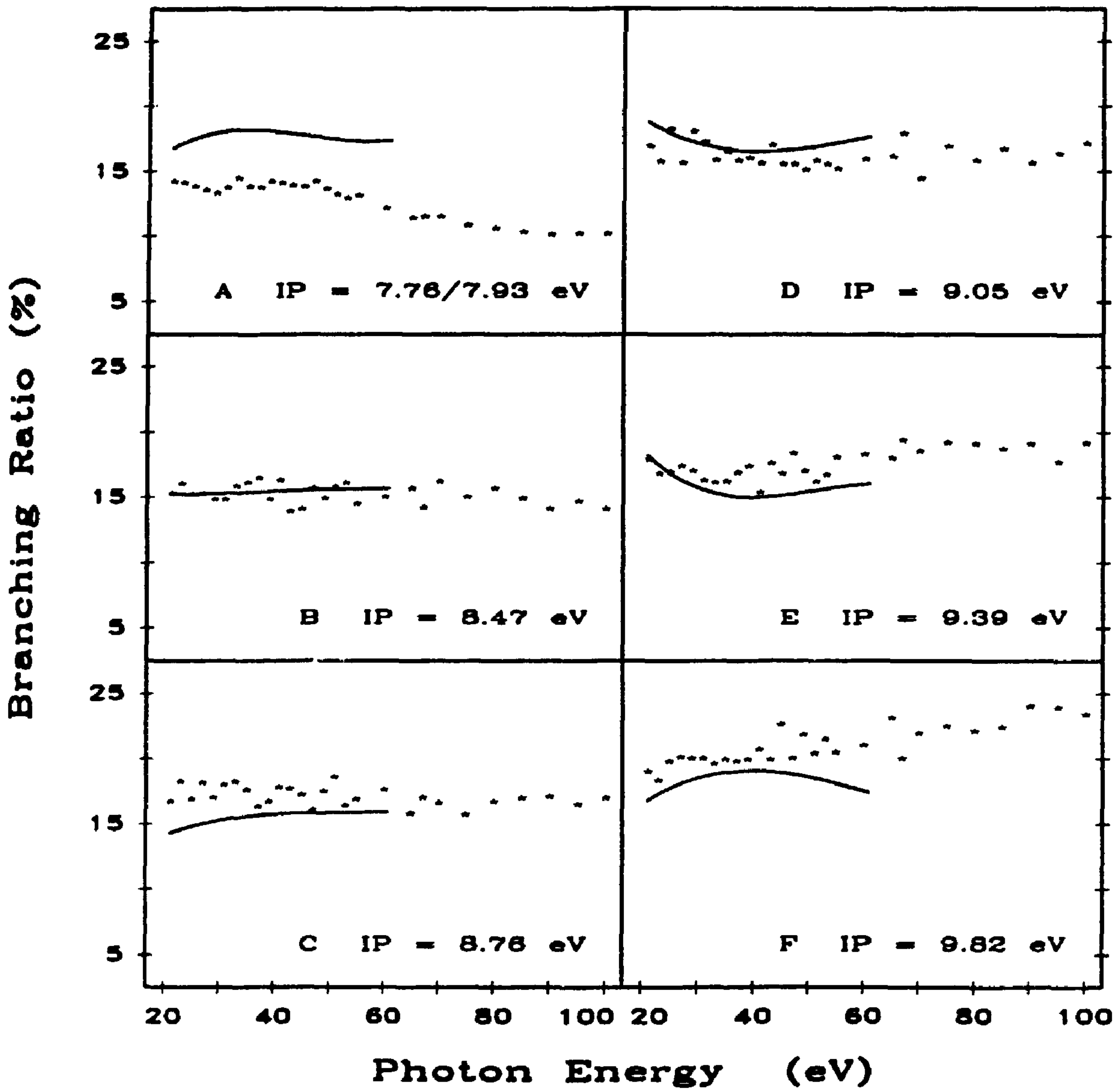

Figure 6.5. Branching ratios of the upper valence orbitals of $Me_2Pt(COD)$ from experiment measurements (***) and Xα-SW calculations (solid lines).

discussion follows.

Based on the HeI and He II photoelectron spectra along with the Xα-SW calculations, bands A and B are assigned to ionizations of MO's with mostly C 2p character, while the bands C-F are due to MO's with mostly Pt 5d character (Tables 2.1 and 2.5). By comparison with $CpPtMe_3$, the orbital character is well reflected in the measured branching ratios for the ionization bands with mostly Pt 5d contributions (C-F), but not for the ionization bands with mostly C 2p character (A and B). Since there is little feature in either the experimental or theoretical branching ratios, it is not possible to explain these observations at the present time.

6.3. CONCLUSIONS

The arguments about the $CpPtMe_3$ spectral assignments from the Xα-SW and Fenske-Hall calculations can be clarified by using the experimental branching ratios and by comparing them with the theoretical values. The agreement between experimental branching ratios and the Xα-SW values strongly supports the Xα-SW assignment for both $CpPtMe_3$ and $Me_2Pt(COD)$. The differences in orbital character are generally reflected in the experimental branching ratios in the absence of resonance effects. A possible resonance resulting from a Pt-ligand σ electron transition to a f-like antibonding orbital is observed in $CpPtMe_3$.

6.4. REFERENCES

1. V. J. Gelius, J. Electron Spectrosc. Relat. Phenom., 4, 985 (1974).
2. B. W. Yates, K. H. Tan, G. M. Bancroft, L. L. Coatsworth, J. S. Tse and G. J. Schrobligen, J. Chem. Phys., 84, 3603 (1986).
3. D. Moncrieff, I. H. Hillier, V. R. Saunders and W. Von Niessen, Chem. Phys. Lett., 131, 545 (1986).
4. D. Decleva, G. Fronzoi and A. Lisini, Chem. Phys., 134, 307 (1989).
5. G. Cooper, J. C. Green, M. P. Payne, B. R. Dobson and I. H. Hillier, J. Am. Chem. Soc., 109, 3836 (1987).
6. G. Cooper, J. C. Green and M. P. Payne, Mol. Phys., 63, 1031 (1988).
7. J. G. Brennan, J. C. Green and C. M. Redfern, J. Am. Chem. Soc., 111, 2373 (1989).
8. J. W. Davenport, Phys. Rev. Lett., 36, 945 (1976).
9. I. Lindau and J. J. Yeu, At. Nucl. Data Tables, 32, 1 (1985).
10. M. B. Robin, Chem. Phys. Lett., 119, 33 (1985).
11. I. Novak, J. M. Benson and A. W. Potts, J. Phys. B: At. Mol. Phys., 20, 3395 (1987).
12. G. Margaritondo, Introduction to Sychrotron radiation, Oxford University Press Inc., 1988, P.261.

CHAPTER 7

EXPERIMENTAL AND COMPUTATIONAL

7.1 SYNTHESIS AND CHARACTERIZATION

^{1}H NMR spectra were recorded on a Varian XL200 spectrometer. 19F and 31P NMR spectra were recorded on a Varian XL300 spectrometer. Mass spectra were obtained by electron impact on a Finigan MAT8230 spectrometer employing an ionization voltage of 70 eV. Melting points were measured in capillary tubes without correction. Elemental analyses were performed by Guelph Chemical Laboratories Ltd., Guelph, Ontario, Canada. Preparations requiring inert atmosphere were carried out by using standard Schlenk techniques. Preparations and characterizations of new compounds will be presented in detail.

7.1.1 Cis-dimethylplatinum(II) Complexes

[$PtMe_2\{P(NMe_2)_3\}_2$]. This general procedure was followed to prepare all of the dimethylplatinum(II) compounds. The starting material, $Pt_2Me_4(\mu\text{-}SMe_2)_2$, was prepared by a literature method.[1] To a suspension of $Pt_2Me_4(\mu\text{-}SMe_2)_2$ (0.350 g, 0.610 mmol) in dry dichloromethane (5 mL) in a Schlenk tube was added tris(dimethylamino)phosphine (0.45 mL, 2.440 mmol) under N_2 at room temperature. After 1 hour, the solvent was removed under vacuum to yield a white residue of cis-[PtMe2{$P(NMe_2)_3\}_2$], which was purified by sublimation at 95°C and 10^{-2} mm Hg to yield a white solid (0.27 g, 40.1% yield). m.p. 90°C. ^{1}H NMR ($CDCl_3$): δ 0.38 [^2J(Pt-H) = 66.0 Hz, Pt-CH_3]; 2.65 [s, NMe]. ^{31}P NMR ($CDCl_3$): δ 116.22 [J(Pt-P) = 2841.0 Hz, Pt-$P(NMe_2)_3$]. Molecular weight 551 (mass spectrum). Anal. Calcd. for $C_{14}H_{42}N_6P_2Pt$: C, 30.46; H, 7.68; N, 15.25. Found: C, 30.19; H, 7.89; N, 15.59%.

cis-[$PtMe_2\{P(OEt)_3\}_2$]. $Pt_2Me_4(\mu\text{-}SMe_2)_2$ (0.250 g, 0.435, mmol) in 5 mL of dichloromethane was treated with triethylphosphite (0.31 mL, 1.31 mmol) to give 0.32 g (65.0%) of the desired product, yellow liquid. ^1H NMR ($CDCl_3$): δ 0.53 [^2J(Pt-H) = 67.0, Pt-CH_3]; 1.29 [t, OCH_2CH_3]; 4.02 [q, OCH_2]. ^{31}P NMR ($CDCl_3$): δ 130.65 [J(Pt-P) = 3106.1 Hz, Pt-$P(OEt)_3$]. Molecular weight 557 (mass spectrum).

cis-[$PtMe_2\{PMe(OEt)_2\}_2$]. $Pt_2Me_4(\mu\text{-}SMe_2)_2$ (0.280 g, 0.487, mmol) in 5 mL of dichloromethane was treated with triethylphosphite (0.30 mL) to give 0.39 g (80.5%) of the desired product, green-yellow liquid. ^1H NMR ($CDCl_3$): δ 0.43 [^2J(Pt-H) = 65.3, Pt-CH_3]; 1.56 [d, PMe]; 1.25 [t, OCH_2CH_3]; 3.93 [q, OCH_2]. ^{31}P NMR ($CDCl_3$): δ 152.5 [J(Pt-P) = 2591.0 Hz, Pt-$PMe(OEt)_2$]. Molecular weight 497 (mass spectrum).

Cis-[$PtMe_2(PMePh_2)_2$], cis-[$PtMe_2(PEt_3)_2$], cis-[$PtMe_2\{P(OMe)_3\}_2$], cis-[$PtMe_2(AsMe_3)_2$], [$PtMe_2$(TMED)], [$PtMe_2$(COD)], and [$PtMe_2$(NBD)] were also synthesized by the above method. Their purity and identity were checked by melting points and by ^{31}P and/or ^1H NMR spectra.[2-8]

The *cis* form of the new compounds was identified by comparing their J(Pt-P) values with those of the similar dimethylplatinum(II) compounds.[2-8] Since the methyl group has stronger *trans* influence than the phosphines or phosphites, the coupling constants (J(Pt-P)) of the *trans* forms are expected to be larger than those of the corresponding *cis* forms. In fact, All of the known dimethylplatinum(II) compounds were previously identified as the *cis* isomers.

7.1.2 Cis-bis(trifluoromethyl)platinum(II) Complexes

Cis-[$Pt(CF_3)_2(PEt_3)_2$]. The starting material, [$Pt(CF_3)_2$(COD)], was prepared according to the literature method and was checked by ^1H and ^{19}F NMR spectra.[8] To a solution of [$Pt(CF_3)_2$(COD)] (0.25 g, 0.567 mmol) in 5 mL of dichloromethane was added triethylphosphine (0.17 mL, 1.186 mmol) under N_2 at room temperature. The solution was stirred for 2 hours and the solvent was removed under vacuum to give a white solid that was recrystallized from dichloromethane (0.5 mL) and n-pentane (10 mL) at 0°C. Yield 0.29 g (90%). m.p. 141-143°C. ^{19}F NMR (CD_2Cl_2): δ -21.65 [^2J(Pt-F) = 617.3 Hz, Pt-CF_3; ^3J(P-F) = 65.8 Hz, CF_3-Pt-PEt_3]. ^{31}P NMR (CD_2Cl_2): δ 17.49 [J(Pt-P) = 2040.0 Hz, Pt-PEt_3]. Anal. Calcd. for $C_{14}H_{30}F_6P_2Pt$: C, 29.42; H, 5.67. Found: C, 29.51; H, 5.38%. The *cis* form of this compound was identified by its J(Pt-P) value.

cis-[$Pt(CF_3)_2(AsMe_3)_2$] and [$Pt(CF_3)_2$(COD)] were prepared by the above procedure and were identified by their melting points and ^1H and ^{19}F NMR spectra.[8]

7.1.3 (η^5-cyclopentadienyl)trimethylplatinum(IV) Complexes

(η^5-C_5Me_5)$PtMe_3$. 1,2,3,4,5-pentamethylcyclopentadiene (0.243 g, 95%, 1.7 mmol) in dry THF (15 mL) was cooled to -78°C. To this solution was syringed n-butyllithium (0.65 mL, 2.6 M in hexane, 1.7 mmol). Upon warming to room temperature, white lithium pentamethylcyclopentadienide precipitated from a very yellow solution. The stirring suspension was cooled to -78°C again and finely powered [$PtIMe_3$]$_4$[9] (0.50 g, 1.36 mmol) was added against a nitrogen counterstream. The mixture was slowly warmed to 50°C (ca. 1 hour), then stirred for an additional 2 hours and finally filtered. The solvent was removed from the filtrate by vacuum to yield a oily yellow residue. This residue was sublimed at 40 and 10^{-2} mm Hg to give a pale yellow solid (0.19 g, 37% Yield). m.p. 90°C. ^1H NMR ($CDCl_3$): δ 0.37 (s, ^2J(Pt-H) = 80.0 Hz, Pt-CH_3); δ 1.46 (s, ^3J(Pt-H) = 7.0 Hz, C_5Me_5-Pt). Molecular weight 375 (mass spectrum). Anal. Calcd. for $C_{13}H_{24}Pt$: C, 41.62; H, 6.45. Found C, 42.64; H, 6.76.

The complex (η^5-C_5H_5)$PtMe_3$ was prepared by published procedures[10] and purified by vacuum sublimation. Purity was established by melting point,[11] ^1H NMR,[12] and mass spectrum.[13]

7.1.4 (β-diketonato)trimethylplatinum(IV) Complexes

[$PtMe_3$(tfa)Me_2S]. To a suspension of [Pt_2Me_8(μ-SMe_2)$_2$][14] (0.260 g, 0.41 mmol) in dry ether (15 mL) was added trifluoroacetylacetone (0.15 mL, 1.20 mmol). The yellow-orange solution was stirred at room temperature for 5 hours. The solvent was evaporated under reduced pressure and the excess free ligand was removed by heating up to 50°C (water bath) for 3 hours. The oily residue was then sublimed at 80°C to give a yellow liquid (0.16 g, 42.9% yield). ^{1}H NMR ($CDCl_3$): δ 0.98 [s, ^{2}J(Pt-H) = 74.1 Hz, Pt-CH_3]; 2.05 [s, CH_3, tfa]; 2.16 [s, Me_2S]; 5.57 [s, CH, tfa]. ^{19}F NMR ($CDCl_3$): -75.6 [s, tfa]. Molecular weight 455 (mass spectrum). Anal. Calcd. for $C_{10}H_{17}O_2F_3SPt$: C, 26.37; H, 4.18. Found: C, 25.95; H, 4.19.

[$PtMe_3$(hfa)H_2O]. [Me_3PtI]$_4$ (0.300 g, 0.82 mmol) was dissolved in warm, glass distilled benzene (20 mL). Tl(hfa) (0.350 g, 0.85 mmol) in 95% ethanol (5 mL) was then added to the orange benzene solution. The mixture was stirred at 70°C under reflux for 3 hours. The thallous iodide that separated was removed and the filtrate was evaporated to dryness. The dry residue was extracted with ether (50 mL) and the extract was evaporated to dryness again. The product was recrystallized from hot hexane (1 mL) additionally purified by sublimation to give a yellow solid (0.23 g, 60.6% yield). m.p. 105-107°C. dec. 125°C. ^{1}H NMR ($CDCl_3$): δ 1.22 [s, ^{2}J(Pt-H) = 78.7 Hz, Pt-CH_3]; 2.09 [s, H_2O]; 5.94 [s, CH, hfa]. ^{19}F NMR ($CDCl_3$): -76.1 [s, hfa]. Molecular weight 465 (mass spectrum). Anal. Calcd. for $C_8H_{12}O_3F_6Pt$: C, 20.65; H, 2.58. Found: C, 19.51; H, 2.05.

Preparation of [$PtMe_3$(tfa)H_2O] followed the procedure for preparing [$PtMe_3$(hfa)H_2O]. white solid. m.p. 101°C (lit.[15] 85°C). ^{1}H NMR ($CDCl_3$): δ 1.17 [s, ^{2}J(Pt-H) = 77.8 Hz, Pt-CH_3]; 2.02 [s, CH_3, tfa]; 2.08 [s, H_2O]; 5.61 [s, CH, tfa]. ^{19}F NMR ($CDCl_3$): -75.3 [s, tfa]. Molecular weight 411 (mass spectrum).

$[PtMe_3(acac)]_2$ was prepared by the literature method[16] and identified by the decomposing point (200°C)[16] and ^1H NMR spectrum[17].

7.2 HE I AND HE II PHOTOELECTRON SPECTRA

7.2.1 Spectrometer and Maintenance

He I and He II photoelectron spectra were all recorded on a McPherson ESCA-36 photoelectron spectrometer. The spectrometer consists of (1) a home-built helium hollow cathode discharge lamp producing both He I (21.218 eV) and He II (40.814 eV) radiation[18], (2) a home-built inlet system with a electric heater introducing solid and liquid samples and calibrant (Ar) gas into the ionization region[19], (3) a home-built vacuum chamber with an Edwards Series 100 Diffstak diffusion pumping system[19], (4) a hemispherical electrostatic analyzer with a 36 cm radius and a 10 cm gap between the spheres and with a turbomolecular pumping system, (5) a channeltron detector and a DEC VT/78 microcomputer interfaced to the spectrometer's PDP8/e computer. More details of the spectrometer have been described previously.[18-21]

Routine maintenance of the spectrometer was necessary for its good performance and is described as follows.

Vacuum Components. The oil level in the rotary and turbomoleclar pumps was checked at regular intervals, at least once a week, to make sure sufficient oil was in the pumps. The oil in the rotary and turbomolecular pumps was refreshed if the oil colour had been changed, usually at intervals of every six months depending on the frequency of the cycling. The oil in the diffusion pump was not easily checked without the dismantlement of the pumping system, but the fluid sufficiency and cleanness was implied by a satisfactory ultimate pressure in a clean leak-free system ((2-3) x 10^{-7} torr), say in a period of 48 hours. I did not add or change the diffusion pump oil in the last three years. The pressure in the air cylinder was checked regularly to make sure that the pressure was enough to operate properly the valve between the diffusion pump and the vacuum chamber, as well as the valve between the turbomolecular pump and the analyzer.

Helium Lamp, Sample Probe, Gas Cell and Sample Chamber. Following each run of experiment, the sample probe was cleaned with spectroscopic grade methanol and the sample chamber was baked out for at least a few hours at temperature higher than the working temperature for the previous compound. The spectrometer performance was then checked by running Ar spectra under both He I and He II radiations. If the Ar spectra were not satisfactory, the helium lamp was dismantled. A special attention was taken to protect the stainless steel capillary of the lamp from bending since it serves to collimate the light source. The lamp components were inspected and adjusted if it was necessary. The quartz jacket in the lamp was replaced if it was blacked or oxidized and the tantalum tube was sanded with a fine sand paper if oxidation spots appeared on the tube surfaces. A cleaning of the lamp components was helpful in improving the lamp performance.

In many cases, however, the minor treatment on the lamp could not significantly improve the spectrometer performance. Thus the gas cell and the detachable components in the chamber were taken off, the entire sample chamber and gas cell were thoroughly cleaned, and all pertinent surfaces were coated with a fine layer of Acheson colloidal graphite.

Analyzer. The slit of the analyzer was cleaned periodically.

ESCA-36 program. Under normal conditions, the ESCA 36 program was retained by the computer memory. But thunderstorms as well as accidental power cutoff caused loss of the program. Much time was spent on reloading the program!

7.2.2 Spectral Measurement

All compounds were sublimed prior to the spectral measurements. If the colour of the compounds changed during the photoelectron experiments, the residuals were checked by NMR spectra to see whether the compounds had decomposed. During the spectral accumulations, possible decomposition of the compounds could also be detected through dramatic changes in the spectra. If a compound undergoes decomposition, first the electron signal will increase rapidly and then vanish in a few minutes.

The spectral measurements for each compound were taken under a typical spectrometer working condition with the Ar $3p_{3/2}$ peak height being 30,000 counts sec^{-1} for the He I and 300 counts sec^{-1} for the He II, and the Ar $3p_{3/2}$ peak resolution defined as the full with at half the maximum height (FWHM) being less than 0.027 eV for the He I and 0.036 eV for the He II radiations.

All samples except for the free ligand TMED (ca. 0.1g) were loaded into an open end quartz tube which was then placed into a copper tip sample probe. This probe was inserted into the gas cell, which could be electrically heated or water cooled. The free ligand TMED was loaded into a glass tube adapted with a rotaflo tap and a 1/4" glass side arm. The side arm was sealed with quick-fit adapters. By cooling the sample tube in liquid nitrogen, the gases were then removed by pumping under high vacuum.

The operating temperatures for the studied compounds ware tabulated in Table 7.1. These temperatures were set to achieve proper vapour pressures (ca. 5×10^{-6} torr in the sample chamber and ca. 0.1 torr in the gas cell) producing spectra with good signal to background ratios. For the compound $[PtMe_3(acac)]_2$, we started collecting spectrum at 90°C and ended at 185°C. The unique, reproducible He I spectrum could only be obtained above 125°C. Spectra were collected with multiscans. The multiscans were limited to a certain period to assure acceptable

Table 7.1 Temperature for photoelectron spectrum measurement

Compound	Operating Temperature (°C)
cis-$[PtMe_2(PEt_3)_2]$	73-80
cis-$[PtMe_2(P(OMe)_3)_2]$	68-73
cis-$[PtMe_2(P(OEt)_3)_2]$[a]	68-70
cis-$[PtMe_2(PMe(OEt)_2)_2]$[a]	77-81
cis-$[PtMe_2(PMePh_2)_2]$	143-148
cis-$[PtMe_2(P(NMe_2)_3)_2]$[a]	139-145
cis-$[PtMe_2(AsMe_3)_2]$	75-80
$[PtMe_2(Me_2NCH_2CH_2NMe_2)]$	100-107
$[PtMe_2(COD)]$	59-64
$[PtMe_2(NBD)]$	55-60
$[Me_2NCH_2CH_2NMe_2]$	22[b]
cis-$[Pt(CF_3)_2(PEt_3)_2]$[a]	163-171
cis-$[PtCF_3)_2(AsMe_3)_2]$	278-281
$[Pt(CF_3)_2(Me_2NCH_2CH_2NMe_2)]$	229-237
$[Pt(CF_3)_2(COD)]$	173-178
$[Me_3Pt(acac)]_2$	175-180
$[Me_3Pt(tfa)H_2O]$	79-81
$[Me_3Pt(tfa)Me_2S]$[a]	83-85
$[Me_3Pt(hfa)H_2O]$[a]	81-86
$[(\eta^5-C_5H_5)PtMe_3]$	29-32[c]
$[(\eta^5-C_5Me_5)PtMe_3]$[a]	36-41

[a]New compounds. [b]The compound was loaded in a glass tube and the vapour pressure of the compound in the chamber was controlled by a rotaflo tap adapted on the sample tube. [c]The sample probe was initially cooled with liquid nitrogen and then cool water.

spectrum shifts and the various multiscans could then be added by a fortran program if they were required by statistical considerations. He I spectra were calibrated with the Ar $3p_{3/2}$ ionization at 15.759 eV and the corresponding He II spectra were simply referenced to the calibrated He I spectra.

7.2.3 Spectral Fitting

The spectra were computer-fitted to symmetric Lorentzian-Gassian peak shapes with the use of an iterative Gauss-Newton procedure.[22] This procedure was used to deconvolute poorly resolved bands and to determine band areas and positions. Four parameters were thus fitted which were band position, full width at half height, band height and Gauss fraction which determines the fraction of the Gaussian component in the fitted peak shape. The reproducibility of the fitted band positions (ionization energies) were about ±0.02 eV. The fitted band areas were reproducible to about ±10% in the He I spectra and about ±15% in the He II spectra based on the good fittings. The band area ratios from the fitted He I and He II spectra were corrected for the energy discriminations of the electron analyzer, by dividing by the kinetic energy of their electrons.

7.3 SYNCHROTRON RADIATION PHOTOELECTRON SPECTRA

Photoelectron spectra of $CpPtMe_3$ and $Me_2Pt(COD)$ were obtained with photons from the Canadian Synchrotron Radiation Facility (CSRF) at the Aladdin storage ring, University of Wisconsin, Madison.[23-25] A 900 groove/mm grating at photon energies >40 eV and A 600 groove/mm grating at photon energies <40 eV were used in *the Grasshopper* grazing incidence monochromator. Practical minimum photon resolutions were 0.06 eV at photon energy 30 eV with 100 µm slits and 0.09 eV at photon energy 80 eV with 30 µm slits. Intensities at these resolutions were comparable to those obtained from a He lamp (~10^{10} photons per second).

The photon beam emerging from the monochromator exit is refocused to the gas cell in the photoelectron chamber. A two stage differential pumping system and a high vacuum gate valve with a rectangular glass light guide (1mm x 10mm x 200mm) supported in a copper tube is used to isolate the optical elements of the beamline from the high pressure interaction region. The light guide results in almost five orders of magnitude differential pumping, so that the entire beamline is at a pressure of less than 2×10^{-10} torr with pressure in the sample chamber of $\sim 10^{-5}$ torr.

As in the He I and He II photoelectron experiments, a larger McPherson electron analyzer (from the University of Alberta) was used. The analyzer was oriented on a frame so that the synchrotron beam is directed across the length of the analyzer slit, and so that electrons are taken off at a pseudo-magic angle ($\theta_x = 55.8°$, $\theta_y = 34.2°$, $\theta_z = 90°$) assuming a 90% polarization of the incident radiation.[26] The synchrotron beam from the glass light guide entered the gas cell through another aligned light guide 2 cm in length. Electrons exiting from a 1 mm exit slit on the gas cell, travelled into the analyzer through a 3 mm slit and a baffles arrangement common to the McPherson 36 electron spectrometer.

The McPherson analyzer and the sample chamber were each pumped by 330 l/sec Balzers turbomolecular pumps. The pressure in the gas cell of 0.1 torr (as measured by an MKS capacitance manometer) resulted in pressures of $\sim 10^{-5}$ and $\sim 10^{-6}$ torr in the sample and analyzer chambers respectively.

A channeltron detector was linked to a specially designed amplifier-discriminator and connected to a counter unit interfaced with a Zenith Z-158 PC microcomputer. This computer also controlled the spectrometer electron energy scanning through a Biodata Microlink interface unit and the McPherson high stability voltage power supply.

The solid samples, $CpPtMe_3$ and $Me_2(COD)$, were introduced through a probe into the gas cell which was heated by a resistance heater for achieving a proper pressure (~$5x10^{-5}$ torr in the sample chamber). The spectra were collected from photon energies 21 to 100 eV, with the energy steps of 2 eV below 55 eV and of 5 eV above 55 eV. A total amount of ~2.5 g of each compound was used in these experiments.

7.4 Xα-SW CALCULATION

7.4.1 Molecular Orbital Energy and Electron Distribution

All calculations in this thesis were performed using the relativistic version of the self-consistent field (SCF) Xα scattered-wave (SW) method.[27-29] The fundamentals of the SCF-Xα-SW method have been described in detail previously.[30-34] In carrying out the SCF-Xα-SW calculation of a molecule, one first performs SCF-Xα calculations for the consistent atom potentials with a computer program of the type developed originally by Herman and Skillman[35] but modified to permit the use of Slater's Xα statistical approximation to exchange correlation.[36-38] The initial molecular potential is constructed by a superposition of the free atom potentials and by spherically averaging of the superposition using a so-called "muffin-tin" approximation. In this approximation, the potential is assumed to be the spherical average inside a cell surrounding each atom, and outerside an "outersphere," that surrounds the entire molecule. In the remaining, "intersphere," region a constant potential is assumed which is equal to the volume average of the superposition over this region. With this averaged potential, the one-electron Schrödinger equation is numerically solved and a charge density is generated from the resultant wavefunctions. The charge density is averaged by the "muffin-tin" scheme and a new potential is determined from the averaging of the charge density. A weighted average of the new potential and the initial potential serves as input for the first iteration. This procedure is repeated until self-consistency of the potential and charge density is attained.

In order to calculate ionization potentials, Slater's transition state procedure is employed.[39,40] One-half electron is removed from the Highest Occupied Molecular Orbital (HOMO) and the molecular potential is again iterated starting from the converged potential of the ground states to self-consistency. In this procedure, orbital relaxation accompanying ionization is taken account.

The parameters employed in the calculations appear in Tables 7.2-7.12. All coordinates and sphere radii are in atomic units. For comparison, a non-relativistic calculation was also performed on the ground state of cis-$[PtMe_2(PH_3)_2]$. The exchange α-parameters used in each atomic region were taken from Schwarz's tabulation,[41,42] except for hydrogen, for which 0.77725 was used.[43] For the extramolecular and intersphere regions, a weighted average of the atomic α's was employed, the weights being the number of valence electrons in neutral atoms. Overlapping atomic sphere radii were used with the outersphere radius tangent to the outermost atomic spheres.[44,45] An l_{max} of 3 was used around the outersphere region and the platinum atom whereas an l_{max} of 2, 1 and 0 was invoked around As and P; O, N and C; and H atoms respectively. The cis-square-platinum(II) complexes were optimized to have C_{2v} symmetry and the trimethylplatinum(IV) complexes to have C_s. The convergence criterion in all calculations was that the maximum change in the molecular potential be about 10^{-4} Rydbergs.

7.4.2 Photoionization Cross Section

Photoionization cross sections were calculated for the valence levels of cis-$[PtMe_2(C_2H_4)_2]$ and $[(\eta^5\text{-}C_5H_5)Pt(CH_3)_3]$, using the X$\alpha$-SW cross section program of Davenport.[64,65] The calculations were performed with the converged Xα-SW transition state potential, modified with a Latter tail[66] to correct for large r behaviour. In addition to the parameters used in the Xα-SW calculations on molecular orbitals, (

Table 7.2 Parameters used in Xα-SW calculation for cis-[$PtMe_2(C_2H_4)_2$][a]

Region[b]	X	Y	Z	R	α
Outer	0.00	0.00	1.0507	6.8965	0.75073
Pt	0.00	0.00	0.00	2.6577	0.69306
C_1	0.00	-2.5617	-2.9512	1.6794	0.75928
C_2	0.00	2.5617	-2.9512	1.6794	0.75928
C_3	1.2992	-2.9794	2.8150	1.6794	0.75928
C_4	-1.2992	-2.9794	2.8150	1.6794	0.75928
C_5	1.2992	2.9794	2.8150	1.6794	0.75928
C_6	-1.2992	2.9794	2.8150	1.6794	0.75928
H_1	0.00	-1.5366	-4.7599	1.2390	0.77725
H_2	1.6976	-3.7557	-2.8320	1.2390	0.77725
H_3	-1.6976	-3.7557	-2.8320	1.2390	0.77725
H_4	0.00	1.5366	-4.7599	1.2390	0.77725
H_5	1.6976	3.7557	-2.8320	1.2390	0.77725
H_6	-1.6976	3.7557	-2.8320	1.2390	0.77725
H_7	2.3601	-4.7110	3.1241	1.2390	0.77725
H_8	2.3601	-1.2478	3.1241	1.2390	0.77725
H_9	-2.3601	-4.7110	3.1241	1.2390	0.77725
H_{10}	-2.3601	-1.2478	3.1241	1.2390	0.77725
H_{11}	2.3601	4.7110	3.1241	1.2390	0.77725
H_{12}	2.3601	1.2478	3.1241	1.2390	0.77725
H_{13}	-2.3601	4.7110	3.1241	1.2390	0.77725
H_{14}	-2.3601	1.2478	3.1241	1.2390	0.77725

[a]The coordinates were derived from the X-ray data of similar compounds. C_{Me}-Pt-C_{Me} = 81.92°,[46] Pt-C_{Me} = 2.068 Å, Pt-ol = 2.169 Å and ol-Pt-ol = 91.25°[47] (ol = midpoint of C=C bond); for the methyl group, C-H = 1.10 Å[48] and H-C-H = 109.5 Å;for the ethylene, C=C = 1.375 Å, C-H = 1.087 Å, H-C-H = 114.9° and H-C-C = 121.08°.[49] [b]C_1, C_2 and H_1-H_6 are the atoms on the two methyl groups, while C_3-C_6 and H_7-H_{14} are the atoms on the two ethylenes.

Table 7.3 Parameters used in Xα-SW calculation for cis-$[PtMe_2(NH_3)_2]$[a]

Region[b]	X	Y	Z	R	α
Outer	0.00	0.00	-0.1025	6.1052	0.74629
Pt	0.00	0.00	0.00	2.6512	0.69306
C_1	0.00	-2.6268	-3.0255	1.6476	0.75928
C_2	0.00	2.6268	-3.0255	1.6476	0.75928
N_1	0.00	-2.7181	2.8642	1.5651	0.75197
N_2	0.00	2.7181	2.8642	1.5651	0.75197
H_1	0.00	-1.6016	-4.8334	1.1880	0.77725
H_2	1.6976	-3.8207	-2.9062	1.1880	0.77725
H_3	-1.6976	-3.8207	-2.9062	1.1880	0.77725
H_4	0.00	1.6016	-4.8334	1.1880	0.77725
H_5	1.6976	3.8207	-2.9062	1.1880	0.77725
H_6	-1.6976	3.8207	-2.9062	1.1880	0.77725
H_7	0.00	-4.4962	2.0726	1.1605	0.77725
H_8	1.5895	-2.4988	3.9660	1.1605	0.77725
H_9	-1.5895	-2.4988	3.9660	1.1605	0.77725
H_{10}	0.00	4.4962	2.0726	1.1605	0.77725
H_{11}	1.5895	2.4988	3.9960	1.1605	0.77725
H_{12}	-1.5895	2.4988	3.9660	1.1605	0.77725

[a]The coordinates were derived from the X-ray data of similar compounds. Pt-C = 2.120 Å, C-Pt-C =81.92°,[46] Pt-N = 2.09 Å and N-Pt-N = 87.0°;[50] for NH_3, N-H = 1.03 Å and H-N-H = 109.5°;[51] for CH_3, see the footnote of the Table 7.2. [b]The H_1-H_6 are the hydrogens of the two CH_3 groups and the H_7-H_{12} are the hydrogens of the two NH_3.

Table 7.4 Parameters used in Xα-SW calculation for cis-[$PtMe_2(PH_3)_2$][a]

Region[b]	X	Y	Z	R	α
Outer	0.00	0.00	0.5708	6.3916	0.73985
Pt	0.00	0.00	0.00	2.6512	0.69306
C_1	0.00	-2.6268	-3.0255	1.6476	0.75928
C_2	0.00	2.6268	-3.0255	1.6476	0.75928
P_1	0.00	-3.2523	2.8403	2.2564	0.72620
P_2	0.00	3.2523	2.8403	2.2564	0.72620
H_1	0.00	-1.6016	-4.8334	1.1880	0.77725
H_2	1.6976	-3.8207	-2.9062	1.1880	0.77725
H_3	-1.6976	-3.8207	-2.9062	1.1880	0.77725
H_4	0.00	1.6016	-4.8334	1.1880	0.77725
H_5	1.6976	3.8207	-2.9062	1.1880	0.77725
H_6	-1.6976	3.8207	-2.9062	1.1880	0.77725
H_7	0.00	-5.4757	1.3548	1.3410	0.77725
H_8	2.1214	-3.1476	4.4647	1.3410	0.77725
H_9	-2.1214	-3.1476	4.4647	1.3410	0.77725
H_{10}	0.00	5.4757	1.3548	1.3410	0.77725
H_{11}	2.1214	3.1476	4.4647	1.3410	0.77725
H_{12}	-2.1214	3.1476	4.4647	1.3410	0.77725

[a]The coordinates were derived from the X-ray data of similar compounds. Pt-P = 2.285 Å, P-Pt-P = 97.75°,[46] P-H = 1.415 Å,[52], H-P-H = 105.0°,[53] for the $Pt(CH_3)_2$, see the footnote of the Table 7.3. [b]The H_1-H_6 are the hydrogens of the two CH_3 groups and the H_7-H_{12} are the hydrogens of the two PH_3.

Table 7.5 Parameters used in Xα-SW calculation for cis-[$PtMe_2(AsH_3)_2$][a]

Region[b]	X	Y	Z	R	α
Outer	0.00	0.00	0.8081	6.7935	0.73496
Pt	0.00	0.00	0.00	2.6512	0.69306
C_1	0.00	-2.6268	-3.0255	1.6794	0.75928
C_2	0.00	2.6268	-3.0255	1.6794	0.75928
As_1	0.00	-3.6186	2.8425	2.3907	0.70665
As_2	0.00	3.6186	2.8425	2.3907	0.70665
H_1	0.00	-1.6016	-4.8334	1.2010	0.77725
H_2	1.6976	-3.8207	-2.9062	1.2010	0.77725
H_3	-1.6976	-3.8207	-2.9062	1.2010	0.77725
H_4	0.00	1.6016	-4.8334	1.2010	0.77725
H_5	1.6976	3.8207	-2.9062	1.2010	0.77725
H_6	-1.6976	3.8207	-2.9062	1.2010	0.77725
H_7	0.00	-6.1751	1.5706	1.3890	0.77725
H_8	2.2331	-3.4372	4.6127	1.3890	0.77725
H_9	-2.2331	-3.4372	4.6127	1.3890	0.77725
H_{10}	0.00	6.1751	1.5706	1.3890	0.77725
H_{11}	2.2331	3.4372	4.6127	1.3890	0.77725
H_{12}	-2.2331	3.4372	4.6127	1.3890	0.77725

[a]The coordinates were derived from the X-ray data of similar compounds. Pt-As = 2.435 Å, As-Pt-As = 103.7° and H-As-H = 102.9°,[54] As-H = 1.511 Å,[55] for the $Pt(CH_3)_2$, see the footnote of the Table 7.3. [b]The H_1-H_6 are the hydrogens of the two CH_3 groups and the H_7-H_{12} are the hydrogens of the two AsH_3.

Table 7.6 Parameters used in Xα-SW calculation for cis-[$PtMe_2(CNH)_2$][a]

Region[b]	X	Y	Z	R	α
Outer	0.00	0.00	1.6179	7.4599	0.74583
Pt	0.00	0.00	0.00	2.6512	0.69306
C_1	0.00	-2.5617	-2.9512	1.6476	0.75928
C_2	0.00	2.5617	-2.9512	1.6476	0.75928
C_3	0.00	-2.5070	2.4636	1.6476	0.75928
C_4	0.00	2.5070	2.4636	1.6476	0.75928
H_1	0.00	-1.5366	-4.7595	1.1880	0.77725
H_2	1.6976	-3.7557	-2.8320	1.1880	0.77725
H_3	-1.6976	-3.7557	-2.8320	1.1880	0.77725
H_4	0.00	1.5366	-4.7595	1.1880	0.77725
H_5	1.6976	3.7557	-2.8320	1.1880	0.77725
H_6	-1.6976	3.7557	-2.8320	1.1880	0.77725
N_1	0.00	-3.9370	4.1993	1.5651	0.75197
N_2	0.00	3.9370	4.1993	1.5651	0.75197
H_7	0.00	-5.0671	5.7840	1.1605	0.77725
H_8	0.00	5.0671	5.7840	1.1605	0.77725

[a]The coordinates were derived from the X-ray data of similar compounds. Pt-C_N = 1.86 Å, C≡N = 1.19 Å,[56] C_N-Pt-C_N = 91°[57], and N-H was the same as in the [$PtMe_2(NH_3)_2$]. For the $Pt(CH_3)_2$, see the footnote of the Table 7.3. [b]The C_1 and C_2 and H_1-H_6 are the carbon and hydrogen atoms of the two CH_3 groups. The C_3, C_4, N_1, N_2, H_7 and H_8 are the atoms (carbon, nitrogen, and hydrogen respectively) of the two CNH groups.

Table 7.7 Parameters used in Xα-SW calculation for cis-[Pt(CF$_3$)$_2$(C$_2$H$_4$)$_2$][a]

Region[b]	X	Y	Z	R	α
Outer	0.00	0.00	0.9660	7.0200	0.74213
Pt	0.00	0.00	0.00	2.6577	0.69306
C_1	0.00	-2.7016	-2.7976	1.6794	0.75928
C_2	0.00	2.7016	-2.7976	1.6794	0.75928
C_3	1.2992	-2.9794	2.8150	1.6794	0.75928
C_4	-1.2992	-2.9794	2.8150	1.6794	0.75928
C_5	1.2992	2.9794	2.8150	1.6794	0.75928
C_6	-1.2992	2.9794	2.8150	1.6794	0.75928
F_1	0.00	-5.0058	-1.7475	1.6802	0.73732
F_2	2.0680	-2.4289	-4.2334	1.6802	0.73732
F	-2.0680	-2.4289	-4.2334	1.6802	0.73732
F_4	0.00	5.0058	-1.7475	1.6802	0.73732
F_5	2.0680	2.4289	-4.2334	1.6802	0.73732
F_6	-2.0680	2.4289	-4.2334	1.6802	0.73732
H_1	2.3601	-4.7110	3.1241	1.2100	0.77725
H_2	2.3601	-1.2478	3.1241	1.2100	0.77725
H_3	-2.3601	-4.7110	3.1241	1.2100	0.77725
H_4	-2.3601	-1.2478	3.1241	1.2100	0.77725
H_5	2.3601	4.7110	3.1241	1.2100	0.77725
H_6	2.3601	1.2478	3.1241	1.2100	0.77725
H_7	-2.3601	4.7110	3.1241	1.2100	0.77725
H_8	-2.3601	1.2478	3.1241	1.2390	0.77725

[a]The coordinates were derived from the X-ray data of similar compounds. Pt-C(CF$_3$) = 2.058 Å and C(CF$_3$)-Pt-C(CF$_3$) = 88.0°,[58] C-F =1.340 Å and F-C-F =109.5°,[59] for the Pt(C$_2$H$_4$)$_2$, see the footnote of the Table 7.2. [b]The C_1 and C_2 are the carbons of the two CF$_3$ groups and the C_3, C_4, C_5, and C_6 are the carbons of the two ethylenes.

Table 7.8 Parameters used in Xα-SW calculation for cis-[$Pt(CF_3)_2(PH_3)_2$][a]

Region	X	Y	Z	R	α
Outer	0.00	0.00	0.5977	7.0803	0.73550
Pt	0.00	0.00	0.00	2.6577	0.69306
C_1	0.00	-2.7016	-2.7976	1.6794	0.75928
C_2	0.00	2.7016	-2.7976	1.6794	0.75928
P_1	0.00	-3.2523	2.8403	2.3080	0.72620
P_2	0.00	3.2523	2.8403	2.3080	0.72620
F_1	0.00	-5.0058	-1.7475	1.7048	0.73732
F_2	2.0680	-2.4289	-4.2334	1.7048	0.73732
F_3	-2.0680	-2.4289	-4.2334	1.7048	0.73732
F_4	0.00	5.0058	-1.7475	1.7048	0.73732
F_5	2.0680	2.4289	-4.2334	1.7048	0.73732
F_6	-2.0680	2.4289	-4.2334	1.7048	0.73732
H_7	0.00	-5.4757	1.3548	1.4000	0.77725
H_8	2.1214	-3.1476	4.4647	1.4000	0.77725
H_9	-2.1214	-3.1476	4.4647	1.4000	0.77725
H_{10}	0.00	5.4757	1.3548	1.4000	0.77725
H_{11}	2.1214	3.1476	4.4647	1.4000	0.77725
H_{12}	-2.1214	3.1476	4.4647	1.4000	0.77725

[a]The bond length and angle of the $Pt(CF_3)_2$ were the same as those in cis-[$Pt(CF_3)_2(C_2H_4)_2$], while the bond length and angle of the $Pt(PH_3)_2$ were the same as those in cis-[$PtMe_2(PH_3)_2$]. See footnotes of Tables 7.4 and 7.7.

Table 7.9 Parameters used in Xα-SW calculation for cis-[$PtMe_2$] and cis-[$Pt(CF_3)_2$][a]

Region	X	Y	Z	R	α
Outer	0.00	0.00	-1.3881	5.5222	0.73618
Pt	0.00	0.00	0.00	2.6577	0.69306
C_1	0.00	-2.5617	-2.9512	1.6794	0.75928
C_2	0.00	2.5617	-2.9512	1.6794	0.75928
H_1	0.00	-1.5366	-4.7595	1.2390	0.77725
H_2	1.6976	-3.7557	-2.8320	1.2390	0.77725
H_3	-1.6976	-3.7557	-2.8320	1.2390	0.77725
H_4	0.00	1.5366	-4.7595	1.2[illegible]	0.77725
H_5	1.6976	3.7557	-2.8320	1.2390	0.77725
H_6	-1.6976	3.7557	-2.8320	1.2390	0.77725
Outer	0.00	0.00	-2.6084	6.4698	0.73287
Pt	0.00	0.00	0.00	2.6577	0.69306
C_1	0.00	-2.7016	-2.7976	1.6794	0.75928
C_2	0.00	2.7016	-2.7976	1.6794	0.75928
F_1	0.00	-5.0058	-1.7475	1.6802	0.73732
F_2	2.0680	-2.4289	-4.2334	1.6802	0.73732
F_3	-2.0680	-2.4289	-4.2334	1.6802	0.73732
F_4	0.00	5.0058	-1.7475	1.6802	0.73732
F_5	2.0680	2.4289	-4.2334	1.6802	0.73732
F_6	-2.0680	2.4289	-4.2334	1.6802	0.73732

[a]The bond lengths and angles of the $PtMe_2$ were the same as the those in cis-[$PtMe_2(C_2H_4)_2$], while the bond lengths and angles of the $Pt(CF_3)_2$ were the same as those in cis-[$Pt(CF_3)_2(C_2H_4)_2$]. See the footnotes of Tables 7.2 and 7.7.

Table 7.10 Parameters used in Xα-SW calculation for C_2H_4, NH_3, PH_3, AsH_3 and CNH[a]

Region	X	Y	Z	R	α
Outer	0.00	0.00	0.00	4.1497	0.76527
C_1	0.00	0.00	1.2623	1.6794	0.75928
C_2	0.00	0.00	-1.2623	1.6794	0.75928
H_1	0.00	-1.7527	2.3310	1.2390	0.77725
H_2	0.00	1.7527	2.3310	1.2390	0.77725
H_3	0.00	-1.7527	-2.3310	1.2390	0.77725
H_4	0.00	1.7527	-2.3310	1.2390	0.77725
Outer	0.00	0.00	0.1478	2.7840	0.76145
N	0.00	0.00	0.00	1.5651	0.75197
H_1	0.00	-1.7715	0.7001	1.1605	0.77725
H_2	1.5342	0.8858	0.7001	1.1605	0.77725
H_3	-1.5342	0.8858	0.7001	1.1605	0.77725
Outer	0.00	0.00	0.2663	3.4933	0.74534
P	0.00	0.00	0.00	2.2564	0.72620
H1	0.00	-2.2480	1.4480	1.3410	0.77725
H_2	1.9469	1.1240	1.4480	1.3410	0.77725
H_3	-1.9469	1.1240	1.4480	1.3410	0.77725
Outer	0.00	0.00	0.2927	3.6760	0.73313
As	0.00	0.00	0.00	2.3907	0.70665
H_1	0.00	-2.3738	1.5870	1.3890	0.77725
H_2	2.0577	1.1869	1.5870	1.3890	0.77725
H_3	-2.0577	1.1869	1.5870	1.3890	0.77725
Outer	0.00	0.00	0.1512	3.1879	0.75742
C	0.00	0.00	2.2488	1.6476	0.75928
N	0.00	0.00	0.00	1.5651	0.75197
H	0.00	0.00	-1.9464	1.1605	0.77725

[a]The coordinates were derived from as follows. For C_2H_4, C=C = 1.337 Å, C-H = 1.086 Å, H-C-H = 117.3°[?] and H-C_1-C_2 = 121.4°;[60] for NH_3, N-H = 1.008 Å and H-N-H = 107.3°;[61] for PH_3, P-H =1.415 Å and H-P-H = 93.45°;[44] for AsH_3, As-H = 1.511 Å and H-As-H = 92.1°,[55] for CNH, C≡N = 1.19 Å[56] and N-H = 1.03 Å.[51]

Table 7.11 Parameters used in Xα-SW calculation for $[(\eta^5\text{-}C_5H_5)PtMe_3]^a$

Region[b]	X	Y	Z	R	α
Outer	0.0387	0.00	0.5427	6.8330	0.75195
Pt	0.00	0.00	0.00	2.6577	0.69306
C_1	-2.4799	0.00	3.1224	1.6794	0.75928
C_2	-2.4799	2.7040	-1.5611	1.6794	0.75928
C_3	-2.4799	-2.7040	-1.5611	1.6794	0.75928
C_4	3.7332	0.00	2.2987	1.6794	0.75928
C_5	3.7332	2.1683	0.7104	1.6794	0.75928
C_6	3.7332	-2.1683	0.7104	1.6794	0.75928
C_7	3.7332	1.3512	-1.8597	1.6794	0.75928
C_8	3.7332	-1.3512	-1.8597	1.6794	0.75928
H_1	-1.3971	0.00	4.8525	1.2105	0.77725
H_2	-3.6559	1.6668	3.0565	1.2105	0.77725
H_3	-3.6559	-1.6668	3.0565	1.2105	0.77725
H_4	-1.3971	4.2022	-2.4263	1.2105	0.77725
H_5	-3.6559	4.1474	-1.5281	1.2105	0.77725
H_6	-3.6559	1.2607	-1.5281	1.2105	0.77725
H_7	-1.3971	-4.2022	-2.4263	1.2105	0.77725
H_8	-3.6559	-4.1474	-1.5281	1.2105	0.77725
H_9	-3.6559	-1.2607	-1.5281	1.2105	0.77725
H_{10}	3.7332	0.00	4.3396	1.2105	0.77725
H_{11}	3.7332	4.1272	1.3410	1.2105	0.77725
H_{12}	3.7332	-4.1272	1.3410	1.2105	0.77725
H_{13}	3.7332	2.5508	-3.5108	1.2105	0.77725
H_{14}	3.7332	-2.5508	-3.5108	1.2105	0.77725

a) The coordinates were derived from the X-ray data of the compound $[(\eta^5\text{-}C_5H_5)PtMe_3]$.[62] $Pt\text{-}C_{Me}$ = 2.11 Å, $Pt\text{-}C_{ring}$ = 2.32 Å, $C_{ring}\text{-}C_{ring}$ = 1.43 Å, C-H = 1.08 Å, $C_{Me}\text{-}Pt\text{-}C_{Me}$ = 85.4°, $C_{ring}\text{-}C_{ring}\text{-}C_{ring}$ = 108.0°. b). The C_1-C_3 and H_1-H_9 are the atoms of the three CH_3 groups and the C_4-C_8 and H_{10}-H_{14} are the atoms of the C_5H_5 ring.

Table 7.12 Parameters used in Xα-SW calculation for $[Me_3Pt(O_2C_3H_3)]$[a]

Region[b]	X	Y	Z	R	α
Outer	1.5079	0.00	1.6463	7.4777	0.74582
Pt	0.00	0.00	0.00	2.6577	0.75928
C_1	3.7795	0.00	0.00	1.6794	0.75928
C_2	0.00	-2.6887	-2.7362	1.6794	0.75928
C_3	0.00	2.6887	-2.7362	1.6794	0.75928
C_4	0.00	-2.8479	5.2223	1.6794	0.75928
C_5	0.00	2.8479	5.2223	1.6794	0.75928
C_6	0.00	0.00	6.5599	1.6794	0.75928
O_1	0.00	-2.8479	2.8979	1.5547	0.74447
O_2	0.00	2.8479	2.8979	1.5547	0.74447
H_1	4.4734	0.00	-1.9595	1.2105	0.77725
H_2	4.4719	-1.6976	0.9798	1.2105	0.77725
H_3	4.4719	1.6976	0.9798	1.2105	0.77725
H_4	0.00	-1.7775	-4.6046	1.2105	0.77725
H_5	1.6976	-3.8729	-2.5432	1.2105	0.77725
H_6	-1.6976	-3.8729	-2.5432	1.2105	0.77725
H_7	0.00	1.7775	-4.6046	1.2105	0.77725
H_8	1.6976	3.8729	-2.5432	1.2105	0.77725
H_9	-1.6976	3.8729	-2.5432	1.2105	0.77725
H_{10}	0.00	-4.7317	6.1009	1.2105	0.77725
H_{11}	0.00	4.7317	6.1009	1.2105	0.77725
H_{12}	0.00	0.00	8.6386	1.2105	0.77725

[a]The coordinates were derived from the X-ray data of $Me_3Pt(C_3H_7CO.CH.COC_3H_7)$.[63] Pt-C =2.03 Å, Pt-C =2.00 Å, Pt-O = 2.15 Å, O-C = 1.23 Å, C-C = 1.46 Å, C-Pt-C =88.6°, O-Pt-O = 88.9°, Pt-O-C =124.4°, O-C-O = 128.0° and C-C-C = 122.0°. For the bond length and angle of the methyl groups, see the footnote of Table 7.2. [b]The C_1-C_3 and H_1-H_9 are the atoms of the three methyl groups, while the C_4-C_6, O_1, O_2, and H_{10}-H_{12} are the atoms of the ß-diketonate anion.

Tables 7.2 and 7.11) the maximum azimuthal quantum number, L_{max}, for final state were extended to 7, 5, 2 and 1 around outersphere, platinum, carbon and hydrogen region respectively. This choice of the L_{max} values should provide convergence in cross section to better than a few percent.[67] All symmetry-allowed photoionization processes based on the dipolar selection rule were included in the calculations.

7.5 REFERENCES

1. J. D. Scott and R. J. Puddephatt, Organometallics 2, 1643 (1983).
2. J. D. Ruddick and B. L. Shaw, J. Chem. Soc. (A) 2801 (1969).
3. T. G. Appleton, M. A. Bennett and I. B. Tomkins, J. Chem. Soc., Dalton Trans. 439 (1976).
4. J. Chatt and B. L. Shaw, J. Chem. Soc. 705 (1959).
5. F. H. Allen and A. Pidcock, J. Chem. Soc. (A) 2700 (168).
6. B. Neruda and J. Lörberth, J. Organomet. Chem. 111, 241 (1976).
7. H. C. Clark, L. E. Manzer and J. E. H. Ward, Can. J. Chem., 52, 1165 (1974).
8. H. C. Clark and L. E. Manzer, J. Organomet. Chem., 59, 411 (1973).
9. M. Rashidi, Personal communication.
10. S. D. Robinson and B. L. Shaw, J. Chem. Soc., 1529 (1965).
11. A. Shaver, Can. J. Chem., 56, 2281 (1978).
12. G. Hamer and A. Shaver, Can. J. Chem., 58, 2011 (1980).
13. K. W. Egger, J. Organomet. Chem., 24, 501 (1970).
14. M. Lashanizadehgan, M. Rashidi, J. H. Hux and R. J. Puddephatt, J. Organomet. Chem., 269, 317 (1984).
15. G. I. Zharkova, I. K. Igumenov and S. V. Zemskov, Sov. J. Coord. Chem. (Russian Translation), 5, 586 (1979).
16. R. C. Menzies, J. Chem. Soc., 565 (1928).
17. K. Kite, J. A. S. Smith and E. J. Wilkins, J. Chem. Soc. (A), 1744 (1966).
18. L. L. Coatsworth, G. M. Bancroft, D. K. Creber, R. J. D. Lazier and P. W. M. Jacobs, J. Electron Spectrosc. Relat. Phenom., 13, 395 (1978).
19. G. M. Bancroft, D. J. Bristow and L. L. Coatsworth, Chem. Phys. Lett., 82, 344 (1981).

20. L. M. Dignard, Ph. D. Dissertation, University of Western Ontario, London, Ontario, Canada, 1986.

21. J. E. Bice, Ph. D. Dissertation, University of Western Ontario, London, Ontario, Canada, 1987.

22. G. M. Bancroft, I Adams, L. L. Coatsworth, C. D. Bennewltz, J. D. Brown and W. D. Westwood, Anal. Chem., 47, 586 (1975).

23. J. D. Bozek, J. N. Cutler, G. M. Bancroft, L. L. Coatsworth, K. H. Tan, D. S. Yang and R. G. Cavell, Chem. Phys. Lett., (submitted).

24. G. M. Bancroft, J. D. Bozek, J. N. Cutler and K. H. Tan, J. Electron Spectrosc. Relat. Phenomen., 47, 187 (1988).

25. B. W. Yates, K. H. Tan, L. L. Coatsworth and G. M. Bancroft, Phys. Rev., 31 A, 1529 (1985).

26. J. A. R. Samson, Philos. Trans. Roy. Soc. London, 268 A, 141 (1970).

27. D. A. Case and C. Y. Yang, J. Chem. Phys., 72, 3443 (1980).

28. D. A. Case and C. Y. Yang, Int. J. Quantum Chem., 18, 1091 (1980).

29. M. Cook and D. A. Case, QCPE, 14, 465 (1982).

30. J. C. Slater, "Quantum Theory of Molecules and Solids", 4, New York: McGraw-Hill. (1974).

31. K. H. Johnson, Advan. Quantum Chem., 7, 143 (1973).

32. K. H. Johnson, Ann. Rev. Phys. Chem., 26, 39 (1975).

33. N. Rösch, in " Electrons in Finite and Infinite Structure ", edited by P. Phariseau and L. Scheire, P.1-143. New York: Plenum. (1977).

34. D. A. Case, Ann. Rev. Phys. Chem., 33, 151 (1982).

35. F. Herman and S. Skillman, " Atomic Structure calculations ", Prentice-Hall, Englewood Cliffs, N. J., (1963).

36. J. C. Slater, T. M. Wilson and J. H. Wood, Phys. Rev., 179, 28 (1969).

37. J. C. Slater, J. B. Mann, T. M. Wilson and J. H. Wood, Phys. Rev., 184, 672 (1969).

38. J. C. Slater and J. H. Wood, Intern. J. Quantum Chem., 4s, 3 (1971).

39. J. C. Slater, Adv. Quantum Chem., 6, 1 (1972).

40. J. C. Slater and J. H. Johnson, Phys. Rew., B, 5, 844 (1972).

41. K. Schwarz, Phys. Rev. B., 5, 2466 (1972).

42. K. Schwarz, Theor. Chim. Acta., 34, 225 (1974).

43. J. C. Slater, Int. J. Quantum Chem., 7s, 533 (1973).

44. J. G. Norman, Jr. J. Chem. Phys., 61, 4630 (1974).

45. J. G. Norman, Jr. Mol. Phys., 31, 1191 (1976).

46. J. M. Wisner, T. J. Bartczak and A. Ibers, Organometallics, 5, 2044 (1986).

47. C. S. Day, V. W. Day, A. Shaver and H. C. Clark, Inorg. Chem., 20, 2188 (1981).

48. S. Obara, K. Kitaura and K. Morokuma, J. Am. Chem. Soc., 106, 7482 (1984).

49. R. A. Love, T. F. Koetzle, G. J. B. Williams, L. C. Andrews and R. Bau, Inorg. Chem., 14, 2653 (1975).

50. M. Barber, J. R. Clark and A. Hinchliff, J. Mol. Struct., 57, 169 (1979).

51. M. Takah·shi, I. Watanable and S. Ikeda, J. Bull. Chem. Soc. Jap., 60, 9 (1987).

52. K. J. Kuchitzer, J. mol. Spectrosc., 7, 399 (1961).

53. L. S. Bartell and R. C. Hirst, J. Chem. Phys., 31, 449 (1959).

54. D. R. Russell and P. A. Tucker, J. Chem. Soc. Dalton Trans., 1752 (1975).

55. K. D. Dobbs and W. J. Hehre, J. Comput. Chem., 7, 359 (1986).

56. A. Scrivanti, G. Carturan, U. Belluco, N. Brescianipahor, M. Calligaris, and L. Randaccio, Inorg. Chim. Acta, 20, L3 (1976).

57. B. Jovanovic, L. Manojlovic-Muir, and K. W. Muir, J. Chem. Soc. Dalton Trans., 1178 (1972).

58. L. Manojlovic-muir, K. W. Muir, T. Solomun, D. W. Meek and J. L. Pertson, J. Organomet. Chem., 146, C26 (1978).

59. M. B. Hall and R. F. Fenske, Inorg. Chem., 11, 768 (1972).

60. J. D. Roberts and M. C. Caserio, "Basic Principles of Organic Chemistry", 2nd, W. A. Benjamin Inc. (1977).

61. "Handbook of Chemistry and Physics", CRC Press, Cleveland, Ohio (1981).

62. G. W. Adamson, J. C. J. Bart and J. J. Daly, J. Chem. Soc., (A), 2616 (1971).

63. A. G. Swallow and M. R. Truter, Proc. Roy. Soc., 254A, 205 (1960).

64. J. W. Davenport, Ph. D. Dissertation, University of Pennsylvania (1976).

65. J. W. Davenport, Phys. Rev. lett. 36, 945 (1976).

66. R. Latter, Phys. Rev., 99, 510 (1955).

67. B. W. Yates, K. H. Tan, G. M. Bancroft, L. L, Coatsworth and J. S. Tse, J. Chem. Phys., 84, 3603 (1986).